MICROFABRICATION OF TITANIUM DIBORIDE PATTERNED ON SILICON SUBSTRATES FOR MONO- AND CO-CULTURE OF ENDOTHELIAL AND MESENCHYMAL STEM CELLS

A Dissertation

Presented to

the Faculty of the Department of Electrical and Computer Engineering

University of Houston

In Partial Fulfillment

of the Requirements for the Degree

Doctor of Philosophy

in Electrical Engineering

by

Susmi Das

May 2014

ACKNOWLEDGEMENTS

I am grateful to Dr. Wanda Wosik and Dr. Fatima Merchant for their support, supervision and guidance during my PhD research. They motivated me tremendously and always had insightful ideas for the project. I would like to thank Dr. Osama Gaber, Dr. Omaima Sabek, Dr. Jarek Wosik, Dr. Steven Pei, and Dr. Earl Joe Charlson for serving as my committee members. I appreciate Dr. Osama Gaber and his islet transplantation group for their financial support and for providing us Islets of Langerhans and Mesenchymal Stem cells cultures for experimentation. Special thanks to my laboratory colleague Alex Leon for helping me with my experiments. I highly appreciate the knowledgeable contribution from Daniel Fraga, Director of Islet transplantation laboratory of Methodist Hospital. I appreciate the help from Jihae Chung for AFM measurements and Andrew Robertson for hardness measurements in chemical engineering department-University of Houston, Dr. Lewis Francis and Dr. James Gu for the use of Multimode8 in their facility for BioAFM measurements at The Methodist Research Institute and Dr. Kloc for cytoskeleton staining of samples.

This achievement would not have been possible without the support of my parents and parents in law, sister Saon, brother-in-law Subit, husband Abhinandan and friends. Special acknowledgement to my husband, Abhinandan Pattanayak, for going through my manuscript and providing helpful suggestions.

MICROFABRICATION OF TITANIUM DIBORIDE PATTERNED ON SILICON SUBSTRATES FOR MONO- AND CO-CULTURE OF ENDOTHELIAL AND MESENCHYMAL STEM CELLS

An abstract

of a

Dissertation

Presented to

the Faculty of the Department of Electrical and Computer Engineering

University of Houston

In Partial Fulfillment

of the Requirements for the Degree

Doctor of Philosophy

in Electrical Engineering

by

Susmi Das

May 2014

ABSTRACT

Transplantation of Islet of Langerhans is a treatment used in Diabetes Type I with an objective to introduce beta cells for secretion of insulin for controlling the glucose level in the body. Our project is focused on in vitro culturing of endothelial cells and mesenchymal cells on biocompatible titanium diboride substrates patterned as circles and lines organized as arrays to induce interaction of these layers with the Islets of Langerhans for their *in vitro* prolonged viability. Our designed BIOMEMS device evaluates the influence of substrate material properties such as mechanical, chemical and electrical using 2D sheet based configurations. The device has matrices of different geometries, to determine factors that affect cell growth and orientation. With the design of patterned geometries on the titanium diboride wafers, modification of the surface properties and biocompatible material usage, we can focus on cell adhesion, growth and orientation. Titanium diboride material was characterized for surface composition, surface roughness, hardness, Young's modulus and wettability.

This BioMEMS device mimics native cellular microenvironment, in terms of topology that provides mechanical support and is expected to regulate the cellular activities such as adhesion, adhesion and viability. Our experiments demonstrated TiB_2 as a probable material showing biocompatibility and three weeks long viability of cells and islets. Silicon integrated circuit (IC) and MEMS technology were used to make the substrates and confocal microscopy on fluorescent dyes was used for imaging the endothelial cell (EC) and islet viability.

TABLE OF CONTENTS

List of Figures

List of Tables

Chapter 1: Introduction

Pancreas comprises of many small clusters of Islets of Langerhans that have alpha, beta, delta and PP cells that secret glucagon, insulin, somatostatin and polypeptide hormones respectively. In Type I Diabetes (T1D), autoimmune destruction of insulin producing beta cells causes an increase in blood glucose levels. Currently the treatments for T1D are insulin injection, pancreas transplantation and islet transplantation. There has been tremendous amount of research for increasing the success of the islet transplantation procedure. Islet transplantation has achieved insulin independence in patients with controlled glucose levels for five years post transplantation. However, after five years the patients have to return back to insulin injection dependence for blood glucose level control.

One of the factors limiting prolonged controlled glucose level is the avascular state of islets of Langerhans post isolation from donors. Islets of Langerhans are highly vascularized and receive 15% of the blood to the pancreas. Following isolation from donors the microvascular networks within the islets is destroyed and post-transplantation islets take about two to three weeks to be revascularized. Between isolation and the transplantation period, the islets gradually lose their vasculature in culturing. Therefore, an approach to retain or enforce the vascular architecture of islets pre-transplantation that would facilitate rapid revascularization after implantation can be envisioned as a solution towards a more successful islet transplantation. Active research is being conducted to improve the revascularization of islets using endothelial cells (EC) culture or endothelial and mesenchymal stem cells (MSC) co-culture in artificial biodegradable grafts [1, 2, 3]. Rackham et al. [4] concluded that co-transplantation of islets with MSCs maintained the

islet structure, function and in turn improved the revascularization of islets. They observed reversal of hyperglycemia (excess blood glucose concentration) in mice with MSC-Islet co-culture [4]. Song et al. [5] improved the *in vitro* post extraction islet survival and its function by co-culturing of freshly extracted islets with ECs. They suggested that various factors released from EC such as Vascular Endothelial Growth Factor (VEGF) had improved the islet survival *in vitro.* Johansson et al. [6, 7] studied a novel approach of EC and MSC co-culture in fibrin gel to enhance the capacity of islets for revascularization. They demonstrated that the MSCs caused EC to migrate into the islets to exhibit sprout formation.

We have designed a two-dimensional biomedical (or biological) microelectromechanical systems (BioMEMS) device based on micropatterning on silicon (Si) wafers that will facilitate formation of a bed of co-culture of Human Umbilical Vein Endothelial Cells (HUVECs/ECs) and Mesenchymal Stem Cells (MSC) on which the islets were cultured *in vitro* on the device for about three weeks. From various materials tested for biocompatibility with *in vitro* HUVEC viability studies, we selected titanium diboride (TiB_2). It exhibited prolonged viability of both HUVECs and MSCs, thus indicating its biocompatibility. The TiB_2 material was characterized with respect to its surface composition, roughness, hardness, Young's modulus and hydrophilicity. Patterns of TiB_2 created on substrates attributed to selective growth of cells, with cells responding to material properties of the patterned surface. The substrates were used to culture ECs, MSC and islets independently and in co-culture for a period of about two-three weeks. Stereomicroscopy and/ or fluorescence confocal microscopy was used to monitor and quantitate the growth of cells on the micropatterned surfaces.

1.1 Thesis organization

The remainder of this thesis is organized as follows; Chapter 2 provides an introduction of the structure of Islet of Langerhans, T1D and its treatments, cell structure, extracellular matrix, cellular adhesion, techniques for islet engraftment and factors affecting HUVEC growth on biomaterails. A brief review of various specific biomaterials and techniques of surface modification has been addressed in Chapter 3. Chapter 4 gives the details of experimental methods that describe the design and fabrication of the BIOMEMS, material characterization of biocompatible TiB_2 material, cell culturing protocols and staining protocols for live / fixed confocal imaging. Chapter 5 provides the results obtained from material characterization of titanium diboride for surface chemical composition, crystalline state, hardness, Young's modulus, roughness and wettability. Chapter 6 explains the biological characterization of titanium diboride with culturing of Human Vein Umbilical Endothelial Cells (HUVEC), Mesenchymal Stem Cells (MSC) and Islets of Langerhans. Chapter 7consists of conclusions and suggestions for future work.

Chapter 2: Theory of Type I diabetes and its treatment

Pancreatic islets form the endocrine portion of the pancreas that is present in the form of many small clusters of cells called islets of Langerhans [8]. The adult pancreas contains approximately one million islets that generally range from 30 to 300 μm in diameter. Even though the islets comprise about 1 to 2 percent of the mass of the pancreas, they receive about 10 to 15 percent of the pancreatic blood flow and are highly vascularized [9]. These islets are located across the pancreatic arterial system, where the bigger ones are close to major arterioles and the smaller are within the pancreas [10]. Approximately 2000 cells are present in the islets, comprising of four major cell types in the islets of Langerhans – alpha, beta, delta and polypeptide (PP) cells that secrete glucagon, insulin, somatostatin and polypeptide hormones, respectively (Figure 2.1). The beta-cells occupy about 75% to 80% of the cells population in an islet and produce insulin to lower the blood glucose concentrations.

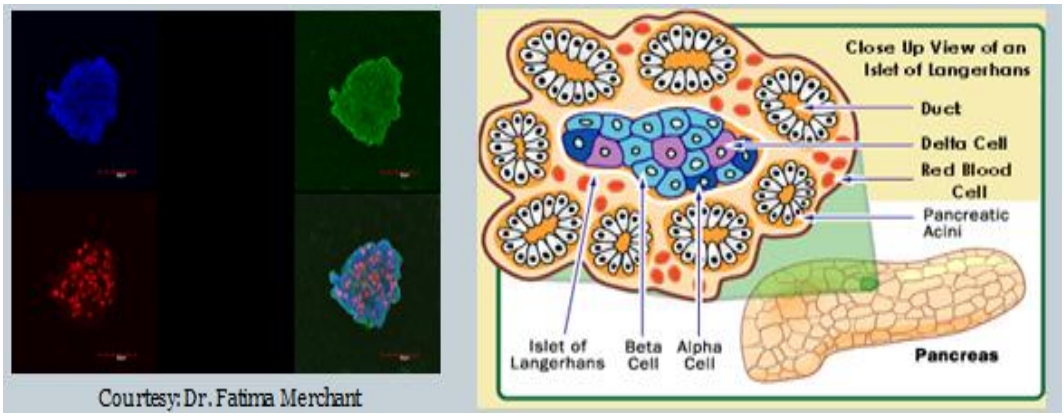

Figure 2.1 Alpha, Beta and Delta cells in the Islet of Langerhans [15].

The density of blood vessels within the islets is greater than the ones outside the islets. The internal blood vessels provide nutrition and oxygen to the islets to facilitate its

normal function. The mature islets retain their assembly due to the blood flow through the dense blood vessel network in the islets [9]. The vascularized state of islets is maintained by the production of the vascular endothelial growth factor-A (VEGF-A) [2, 11].

2.1 Type 1 diabetes

The autoimmune destruction of beta cells that produce insulin in the pancreas causes type 1 diabetes (T1D). The loss of beta cells results in increase of blood glucose level in the body. It has been diagnosed that beta cells are reduced by about 70% in type 1 diabetes [12]. Type 1 diabetes accounts for about 10 % of all cases of diabetes and allthough the increase in incidence of type 2 diabetes has received most attention, a rapid increase in type 1 diabetes has been observed. Approximately 3 million Americans might have type 1 diabetes. About 15,000 children and 15,000 adults every year are diagnosed with this diabetes and accounts for $14.9 billion per year in healthcare costs in US in 2013 [16].

2.2 Diabetes type I treatment

2.2.1 Islet transplantation

One of the treatments for type 1 diabetes is the transplantation of insulin secreting beta cells either by whole pancreas transplantation or transplantation of isolated islets. Often transplantation of whole pancreas is conducted along with kidney transplantation. Hence it is performed mainly in diabetes patients having renal complications as well. Isolated islet transplantation instead of whole pancreas transplantation has relatively small risk for patients since it is technically simpler with reduced medical costs for the

procedure. Therefore islet transplantation is more favorable than whole pancreas transplantation.

However, the islet transplantation does not ensure complete insulin independence in patients. One of the reasons being that for the islet transplantation procedure a large number of islets are needed in order to achieve insulin independence and since there is shortage of donors it restricts the number of patients that can be cured [1]. The location of islet transplanted in the body is also crucial for the success of the transplantation. The Edmonton protocol has been adapted since 2000 in transplant centers worldwide. In the Edmonton protocol, cadaveric donor pancreases are used to isolate islets and about one to three donors are needed for each recipient patient. These isolated islets are injected into the recipient portal vein and the destruction of the foreign islets are avoided by use of immunosuppression drugs (Figure 2.2). This protocol still continues to get improved in terms of immunosuppressant drugs to avoid rejection of injected islets in recipient patient. Even though the Edmonton protocol has tremendously increased the success rate of islet transplantation [13], the long term islet survival is still poor giving 10% insulin independence after duration of five years [14].

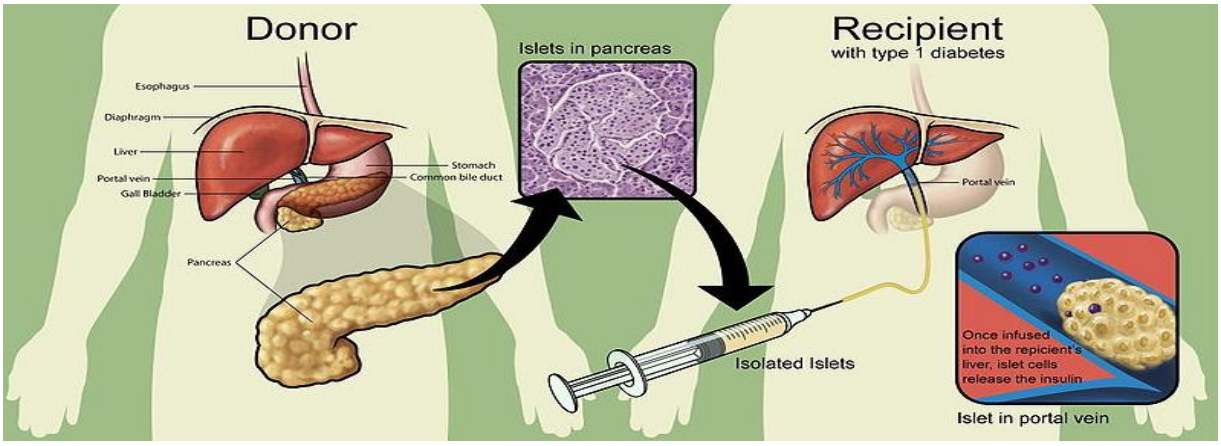

Figure 2.2 Edmonton Protocol for Islet transplantation. [17]

Another reason for not achieving long term insulin independence is due to the loss of blood vessel connections within the islet vasculature during the procedure of islet isolation. In case of whole organ transplantation, the organ reconnection is quickly reestablished with the recipient's blood vessels while for isolated islet transplantation the reestablishment of the blood vessel network within the islets takes several days for angiogenesis (new blood vessel formation from pre-existing blood vessels). After the transplantation, the islets are unable to become vascularized for several days and eventually are less vascularized [18, 19]. The inadequate amount of blood supply after transplantation might cause loss of the injected islets or might impair their function and survival. Thus, the success rate of islet transplantation might be improved by revascularizing islets prior to transplantation [1].

Previous studies have indicated that the endothelial cell required for new vessels inside the islet come from three different sources [1] (Figure 2.3). The first source of the endothelial cells is from islet transplant receiver and the second source is the intraislet endothelial cells that exist inside the isolated islets [2, 20]. The functional vessels within a revascularized transplanted islet were found to consist of endothelial cells from both the transplant receiver and donor derived intraislet endothelial cells. The third small source of endothelial cells is the bone marrow derived progenitor cells [21, 22] (Figure 2.3). The formation of new vessels also requires vascular remodeling involving the basement membrane, vascular cells such as pericytes and the extracellular matrix [1, 11].

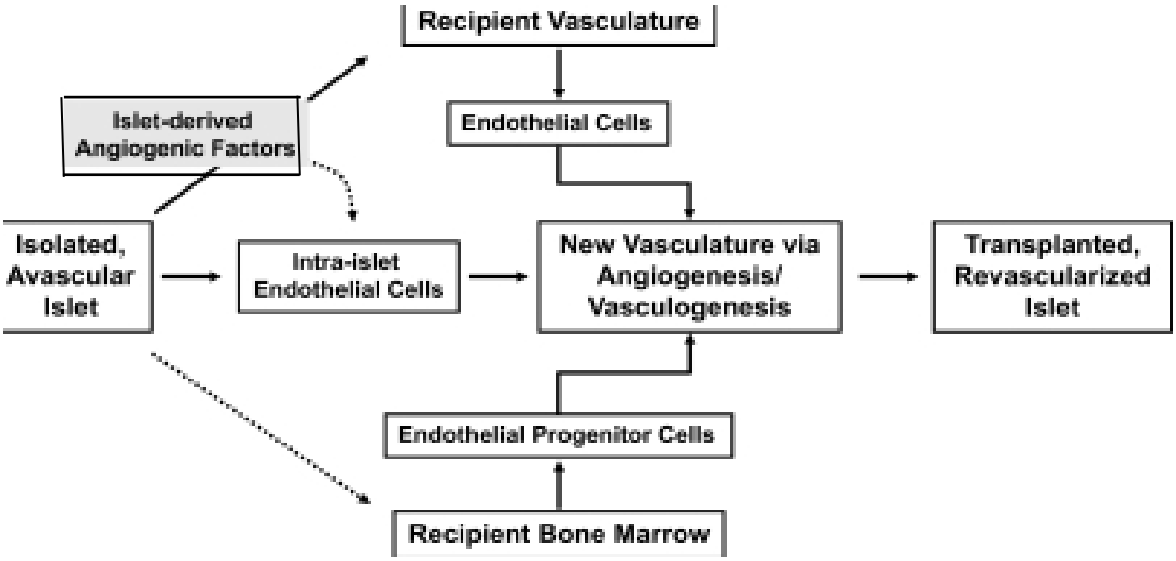

Figure 2.3 Possible key factors for islet vascularization [1].

2.2.2 Islet engraftment and revascularization

The process of engraftment of islets after implantation is possible by revascularization and reorganization of endothelial and stromal cells. A longer period prior to transplantation possibly leads to death of the intraislet endothelial cells [23, 24]. Even though studies have shown revascularization of transplanted islets occur in 7 to 14 days, there have been *in vivo* mice studies that indicate low oxygen and inadequate revascularization within a month of the transplantation [3, 21, 25, 26, 27].

One of the techniques for successful islet transplantation would be to create an *in vitro* vascular environment and implant it to accommodate to the host vascular system [3, 28, 29, 30]. In order to develop methods to build *in vitro* vasculature microenvironment, it is critical to understand the reaction of endothelial cells and islets in such an environment [31]. Since HUVECs constitutes the inner lining of blood vessels, they are considered as one of the cell types to be used for the *in vitro* culturing for possible blood vessel formation [29, 31].

Microfabrication technologies have been used in order to mimic the cellular microenvironment *in vivo* [32, 33]. Endothelial cells self-assemble into vascular tubes of capillaries when surrounded by extracellular matrix [34, 35]. The new blood vessel formation might need interaction between HUVECs and Mesenchymal Stem Cells (MSCs) to enable maturation of the in vitro vascular system [36, 37, 38]. Studies have shown that with the use of only HUVECs for in vitro vascular formation, the vascular system does not retain maturation for a long term [36]. However when the HUVECs are co implanted with MSCs, a mature vascular assembly was obtained [37]. Koike et al. [39] co-implanted HUVECs and perivascular cells in a three dimensional fibronectin-collagen gel in mice to observe that the implanted vascular system was stable for a year. However, implantation of vascular system of capillaries of HUVECs only survived for about 60 days due to the delay in recruitment of MSC's from host tissue resulting in instability of the capillaries [38, 39].

Mesenchymal Stem Cells (MSCs) derived from bone marrow have a great potential *in vitro* for culturing and differentiation. MSCs can be differentiated into other cell types such as endothelial, neuronal, skin, renal epithelial, or cardiac pacemaker cells and are used currently in tissue engineering. Still researches are being conducted to identify proper markers for undifferentiated MSCs [40 - 44]. Despite a lot of research on control of the MSC behavior such as adhesion, spreading and differentiation, there is still little knowledge on the cell-cell and cell-matrix interactions [45, 46]. One of the most significant influences of MSC behavior comes from mechanical properties of tissue or substrates used for MSC culturing and/or for *in vivo* differentiation. On a soft substrate/ tissue MSC differentiate to neurons (substrate stiffness 0.1 – 1 KPa), chondrogenic,

myogenic (8 – 17 KPa), and adipogenic lineages while on harder substrates such as bone MSC differentiate to osteoblasts (25 – 40 KPa) [47].

2.3 Techniques for in vitro islet culturing

In vitro culturing frequently relies on identified natural cues occurring *in vivo*. During the formation of the primary capillary like structures in an embryo, the angioblast differentiate into ECs and MSCs differentiate into pericytes to surround the endothelial cells in the newly forms capillary structures as seen in Figure 2.4 [48]. The pericytes regulate maturation and stabilization of the vascular network. Different approaches have been proposed and conducted as strategies to achieve successful angiogenesis from co-cultured cells in biomaterial/scaffolds such as matrigel [49, 50]. Co-implantation of human mesenchymal progenitor cells and endothelial progenitor cells induces *in vivo* vascularization of a tissue construct [51]. Melero-Martin [52] reproduced vasculogenesis in a tissue construct using Matrigel as the scaffold. Cord blood–derived endothelial progenitor cells or adult blood endothelial progenitor cells were co-implanted with either bone marrow–derived or cord blood–derived mesenchymal progenitor cells to produce a stable and mature vascular network [50].

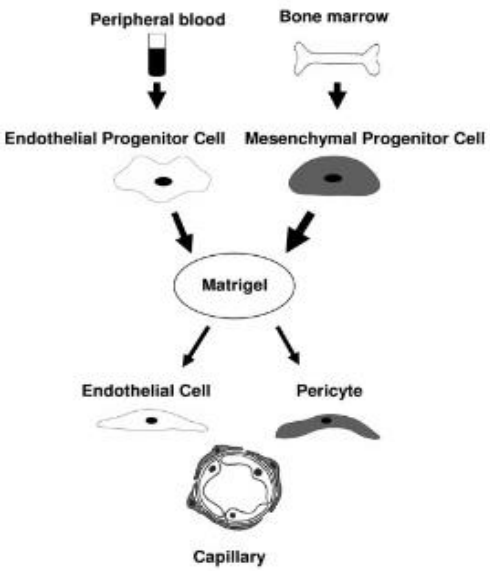

Figure 2.4 Therapeutic vasculogenesis technique [48].

There have been several approaches to enhance the revascularization of islets before transplantation such as increasing angiogenic factors to stimulate the movement of endothelial cells into the islets and its maturation into functional vessels after seeding in collagen or Matrigel suspension [34, 35] co-culturing of different cell types such as MSCs and ECs to enhance the formation of mature functional vessels was also used [53]. These techniques can be used *in vitro* cell culturing or could be implemented at the transplantation site before the isolated islet transplantation.

Johansson et al. [6] studied the *in vitro* co-culture of endothelial cells and bone marrow derived MSCs with human islets and showed the formation of vessel type structure to possibly increase the engraftment of islet post transplantation. The presence of MSC or the growth factors released by MSCs probably promotes the proliferation and migration of endothelial cells within the islets to form vessel like structures by its interaction with intra islet endothelial cells [1, 2]. With successful *in vitro* co-culture of EC, MSC and islet that results in improvement in islet viability due to pre-vascularization

of islets, the next step could be *in vivo* models to study the survival of these transplanted islets [3, 7, 49, 54]. Their data demonstrate that addition of MSCs to composite islets enhanced the capacity of ECs to enclose the islets without compromising the functionality of the islets. Importantly, the MSCs stimulated EC sprout formation not only into the surrounding matrices, but also into the islets where intra- islet capillary-like structures were formed [6]. However the *in vitro* pre vascularization had limited *in vivo* success after a month since the connection between the transplanted and the host vasculature did not take place completely [55].

Further improvement in *in vitro* revascularization of islets was achieved by using heparin for encapsulating islets before transplantation. Heparin is present in the form of a complex polymer that interacts with proteins in the body [56]. It is used for surface modification of biomaterial to increase their biocompatibility after implantation. Heparin has been used to immobilize on islets in order to increase its good blood biocompatibility, inhibit rejection and enhance its activation post transplantation. The transplantation of the heparinized islets in mice showed results of normalized blood glucose in 10 days as compared to untreated islets [56]. Their studies also showed that the heparinized islets attached to the isolated islets and in turn elevated the islet viability, the expression of insulin and sprouting of intra-islet endothelial cells. Heparin was used as a synthetic material to mimic the extra cellular microenvironment to possibly improve the outcome of islet transplantation.

2.4 Cell structure and its microenvironment

2.4.1 Cell structure

Cell is the functional basic unit of all organisms. The outer membrane of the cell also known as cell membrane or plasma membrane controls the flow of ions between the intracellular and extracellular fluid. The cell membrane has surface receptors known as integrins that play a critical role in the adhesion of cells to its microenvironment. The cell adhesion takes place by linking the cell surface receptor, α and β integrin, to the extra cellular matrix/ culturing substrate [57]. The intracellular fluid, cytoplasm, comprises of various organelles and proteins. The main cell components in cytoplasm that play an important role in cell spreading, migration and providing shape to the cell is the cytoskeleton (actin filament network) which further comprises of microfilaments, microtubules, intermediate filaments. These cell components react to signals from the extracellular microenvironment. The cytoskeleton is the internal skeleton network that transports specific protein from the cell surface to the nucleus of the cell and reacts to the forces from the extra cellular microenvironment. The extra cellular microenvironment force is sensed by mechanosensors via cytoskeleton and provides chemical signaling and corresponding cell response.

Microfilaments (Actin filaments)

The microfilaments (actin filaments) are long, thin fibers of polymers of actin. They are about 8 nm in diameter and are the thinnest of the cytoskeleton filaments (Figure 2.5) [58]. They form a network below the cell membrane to provide mechanical support to the cell. The physical connection between the actin and the microenvironment takes place through the focal adhesion complex. The actin filaments along with the focal

adhesion complex act as the mechanosensors. Actin filaments transduce the signals from the extra cellular environment to inside the cell. Actin associated motor protein uses the energy from ATP hydrolysis to form tensile forces to facilitate in the locomotion of the cells at the trailing edge [59]. The orientation and the elasticity of the actin filaments takes place by the force exerted from the microenvironment. With the increase of forces, the actin filaments become more stretched and more rigid [60]. Hence, the stiffness of the cell can be co related to the stretching of the actin filaments.

Microtubules

Microtubules are straight, hollow like cylinders that have a diameter of 25 nm and can grow in its length to about 1000 times its width. The microtubule organizing center – MTOC (small blue circle in Figure 2.5) [60] holds the " – " ends while the " + " end grows and moves towards the periphery of the cell. They are very dynamic due to its rapid cycles of polymerization and depolymerization. The microtubules form an internal transport network to move essential proteins to the cell via the motor protein. These motor proteins produce forces for the movement of lamelipodia during cell locomotion.

Intermediate filaments

The size of intermediate filaments is in between the actin filaments and the microtubules having a diameter of 10 nm. They provide the internal framework inside the cytoplasm similar to the actin filaments and also in the form of lamina within the nucleus [60]. They form a cage like structure around the nucleus. They do not play any role in cell locomotion.

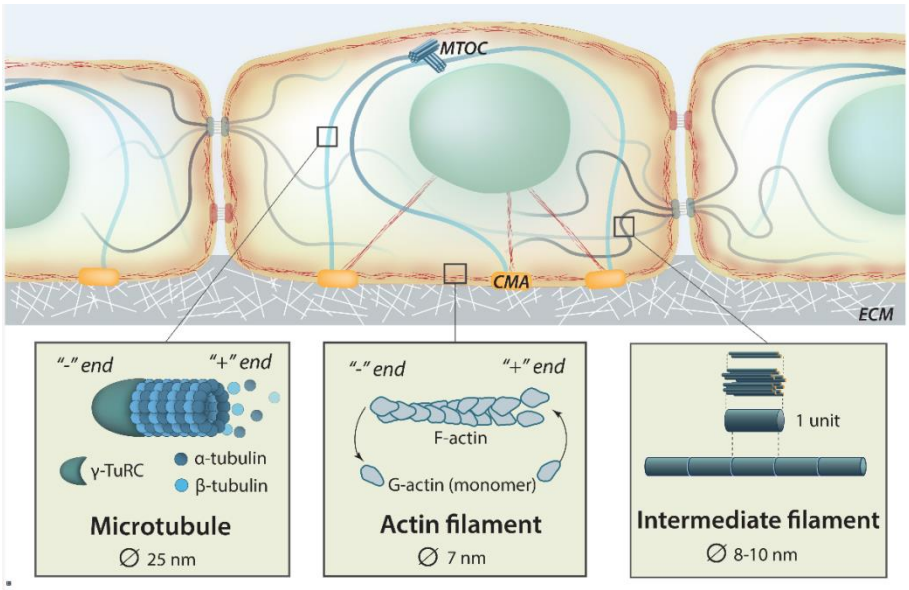

Figure 2.5 Three main components of cell cytoskeleton include actin filaments (microfilaments), microtubules and intermediate filaments. MTOC: microtubule organizing center, ECM: extra cellular matrix and CMA: cell matrix adhesion. Used by permission from MBInfo: ww.mechanobio.info; Mechanobiology Institute, National University of Singapore [60].

2.4.2 Extra cellular microenvironment

The extra cellular matrix (ECM) forms the extra cellular microenvironment as the scaffold to support the cells and provides specific proteins such as fibronectin, proteoglycan, laminin and collagen as shown in Figure 2.6 needed for cellular functions such as adhesion, migration and stretching [61].

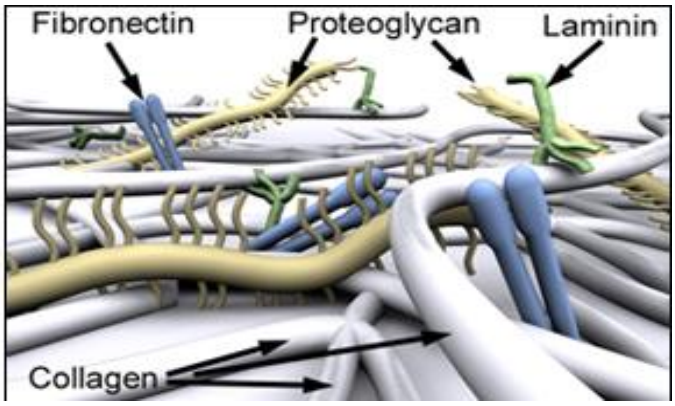

Figure 2.6 Extra Cellular Matrix (ECM) [61].

Collagen forms the major component ECM and hence is preferably used by many researchers for in vitro cell culturing. There are 28 different types of collagen fibrils. Fibronectin are proteins that connect the cells to the collagen fibers through the cell surface receptors, integrin and causes a reorganization of the cells cytoskeleton and in turn facilitates cell locomotion. The laminin is an important glycoprotein that forms independent network to influence cell adhesion, migration and differentiation. Proteoglycans are carbohydrate polymers that maintain hydration in the ECM and the cells [58]. These proteins and carbohydrates together forms the connective 3D scaffold for cell adhesion and growth.

Cell adhesion

The cell interaction with neighboring cells or underlying extracellular matrix takes place due to multi-protein adhesive structure that are specialized based on the cells functionality. The cell adhesion is contributed from the cell surface receptor, α and β integrin, to the scaffolding proteins. The complexes contributing to cell to matrix and cell to cell adhesion are known as anchoring junctions as shown in Figure 2.7 [58].

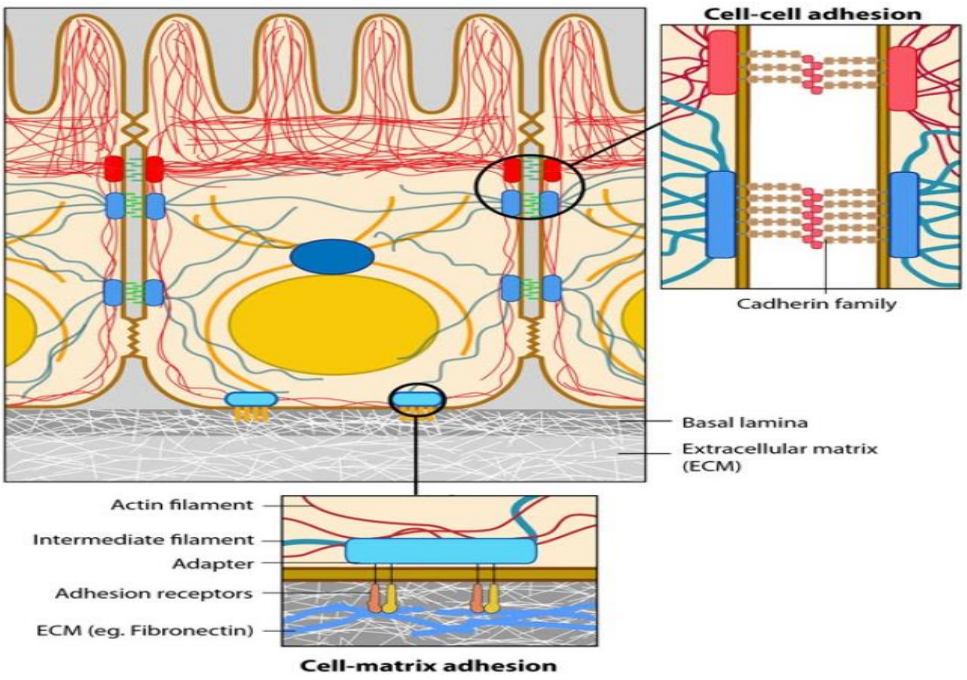

Figure 2.7 Anchoring junctions contributing to cell-matrix and cell-cell adhesion. Used by permission from MBInfo: www.mechanobio.info; Mechanobiology Institute, National University of Singapore [58].

The cell plasma membrane has cell adhesion molecules (CAMs) or cell adhesion receptor known as cadherins that form linkage with another cells and the cell matrix linkage takes place with integrin and syndecans. The adapter protein (Figure 2.7) such as catenins, talin, filamin, tensin, vinculin, and α- actinin forms a connection between the integrin and the cytoskeleton. The matrix chemical composition, topography or rigidity affects the information relayed to the intracellular region from the cell adhesion receptors [59].

Cell matrix adhesion

The integrin, that are receptor to various ECM proteins such as fibronectin, collagen, laminin and hyaluronan, first links to the ECM proteins to form focal points or also knows as focal adhesion complex. The initial cell adhesion takes place through the focal adhesion complex in response to its microenvironment. Focal adhesions (FA) act as

the communication centers between the signals from the extra cellular microenvironment to the intercellular cytoplasm [62]. At the initial interface of the cell and the substrate, the cells are rounded (Figure 2.8) [63] with surface receptor integrin getting attached to the tissue/ substrate.

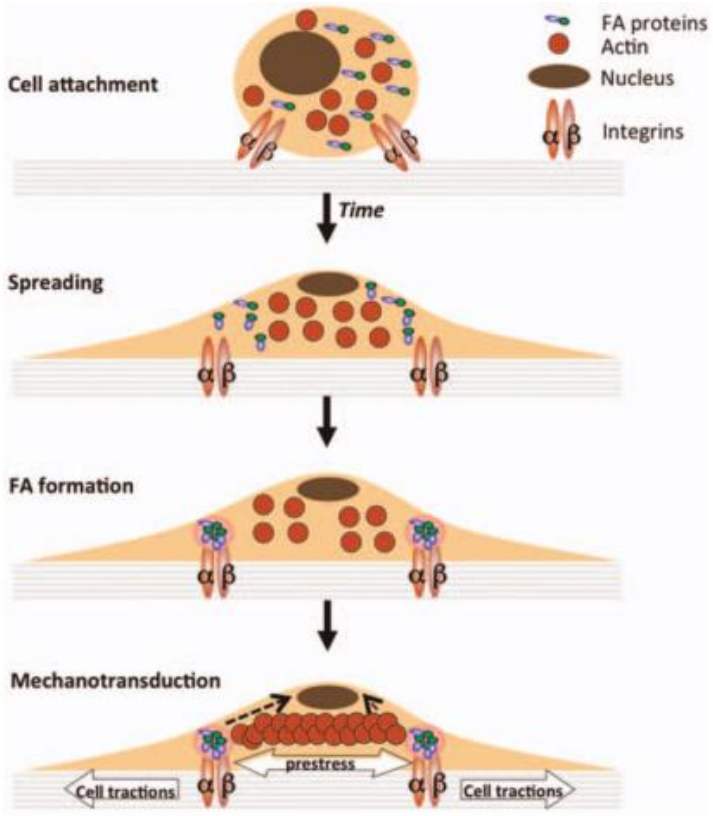

Figure 2.8 Changes in cell shape after adhesion on substrate [63].

The extra cellular matrix or the substrate used for in vitro cell culturing possesses surface properties such as chemical composition, topography, and rigidity that transduce signals from the cell's external environment to its internal organelles thus regulating the cellular function. Post attachment the cells sense the surface to spread and change the cell spread area along with their shapes. As the focal adhesions (protein such as talin, vinculin and paxillin) are formed, the cytoskeleton assembly stress fibers are formed that increases

the extent of adherence of the cells on the surface. The cells translate the shape change to molecular signals that regulate the cell function. The Rho family of GTPases, a family of proteins, plays an important role relaying transmitting signals from various stimuli outside the cell into the inside of the cell. The Rho family GTPases changes cell morphology by formation of lamellipodia, filopodia and actin filaments that further facilitates strong attachment to the ECM. [63].

Growth of endothelial cells in vitro on artificial substrates is important in our research of islet revascularization, therefore their adhesion to the substrates is of interest. The adhesion of endothelial cells on the in vitro substrates is also important in vascular implants/ devices (ex. stents) as it determine the antithrombic nature of the artificial material [64]. Cell adhesion is related to proteins adsorption from the cell culture medium on the culturing substrates and cells are attached to them [65]. In addition, cells also produce and secrete ECM proteins into its cellular microenvironment. The ECM signals and guides the attached HUVEC whether they proliferate, stretch, change shape, types of genes they have to activate or deactivate and types of proteins that they secrete on cellular surface [66, 67]. The proteases secreted by cells degrade the ECM to smaller polypeptides or constituents of amino acids. This degraded ECM further facilitates the cells to synthesize other proteins. Anderson et al. [68] observed more ECM production (collagen and laminin) from endothelial cells on micropatterned substrates than on non patterned substrates. They attributed the difference in ECM secretion to the TGF integrin signaling pathways.

Cell-cell adhesion

Cell to cell adhesion takes place by the cell adhesion molecules (CAMs) such as cadherins, Ig CAMs, and selectins between cells [59]. Cell-cell adhesion forms junction that communicates by the chemical, electrical or mechanical signals. The three different types of junctions formed are tight junctions, adherens junctions and desmosomes. The tight junctions functions as semi permeable diffusion barriers that are selctive to ions [58]. The tight junctions (Figure 2.9) guides the cell behaviour by regulating paracellular permeability to junction associated signalling mechanism [69]. The yellow arrow indicated the paracellular pathway for ion and hydrophillic solutes diffusion.

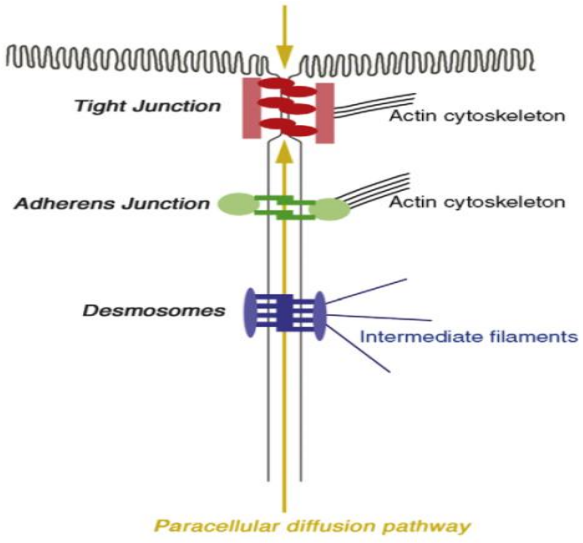

Figure 2.9 Tight junction, adherens junction and desmosomes formed between cells and its interaction with the actin cytoskeleton and intermediate filaments. The yellow arrow indicated the route for diffusion of ions and hydrophilic solutes [69].

The adherens junction, shown in Figure 2.10, controls the shape of the cell and is a kind of anchoring junction keeping cells interconnected to the neighboring cells. The red rectangles in Figure 2.10 are the adherens junctions that connect the red actin filaments.

The large blue rectangles are the desmosomes and small blue rectangles are hemi desmosomes connecting intermediate filaments of the cells to the plasma membrane. These junctions gives mechanical stability to the cells [59]..

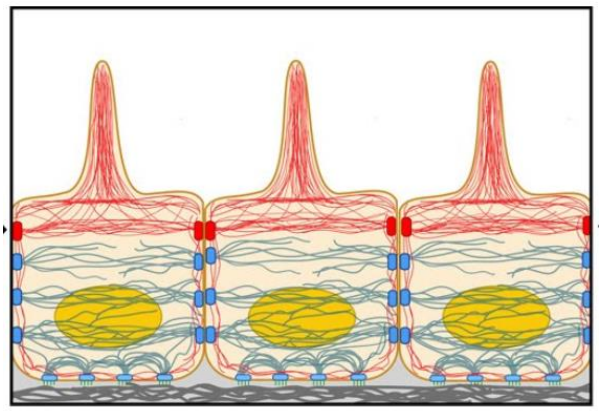

Figure 2.10 Adherens junction (red rectangle) linking the actin filaments of cells, desmosomes (big blue rectangle) and hemi desmosomes (small blue rectangle) connecting intermediate filaments. Yellow ellipse is the nucleus. Used by permission from MBInfo: www.mechanobio.info; Mechanobiology Institute, National University of Singapore [58].

2.5 Factors effecting in vitro HUVEC cell culture

Cell attachment and function on an artificial biomaterial is affected by various material properties such as surface roughness [70], pattern [71], surface chemistry [72], surface elasticity [73], surface energy [74] and surface charge [75]. Few of the factors affecting protein adsorption are shown in Figure 2.11 [76].

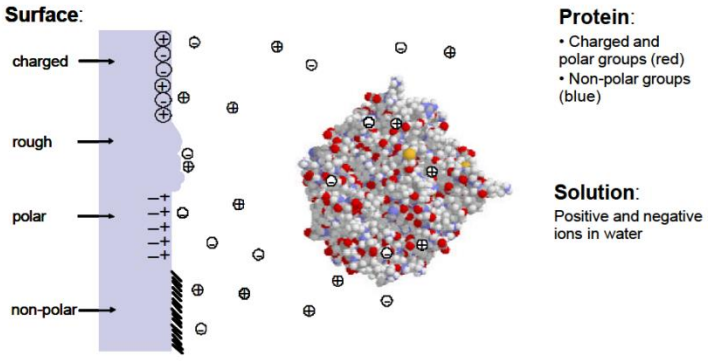

Figure 2.11: Schematic view of protein and surface [76].

Material surface possess non polar groups, polar groups, charges and roughness that affects the adsorption of ions form the solution as well as protein that have charged polar groups and non polar groups. Some of these factors will be discussed below and will be addressed in our experiments.

2.5.1 Surface roughness

The internal structure of the ECM comprises of well-defined nanoscale topographical structures. The ECM has many proteins forming large scale structures ranging from nanoscale to several microns. Interaction of the cells with ECM will be affected by nanoscale physical features such as microfilaments, intermediate filaments, microtubules and focal adhesion complexes of the cells [77]. The nanostructure and topography of the extra cellular microenvironment provides mechanical support to cells for adhesion and growth. The same cellular microenvironment that the cell experiences *in vivo* can be possibly replicated on a substrate to culture cells *in vitro* to provide them adhesion, growth and guidance [47].

Cell behavior on different rough surfaces has been contradictory in the literature. Nanoscale material surface seems to mimic the natural nano surface of the extra cellular microenvironment. Gentile et al. [78] studied the attachment and proliferation of HUVECs on electrochemically etched silicon surfaces having roughness in the range of 2 nm to 100 nm with a moderate roughness of 45 nm. The silicon (111) wafers were etched in KOH solution (KOH: H_2O=1:4 v/v) at 70 °C for different times ranging from 2 to 60 min. They showed that nanotopography increases the cell adhesion, growth and proliferation until the roughness is in the moderate nm range. Their moderate rough

substrate (R_a 40 to 50 nm) showed low contact angle 10° to 8 ° (high effective surface energy) indicating high hydrophilicity.

Chen et al. [79] fabricated titanium oxide thin film on silicon wafer with amorphous and crystalline surface by plasma immersion ion implantation and deposition. Crystalline Ti-O was formed with the presence of TiO, Ti_2O and Ti_2O_3 (specific roughness not specified) by annealing at 700 °C for 30 min at vacuum pressure of 1.2 x 10^{-2} Pa. HUVECs cultured on the crystalline surface exhibited more adhesion, growth and proliferation maintaining the natural cobblestone morphology.The surface energy of the annealed Ti-O sample is low (40 dyn/cm) with crystalline surface while the amorphous surface had a surface energy of 60 dyn/cm. The annealed crystalline surface showed better cell growth than the amorphous surface. The lower interfacial tension indicates less distortion of the protein adsorbed on its surface and better endothelial cell growth.

Chung et al. [80] cultured HUVECs on Polyurethane – polyethylene glycol-Gly-Arg-Gly-Asp PU-PEG-GRGD surface having 40 nm roughness showed better adhesion and growth as compared to PU-PEG2000 (PEG of molecular weight 2000) of 20 nm roughness. Lai et al. [70] studied the HUVEC cell growth on nanostructured surfaces of titanium alloys such as Ti-3Zr2Sn-3Mo-25Nb (TLM). They used a surface mechanical attrition treatment (SMAT) technique for nanocrystallization (~25 nm) of TLM surface in which flying steel balls of 8 mm diameter were hit on the material with high velocity and vibration frequency of 50 Hz. The SMAT treatment improved the titanium surface bioactivity by formation of TiOx oxide. The oval cell morphology and the more expression of focal adhesion protein, vinculin, on treated TLM as compared to untreated

TLM (roughness ~ 7 to 8 nm) indicated enhanced HUVEC adhesion and proliferation due to presence of nanostructures.

2.5.2 Surface rigidity

The surface chemistry of the cell microenvironment or the substrate regulates the function of the cell. It has been observed that the physical properties of the substrate also affect the cell functions. Cells respond to the stiffness of their microenvironment by altering integrin expression, focal adhesion complex formation, cytoskeleton assembly in order to establish a force balance between cell generated traction forces and the resistance provided by the environment [47, 81].

The position dependent mechanism, shown in Figure 2.12, can be used to link ECM stiffness, through integrin clustering, to cytoskeleton tension and the biochemical signal pathways by the integrin and RPTP- α (receptor-like protein tyrosine phosphate-α). The critical feature in this mechanism is the enzyme Fyn within the cell and kinase on the substrate. As seen in Figure 2.12 (b), if the surface is rigid, then the components Fyn kinase are close to each other to activate phosphorylation while if the substrate is soft (Figure 2.12 (c)), the components are separated and do not activate the phosphorylation phosphate [82].

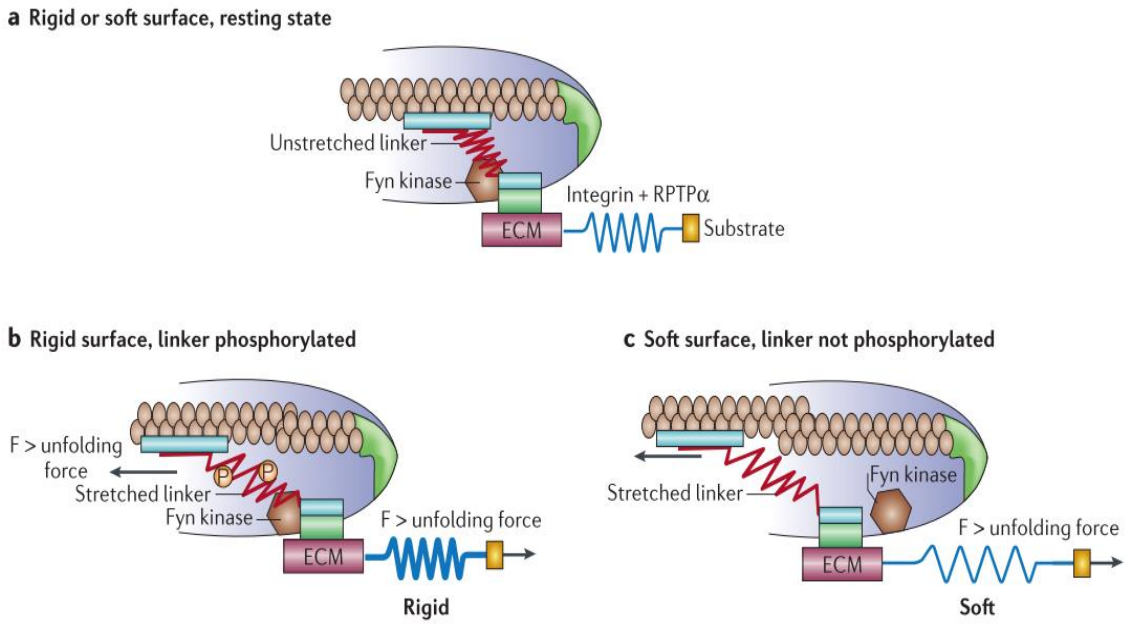

Figure 2.12 Position dependent mechanism: Cell mechanism of sensing substrate stiffness. ECM: extra cellular matrix, SFK: stretched linker fyn kinase F=X: force-displacement [82].

Mechanical properties such as stiffness of the extra cellular environment have profound effect on cell attachment and behavior. Ingber et al. [83] were the first to conclude that the cell function depends on the balance of mechanical forces from the rigidity of the adhesion substrate (biomaterial or ECM) to biochemical signals to the cells. Their tensigrity model explained the cell behavior where the various structural elements within the cell and its shape are altered by the rigidity of the substrate or extra cellular matrix. The tensigrity model describes cells composed of sticks and elastic string in order to explain the effect of substrate mechanical properties on the internal cell organelles such as cytoskeleton. It also states that the nuclei and cells are hardwired and respond based on the physical coupling between extracellular matrix and cells [84]. The cells and nucleus on a soft substrate exhibit a round morphology while the cells on rigid substrate showed cell and nucleus stretching as seen in Figure 2.13 [85].

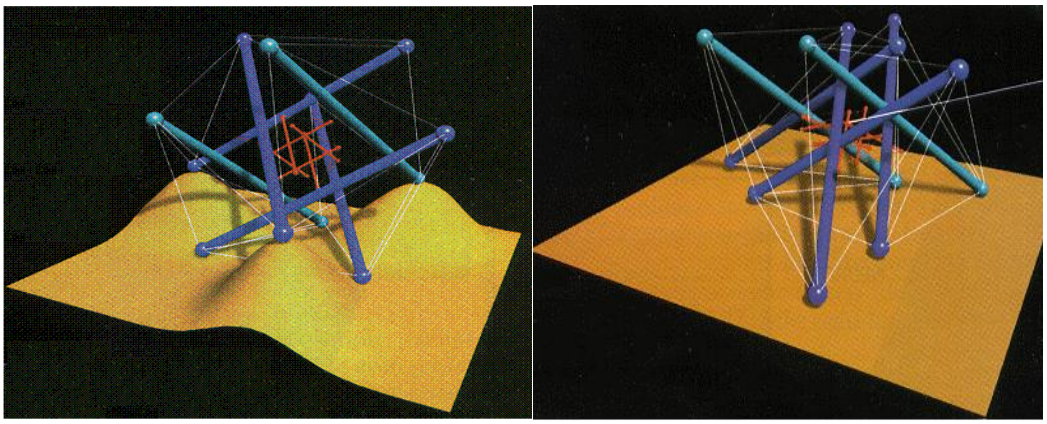

Figure 2.13 Tensigrity model. Cells placed on flexible or rigid substrate. The blue rods indicate the cytoskeleton organization while the red rods show the nucleus structure. Cells on flexible substrate have round nucleus while nucleus on rigid substrate is elongated and flattened [85].

Cells on compliant surfaces show reduced spreading and more random lamellipodial protrusions. Rigid surfaces had stable focal adhesions, cells are more strongly adhered to the surface [86, 87, 88]. A cell possesses mechanism for internal force generation through cytoskeletal polymerization and mechanism for exerting force to its microenvironment. Coupling of these two mechanisms that generate internal force from cytoskeletal polymerization and force form microenvironment to enable cell matrix adhesion and cell spreading. The development and maturation of cell material adhesions depends on exertion of forces at the adhesion site and is directly affected by surface stiffness [89, 47]. ECM *in vivo* can be replicated for *in vitro* cell culturing on substrates. This substrate possibly might have similar characteristics such as hardness and Young's modulus as that of ECM which plays an important role in the initial adhesion and subsequent growth of the cells. However many substrates such as glass have Young's modulus much larger and not all the results obtained in vitro are applicable to in vivo conditions.

Byfield et al. [73] exhibited that endothelial cells cultured on top of stiffer polyacrylamide (9000 Pa) had better cell attachment and more pronounce stress fibers as

compared to softer gel (1700 Pa). Yeung et al. [89] reported culturing of endothelial cells on fibronectin or collagen gel with stiffness from 2 to 55,000 Pa. The endothelial cells cultured on polyacrylamide gel of stiffness 1600 Pa showed less stress fibers while cells on 3200 Pa or greater had stress fibers in abundance. They observed no cell growth on surface stiffness of 1000 Pa.

2.5.3 Surface wettability

Wettability of a surface indicates the hydrophilicity and hydrophobicity of substrate material. The surface energy is the capability of surface wetting of the material and can be characterized from the contact angle of wettability. The contact angle measurement for wettability is shown in Figure 2.14 [90].

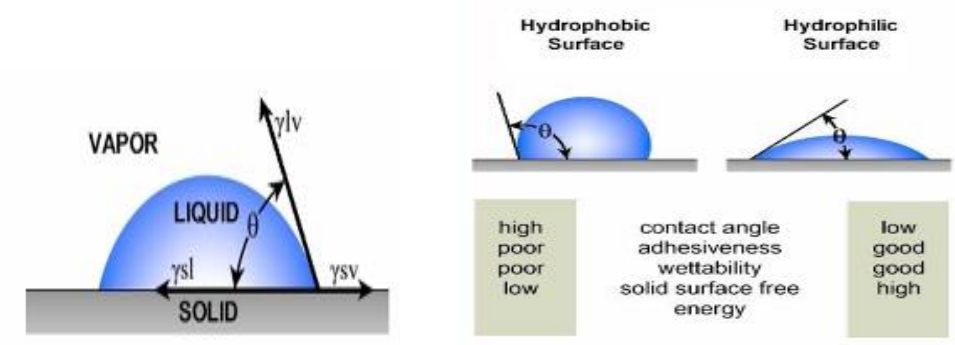

Figure 2.14 Contact angle of Hydrophilic and Hydrophobic surfaces [90].

A contact angle less than 90 ° indicates the hydrophilic nature (high surface energy) of the substrate while a contact angle greater than 90 ° shows hydrophobic surface (low surface energy). The surface free energy of the substrate-liquid (liquid drop), liquid-vapor and contact angle is used to obtain the surface energy of the substrate-vapor from the Young's equation as given below.

$$\gamma sv = \gamma lv * cos\,\theta + \gamma sl\,, \qquad \text{Equation2.1}$$

where θ is contact angle, γsv is substrate surface free energy, γlv is liquid surface energy and γsl is substrate-liquid free energy [90].

The hydrophilic substrate interface has polar interaction bonds such as ion-ion, hydrogen bonding, dipole-dipole and dipole induced dipole interaction bonds while the hydrophobic surface has non-polar interaction bonds (hydrophobic or dispersion forces). Hydrophilic surfaces have a high surface energy in air while hydrophobic surfaces have low surface energy in air [91, 92] (Figure 2.14).

Hydrophilic or hydrophobic properties of various materials depend on surface termination, which can be modified by special cleaning processes and/or functionalization. For biomaterials, the wetting properties can result in increased or decreased cell attachment depending on the type of cells [93, 94]. An example of surface modification is deposition of self-assembled monolayers (SAMs) of alkanethiols of different wettabilities, which were obtained by mixing alkanethiols with terminal methyl (CH_3), hydroxyl (OH), carboxylic (COOH) or amino (NH_2) groups. The HUVEC adhesion on these surfaces pre adsorbed with albumin were studied. Maximum number of cells adhered to the CH_3/OH mixed SAMs that had a contact angle of 40 ° and fewer cells attached to hydrophobic (109 °) CH_3 SAM surface. With increasing composition of COOH and NH_2 in CH_3 /COOH and CH_3 / NH_2, hydrophillicity decreased and the number of cells increased.

However, the cell adhesion not only depended on the surface wettability but also on the type of functional groups. Arima et al. [93] reported maximum endothelial cell adhesion for surfaces with contact angle of 35 ° to 50 ° based on surface chemistry of SAM of alkanethiols. They used four different alkanethiols for specific surface functional

group to obtain different wettability; 1-Dodecanethiol (for CH_3 functional group), 11-mercaptoundecanoic acid (for COOH functional group), 11-amino-1-undecanethiol hydrochloride (for NH_2 functional group), and 11-mercapto-1-undecanol (for OH functional group). Tzoneva et al. [95] prepared hydrophilic (~ 24 °) and hydrophobic (~ 86 °) glass coated with extra cellular matrix protein fibronectin and fibrinogen to understand the effect of surface wettability on endothelial cells. These studies indicate that a highly hydrophobic and highly hydrophilic surface do not induce good biocompatibility due to limited adherence on proteins on them and reduced cell growth. Moderate hydrophilicity or depending on surface chemistry a balance of hydrophobic and hydrophilic surfaces can provide ideal surface for biocompatibility [74].

The need for controlling the amount of adsorption of protein on the surface decides the wettability of the surface. Absolom et al. [96] studied the adsorption of four different proteins such as fibrinogen (most hydrophobic) IgG, human serum albumin (HSA), and bovine serum albumin (BSA) (most hydrophilic) on four different hydrophobic substrates; siliconized glass, Teflon, polyvinylchloride, and Nylon-6,6. On all the four surfaces the extent of protein adsorption reduces in the sequence of fibrinogen, IgG, HSA, and BSA. The greatest amount of protein adsorption took place on surfaces siliconized glass and Nylon-6,6 that were more hydrophobic than Teflon and polyvinylchloride. Wilson et al. [97] provided a review of adsorption of fibronectin and vitronectin protein present in the fetal bovine serum (FBS) on hydrophilic surfaces; hydroxyapatite, titanium and stainless steel. These proteins had enhanced adsorption on hydroxyapatite, as compared to titanium and stainless steel. Previous studies have

indicated that extreme hydrophobicity and extreme hydrophilicity resists protein adsorption and in turn results in decrease in endothelial and Hela cell adhesion [47, 98].

Other studies also reported more IgG protein adsorption on hydrophobic surfaces than on hydrophillic surfaces. Mathes et al. [99] utilized borosilicate glass with different sterilization treatments such as autoclaving and heat sterilization from 300 °C to °600 C (1 h each) and Ar plasma treated for 30 s for IgG1 protein adsorption studies. The untreated glass surface were superhydrophilic (low contact angle of 0 ° and higher surface energy of 66.3 mN/m) while the heat sterilized samples had higher contact angle of 46.4 ° (lower surface energy 50.3 mN/m). IgG1 adsorption was enhanced on glass sample sterilized up to 400 °C (contact angle of 28.2 °) while the glass substrates sterilized at 500° C (contact angle of 15.4 °) and higher temperatures had less protein adsorption. The heat sterilized surfaces were hydrophilic. The hydrophilicity increased with increasing heat sterilization temperatures. They correlated the protein adsorption to the polar component of surface energy also known as surface polarity (hydrophobic surface). The increase in surface polarity (hydrophobic surface) caused more IgG1 protein adsorption due to the attractive forces between IgG1 molecules with net positive charge and the glass being negatively charged.

Marsh et al. [100] showed hydrophobic silicon surface had more globular protein β-lactoglobulin adsorption than hydrophilic silicon surface. This protein has a net negative charge at pH 7. The silicon surface had a native oxide layer with Si-OH functional group formed on contact with water rendering the silicon surface hydrophilic characteristics. For obtaining hydrophobic surfaces, the hydrophilic surfaces were grafted with octadeyltrichirosilane (OTS). The charge of the hydrophilic surface is the same as

that of the protein molecule at pH 7 causing electrostatic barrier to protein adsorption and has less protein adsorption while the hydrophobic surface with no charged groups had more protein adsorption.

2.5.4 Surface charge

Surface charge plays an equally important role in the cell adhesion on a material surface. Wittmer et al. [75] examined multilayer assembly of two polymer, poly(L-lysine) (PLL) and dextran sulfate (DS) for HUVEC cell attachment and growth. PLL terminated film was positively charged while DS terminated surface was negatively charged. PLL terminated surface showed more fibronectin adsorption and better HUVEC attachment and growth as compared to DS terminated surface. Fields et al. [101] conducted electrostatic endothelial cell seeding on e-PTFE vascular grafts using static pool apparatus, a voltage source, and a parallel plate capacitor. These grafts were then implanted in canine femoral artery for 6 weeks. The presence of electrostatically seeded endothelial cells reduced the occurrence of thrombosis.

Macdonald et al. [102] studied the fibronectin protein adsorption on thermally treated titanium oxide surface at 800 °C for 1 h , peroxide chemically treated titanium oxide surface, and titanium oxide surface (control). A batch of these annealed and chemically treated samples was further treated with butanol. The chemically treated or annealed surfaces had more negative zeta potential and more hydrophilic nature as compared to the control titanium oxide surface. Butanol treated (along with thermally or chemically treated) titanium oxide sample had hydrophobic surface with a negative zeta potential and better protein adsorption than the other treated surfaces. All the treated samples had negative surface charge but difference in wettability caused difference in

protein adsorption. The chemical composition of all the surfaces showed similar level of oxygen species, however, the peroxide treated substrates showed more basic hydroxyl group on its surface.

2.5.5 Surface chemistry

The adhesion of mammalian cells requires the presence of surface immobilized protein to bind to the cell surface receptors, integrin. The surface chemistry of the substrate can be altered by patterning layers of adhesive molecules on it such that the shape of the cells will be as per the dimensions of the adhesive pattern. SAMs can be used to pattern layer of adhesive or non adhesive features on the substrate. SAMs are used having different functional groups such as methyl (-CH3), hydroxyl (-OH), amino (-NH2) and carboxyl (-COOH) that possibly modulates the cell focal adhesion on the surface. Hydroxyl and methyl groups had hydrophilic and hydrophobic properties respectively while the carboxyl and amino groups had positively and negatively charged surfaces respectively [72]. The differing responses of cell lines to differing surface chemistry is thought to be due to the changes induced on the pre-adsorbed protein layer which mediates cell attachment.

2.5.6 Surface functionalization

Liu et al. [103] multifunctionalized titanium surfaces with Arg-Glu-Asp-Val (REDV) peptide-conjugated poly (poly(ethylene glycol) mono-methacrylate) P(PEGMA) to improve the endothelial cell adhesion and growth as compared to EC adhesion on pristine Ti surfaces. REDV is a peptide sequence that had been used due to ECs enhanced growth on them. REDV functionalized titanium surfaces formed a better

endothelialization and confluent monolayer as compared to the unmodified titanium surface.

2.5.7 Surface pattern

The substrate design/ pattern affect the behavior of cells *in vitro* by providing contact guidance. The restricted design provides contact guidance to the cells for growth and orientation. Micropatterning can provide information about the cell function of cytoskeleton and cell morphology on square (10 to 50 µm) and line patterns (width of 10 to 30 µm) fibronectin [71]. Various lithographic techniques are used such as soft lithography, photochemistry, inkjet printing, laser bioprinting and micro scale direct printing for micropatterning. The morphology of the cells and their alignment depended on the pattern size and shape. Moon et al. [104] patterned Arg-Gly-Asp-Ser (RGDS) of different line widths of 50 and 200 µm. The HUEVCs grew specifically on the line patterns and not on the non adhesive PEGDA surface. They observed the cell morphology, viability and alignment for 18 days in culture. Lele et al. [105] studied the cell morphology and stretching on fibronectin coated micropatterned squares of length 5 µm, 10 µm, 20 µm, 30 µm, 40 µm and 50 µm. These adhesive islands kept the cells confined only on the square islands. The 5 µm is too small area for a cell to adhere to it while 10 square had cells rounded on it. The 30 µm to 40 µm squares provided good amount of surface for adherence and stretching.

2.5.8 Cleaning & sterilization

Cleaning and sterilization method should be compatible with biomaterial. Kotzar et al. [106] studied the effect of cell growth on titanium with two different sterilization processes; one method was 2 x gamma irradiation of 2.5 Mrad per exposure and the other

method was autoclaving 2 cycles for 25 min/ 10 min dry at 121 °C. The surface properties of biomaterial are influenced by surface cleaning and the surface contaminations that remain on the surface and can have both organic and inorganic components [107]. The titanium surface on exposure to atmosphere always has a native oxide layer formed on its surface. Inorganic and organic contaminant molecules present on the surface of biomaterials are removed by cleaning and sterilization to facilitate better biocompatibility.

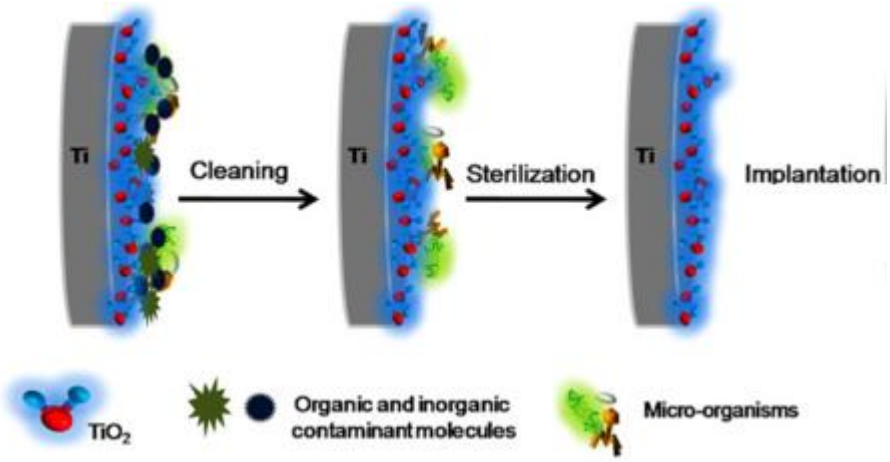

Figure 2.15 Titanium surface cleaning and sterilization [108].

2.5.9 Synergistic surface material properties

In most of the cell culturing studies more than one factor facilitates its adhesion and growth on biomaterial surface. Synergistic effect of surface roughness, chemistry, wettability, hardness and charges has been observed to play an important role in the attachment of cell on the material.

As seen in Figure 2.16 and 2.17, surface roughness increases the wettability of the material surface and conditions the protein adsorption on them. The relationship of roughness and wettability was described by Wenzel [109] and they reported increase in wettability due to increased roughness, for originally hydrophilic surface. The micro

scale roughness as well as nano scale rough effects the surface wettability of material. Wenzel effect can be given as the equation below

$$cos\ \theta m = \mathrm{r} * \cos \theta \mathrm{y}, \qquad \text{Equation 2.2}$$

where θm is measured contact angle, θy is Young contact angle and r is the roughness ratio. r=1 for smooth surface and r > 1 for rough surface [109].

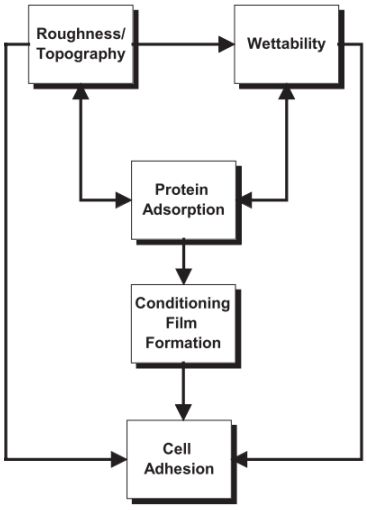

Figure 2.16 Synergistic effect of roughness and wettability on protein adsorption and cell adhesion [110].

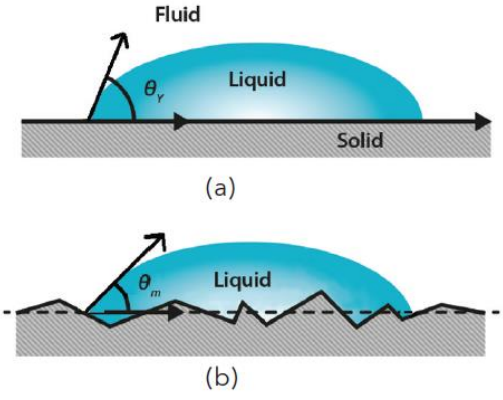

Figure 2.17 Wettability effected by surface roughness [109].

Synergistic behavior of surface material is affects the HUVEC culturing. An et al. [111] studied the response of four different titanium surfaces having different roughness and hydrophilicity on the HUVEC culturing. The substrates were acid etched hydrophobic surface (A), coarse-grit blasted and acid etched hydrophobic surface (SLA), acid etched hydrophilic surface (ModA) and coarse-grit blasted and acid etched hydrophilic surface (ModSLA). The acid etched substrates were smoother than the coarse-grit-blasted substrates. The wettability of the surfaces was modified to acquire hydrophilic surface by submersion of the surface in isotonic solution in N_2 protection [112]. Better HUVEC proliferation was observed on ModA (smooth hydrophilic) >SLA (rough hydrophobic) >A (smooth hydrophobic) >ModSLA (rough hydrophilic) with ModA showing HUVEC proliferation similar to the polystyrene plastic control group. The HUVEC showed better proliferation and viability on the smooth hydrophilic surfaces and least on rough hydrophilic surfaces. Their rough surface might have possibly inhibited the intercellular contact and activity of the HUVEC. The greater cell proliferation on hydrophilic surfaces was explained to be due to increased fibronectin protein adsorption.

The effects of surface topography, electric charge, chemistry, hydrophilicity and isoelectric points of protein have an important influence on adsorption of albumin and fibrinogen. The isoelectric point of titanium, fibrinogen and albumin are 6.0, 5.5 and 5.0 respectively and are negatively charged at physiological pH. Lower isoelectric point of albumin than fibrinogen causes larger charge repulsion and less protein adsorption of albumin on titanium. Cai et al. [113] reported that the molecular size of the protein might give different adsorption sites. Fibrinogen had length 46 nm while albumin has length of

14 nm. They also performed albumin and fibrinogen adsorption on titanium surfaces with roughness varied from 2 nm to 21nm. They reported no statistical difference in their protein adsorption measured by bicinchoninic acid assay. Klinger et al. [114] studied the mechanism of albumin adsorption on titanium surface. They conducted experiments on calcium or magnesium ion treated titanium surface and titanium surface as control substrate. Both the surfaces exhibited albumin adsorption but the pre-treated surfaces showed better albumin adsorption. The presence of calcium and magnesium ions in the culture medium facilitated the adsorption of negatively charged albumin on the negatively charge titanium oxide surface at neutral pH. Sommerfeld et al. [115] studied the interaction of human plasma fibronection on nano-scaled and rippled titanium dioxide and silicon surfaces. The short wavelength rippled titanium dioxide surface provided decreased protein adsorption as compared to long wavelength rippled titanium dioxide surface mainly due to surface curvature.

2.6 Desired surface properties of artificial biomaterials

Artificial materials are increasingly being used for construction of prosthetic devices and biomedical applications. As discussed before, cells can sense the physical properties and chemical composition of these materials and regulate their behavior accordingly. For surface modification of the blood-contacting biomaterials, the seeding of HUVEC is believed to serve best based upon their unique biocompatibility and bioactivity. To enhance HUVEC adhesion, survival, and proliferation on the artificial biomaterial, attempts have been made mainly to optimize the cell-biomaterial interface. For example, the positively charged surface modification can largely enhance the HUVEC adhesion, and the elevated surface hydrophilicity directly affects the growth

morphology of HUVEC, leading to a better spreading condition [116]. The most successful strategy from various studies is the surface immobilization of cell growth-promoting factors, through which the chemical environment on the material interface can be adjusted and the protein components of the *in vivo* extracellular matrices can be imitated. The most important bioactive ECM proteins used include fibronectin (Fn), laminin, and collagen [72].

Cell adhesion, differentiation, migration and function of the material protein interaction may be controlled by mechanical properties such as stiffness, wettability, elemental surface composition, topography and surface charge of the material. The surface phenomena possibly results in the formation of a positively charged biomaterial interface due to layer of adsorbed protein or serum from the culture media. The observed positive charge of the protein adsorbed biomaterial surface facilitates HUVEC attachment since its cell membrane is negatively charged [117].

It is very critical that along with the desired physical and chemical properties of the material, the material should be biocompatible. *In vivo*, the biocompatibility of a material is decided based on its inflammatory and healing reactions while *in vitro* the interaction of cells with the material are studied [87, 94, 118, 119, 120, 121]. Hence, the biocompatibility of a material closely depends on the adhesion and the sequence of events following adhesion [53, 55]. Few applications also require the biodegradability of the material which is possible by forming the material in porous formation.

Chapter 3: Literature review of specific biomaterials

There has been progress in the development of biomaterials for various applications such as dental [122], orthopedic [123], stent [124], and cardiovascular applications [125, 126]. These biomedical applications require the use of biomaterials with optimal surface characteristics. Biocompatibility of a material in body fluid or cell culture medium is affected by factors such as surface chemistry, surface topography, shape and pattern. Some of the artificial biomaterials are discussed below.

3.1 Metallic biomaterials

Metals having superior mechanical properties, corrosion resistance and biocompatibility have been used in biomedical applications. Metallic alloys are developed to obtain desirable mechanical properties of biomaterials based on the application. Alloys are made with metals and two or more elements. The mechanical properties to be considered for biomedical application for implantation/prosthetics are wear resistance, hardness, and elastic modulus. Biological properties of metals are corrosion resistance and biocompatibility. Corrosion resistance and biodegradability are correlated to each other. Modification of some properties can be obtained by surface cleaning, patterning, and functionalization. The physiological environment of neutral pH at 37 °C with electrolytes, dissolved oxygen, proteins and cells is used to test the corrosion of metallic alloys. The corrosion is an electrochemical reaction that causes release of metal ions from the biomaterial alloy such as release of Al and V from titanium alloy Ti-6Al-4V in simulated buffer solution. For a biomaterial in neutral pH environment, the corrosion rate will be so low that it would be experimentally difficult to measure [127]. The surface properties should be varied depending on the requirement of

the biomedical application. Orthopedic implants needs a stable integration of biomaterial with bone, corrosion and wear resistant, Young's modulus value close to bones. Stents need biomaterials with no reaction with blood contact, corrosion and wear resistant [128].

Surgical implants are most commonly made of metals and its alloys. Titanium and its alloy have been successfully used for implants due to its biocompatibility [128, 129]. Titanium and its alloys are used for hip, knee joint replacements, dental implants, cardiac and cardiovascular applications due to its properties such as wear and corrosion resistance. They have been incorporated in prosthetic heart valves, artificial hearts and, pacemaker casings. However, to increase the wear resistance or the hardness of titanium, various techniques such as furnace processes and glow discharge are used [119].

Titanium based alloys are classified as α type (HCP: hexagonal-closed packed crystalline structure), α + β type and β type (BCC: body centered cubic crystalline structure). Adding elements such as Al, Sn, Ga, Zr into titanium provides slight change at transformation temperature from HCC (α) to BCC (β) while heating and BCC to HCP while cooling. These elements are called α stabilizers and have good high temperature performance and β stabilizers reduce the phase transformation temperature [128]. Other elements such as V, Mo, Nb, Ta and Cr are β stabilizers. Ti-6AL-4V is a α + β alloy with 6 wt% of Al and 4 wt% of V and is used widely but studies have reported possible effect of vanadium degradation when implanted in body as hip joints [130]. Alternative titanium alloys are being developed based on the desirable mechanical, wear resistance and corrosion resistance properties for biomedical application. Titanium has affinity to oxygen and oxidation occurs even at room temperature. Studies have indicated the presence of an inert passive stable titanium oxide layer in amorphous form over titanium

surface. Native oxide layer on titanium alloys typically comprises of mixture of titanium dioxide and sub oxides depending on the composition of titanium alloy but TiO_2 is the mainly dominant [128, 118]. This oxide layer gives good corrosion and wears resistance.

Titanium alloys are being used in the biomedical field for several implants due to its biocompatibility, stiffness and strength [129]. Rough surfaces of titanium and its alloys have been observed to enhance bone deposition apatite for bone implants. In order to follow up with new requirements of light alloys with moderate stiffness, hardness, reduced friction and good stability in physiological media, the one variant is to incorporate boron as a stiffener and strengthener. The presence of boron in the titanium has been reported in previous studies to increase the elastic modulus of the TiB_2 material [131, 132]. Increase in boron concentration in titanium had led to super hardness of the TiB_2 material [133, 134]. Oshida et al. [128] found that the addition of boron in titanium enhanced the alloys stiffness.

A great number of favorable properties take place due to the formation of native surface oxide of few nanometers on the titanium biomaterial exposure to air giving a hydrophilic surface. Few organic species such as hydrocarbons, alkoxides and carboxylates might be present on the titanium surface due to cleanliness, duration of air exposure and air quality of storage atmosphere as seen in Figure 3.1 [135].

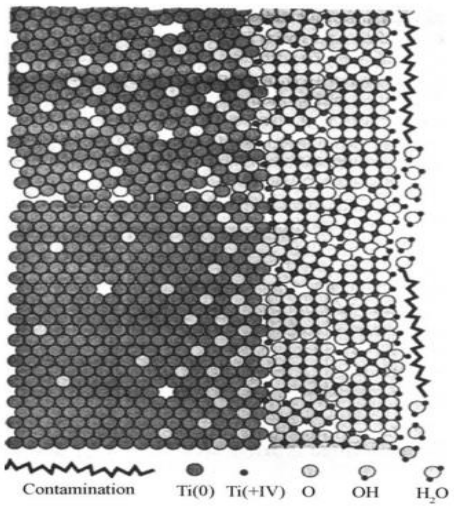

Figure 3.1 Oxide film on pure titanium surface [135].

The hydrolysis equation of titanium in an aqueous solution is expressed as [135]

$$Ti - OH + H2O \leftrightarrow [Ti\text{-}O] + H3O+ \text{ and} \qquad \text{Equation 3.1}$$

$$Ti - OH + H2O \leftrightarrow [Ti\text{-}OH2] + OH-. \qquad \text{Equation 3.2}$$

where equation 3.1 shows formation of a negative surface charge while the equation 3.2 provides a positive surface charge. The titanium surface oxide is mentioned to have both acidic and basic type hydroxide. In neutral pH deionized water, a negative surface charge is formed on titanium oxide since a fractional amount of the acidic hydroxides gets deprotonated and the remaining basic and acidic hydroxide stays in neutral group. The titanium surface charge becomes more negative with increase in pH when placed in a basic solution.

3.2 Surface modification of titanium and its alloys

Appropriate surface treatments of titanium and its alloys increase its use as biomaterials for *in vitro* and *in vivo* applications [129, 136]. The material plays a very critical role when implanted and brought in close proximity of biological environment.

The surface modification method retains the excellent bulk properties of titanium and its alloys and additionally improves the surface material to obtain desirable properties for specific implantation. The surface modification techniques such as sand blasting, chemical etching and plasma spraying are used to increase the titanium implant capabilities for dental applications. The material characteristics that provides adhesion site to cell on the biomaterial are surface roughness, surface topography, surface composition, surface energy (hydrophilicity or hydrophobicity), surface charge, surface hardness and its Young's modulus. Surface modification of biomaterials allows to maintain it's excellent bulk properties along with appropriate surface properties needed for different biomedical application. Biomaterials used as implants for dental and orthopedic applications are surface modified to accommodate good corrosion resistance and optimal biological response.

Titanium alloys were developed to fulfill the need of biomaterials with enhanced biocompatibility and elastic modulus. Addition of Cu to titanium caused an increase in the elastic modulus of Ti-Cu alloy as compared to titanium. The copper acted as a moderate stiffener in the alloy giving precipitation of intermetallic compounds of Ti_2Cu [128]. Ti-Mo alloys had increased corrosion resistance to be used for orthopedic applications.

3.2.1 Mechanical methods

Mechanical methods such as machining, grinding, polishing and blasting modify the surface topography, clean or remove the surface material. These methods cause increase surface roughness with increase in surface area on the material based on the method used thus exhibiting different behavior of cells or biological environment on

them. Most of the orthopedic applications need sandblasting surface treatment. Blasting is used for cleaning off the oxide layer and producing specific roughness by bombarding the surface with high velocity hard particles. Grinding and polishing uses hard abrasive medium such as SiC, alumina and diamond to obtain the desired roughness [137]. Annealing is a heat treatment performed to change the surface morphology of biomaterials. Amorphous titanium oxide when heat treated between 300 to 600 °C gets transformed to anatase content and lesser change on surface roughness. A further increase of heating above 700 °C leads to complete transformation to rutile content with a rougher crystalline surface [129].

3.2.2 Chemical methods

Some of the chemical methods of titanium modification include chemical treatment, anodic oxidation, chemical vapor deposition and biochemical methods [128]. Puippe et al. [138] used electrochemical and chemical surface treatments such as passivation, alkaline anodizing and eletropolishing to form thin or thick titanium oxide passivation layer. Their surface treatments modified the surface topography and also the surface chemical composition. The passivation treatment of titanium formed a stable thin (2 – 6 nm) oxide layer that enhanced wear resistance without causing any modification of titanium surface topography.

The common chemical treatments of titanium and its alloys are done in acid, alkali and hydrogen peroxide. Surface passivation techniques are also performed to obtain a passivating layer on the alloy by chemical reaction [129]. Acid treatment generally removes the contamination and cleans the material surface. 10-30 vol % of HNO_3 and 1-3 vol % of HF in deionized water is the standardized solution used for

cleaning titanium surfaces. The hydrofluoric acid (HF) reacts with TiO_2 to form titanium fluoride and hydrogen on the surface. These acid treatments change the surface chemical composition that further can facilitate its application as implants. The reaction of titanium with hydrogen peroxide results in the formation of amorphous titania on the titanium surface. Another method to form titania gel on the surface in porous form is done by a chemical reaction between titanium and H_2O_2/ 0.1 M HCl solution. Titania gel thickness depends on the chemical reaction duration. Subsequent heating of this gel causes transformation of anatase phase (below 600 °C) and to rutile phase (above 600 °C) where anatase and rutile phase are the two mineral forms of titanium dioxide. The anatase phase is recorded to have better bio activity as compared to rutile phase. Takeuchi et al. [139] conducted acid surface treatment of titanium implants with 5 % $Na_2S_2O_8$ for 30 min, 10N H_2SO_4 for 30 min and 10 N HCl for 30 min. These surface treatments removed the surface contamination from titanium. The HCl etched treatment provided the best decontamination of titanium surface. Young's modulus measured was also not altered by the different acid treatment on titanium.

The alkaline anodization formed thick oxide layer (30 – 300 nm) along with modification of surface roughness. Anodic oxidation is electrochemical method of formation of oxide layer on the anode (titanium surface) using electrolytes such as H_2SO_4, H_3PO_4, acetic acid, and others [129, 136]. The chemical properties of oxide largely depend on the anode electrode potential, composition of electrolyte, current, and temperature.

The biochemical method is performed by a biochemical reaction between titanium surface and the solution. Alkaline treatment also forms a porous surface on titanium

material. The titanium is immersed in 5 -10 M NaOH or KOH for 1 day and rinsed with distilled water leads to formation of sodium titanate porous hydrogel on titanium. Subsequent heating of this layer at 800 °C for 1 h results in anatase and rutile precipitation on the surface. This surface also increases the bioactivity of the material.

3.2.3 Physical methods.

In physical methods such as thermal and physical vapor deposition, the surface modified layer is formed on titanium and its alloys by using processes relying on various energy sources such as kinetic, thermal and electrical energy. Flame spraying and plasma spraying are two types of thermal spraying techniques depending used for deposition of melted material on the metal surface [129]. The material to be deposited is heated and melted by thermal, flame or plasma method to form liquid droplets and are accelerated to the titanium surface for adhesion and condensation on it. The characteristics of the coating material depend on the accelerating method and the surrounding chamber atmosphere. Titanium with bioinert ceramic coating such as Al_2O_3, ZrO_2 and TiO_2 deposited by plasma spraying are used as implants in orthopedics. Another implant used for strong connection with bone tissue is titanium with plasma sprayed coating of hydroxyapatite (HA) [238].

3.2.4 Glow discharge plasma treatment

Plasma processes are frequently used for removing organic contaminants (if O_2 gas is used), chemical etching and/ or sputtering assisted etching [142]. Therefore this treatment could be used for surface cleaning and also surface processing. The surface exposed to ion bombarded in plasma (sputtering or reactive ion etching) can also lead to roughness and damage formation at the surface. Plasma treatment of titanium in Ar and

O_2 were used for removing native oxide layer, contaminants, and oxides (both native layer and thick film). Presence of O_2 also causes reoxidation of the material due to strong affinity of Ti to oxygen.

3.2.5 Ion implantation and deposition

Ion implantation is a process where ion beam obtained from an ion source are accelerated and bombarded on substrate surface at energy required for penetration into titanium or its alloy to produce surface modification [143]. This provides the surface with possible impurity construction and distribution of particular specificity. In plasma immersion ion deposition, the beam scans the surface to ensure uniform coating. This deposition process can be used as a convenient method for depositing various thin films.

Few surface modifications of titanium and its alloys have been tabulated in Table 3.1. This table provides a summary of the surface modification techniques, the modified layer formed and objective of the surface modification based on the biomaterials application.

Table 3.1 Overview of surface modification methods for titanium and its alloys implants [129].

Surface modification methods	Modified layer	Objective
Mechanical methods		
Machining Grinding Polishing Blasting	Rough or smooth surface formed	Produce specific surface topographies; clean and roughen surface; improve adhesion in bonding to bones
Chemical methods		
Acidic treatment	< 10 nm of surface oxide layer	Remove oxide scales and

Table 3.1 Continued		
		contamination
Alkaline treatment	~ 1 μm of sodium titanate gel	Improve biocompatibility, bioactivity or bone conductivity
Hydrogen peroxide treatment	~ 5nm of dense inner oxide and porous outer layer	Improve biocompatibility, bioactivity or bone conductivity
Anodic oxidation	~ 10 nm to 40 μm of TiO_2 layer, adsorption and incorporation of electrolyte anions	Produce specific surface topographies; improved corrosion resistance; improve biocompatibility, bioactivity or bone conductivity
Chemical vapor deposition	~ 1 μm of TiN, TiC, TiCN, diamond and diamond like carbon thin film	Improve wear resistance, corrosion resistance and blood compatibility
Biochemical methods	Modification through silanized titania, photochemistry, self-assembled monolayers, protein-resistance, etc.	Induce specific cell and tissue response by means of surface immobilized peptides, proteins, or growth factors
Physical methods		
Thermal spray Flame spray Plasma spray	~ 30 to ~200 μm of coatings, such as Hydroxyapatite, titanium oxide.	Improve wear resistance, corrosion resistance and biological properties.
Ion Implantation and deposition	Thin layer deposition to modify surface layer.	Modify the surface to get distribution of specificity.
Beam-line ion implantation	~ 10 nm of surface modified layer	Modify surface composition;

Table 3.1 Continued		
Plasma Immersion Ion Implantation (PIII)	and/ or ~ μm of thin film	improve wear, corrosion resistance and biocompatibility
Glow discharge plasma treatment	~ 1 nm to ~100nm of surface modified layer	Clean, sterilize, oxide, nitride surface; remove native oxide layer

3.3 Material characterization techniques

Since substrate material properties have such as important influence on cell attachment, growth, and behavior, both the surface and bulk characterization of the biomaterials should be conducted. To qualify the material for bio-application, surface analyses can be performed that will identify the surface chemical composition, termination and roughness. Surface analyses of biomaterial was done by methods such as X-ray photoelectron spectroscopy (XPS) and Atomic force microscopy (AFM). In addition, complementary techniques such as Transmission electron microscopy (TEM) can be used to observe bulk and surface regions of the substrates used.

3.3.1 X-ray photoelectron spectroscopy (XPS)

X-ray photoelectron spectroscopy provides surface analysis of chemical elements and its electronic state. Photo ionization caused by x-rays provide the chemical composition information based on relation given below

$$KE = h\upsilon - BE\ , \qquad \text{Equation3.3}$$

where h is Planks constant (6.62 x 10-^{34} J.s), υ is frequency (Hz) of radiation, KE is the kinetic energy and BE is the binding energy.

The binding energy of the electron is the difference between the ionized and the neutral atoms. Each surface element has a signature characteristic binding energy depending on the core atomic orbital and the set of peaks provides molecular bonding of the elements. The intensity of the peaks indicates the concentration of the element.

In the XPS of titanium dioxide, the presence of only Ti^{4+} valence state for unannealed sample while the presence of annealed sample in oxygen background (900 – 1200 °K) with Ti^{3+} and Ti^{2+} states due to partial reduction are shown in Figure 3.2 [141].

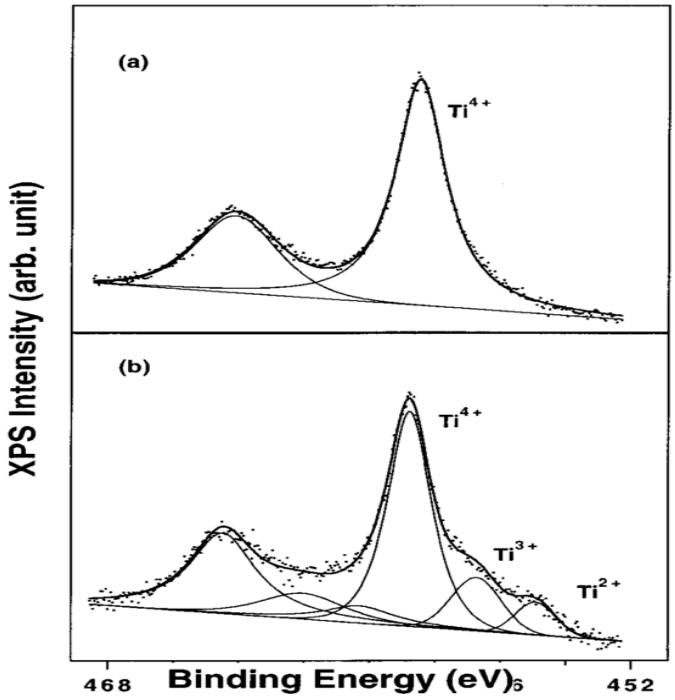

Figure 3.2 Ti 2p XPS spectra for 15A° TiO2/ MO. (a) As prepared at 600K (b) annealed to 1200 K in the oxygen ambient. Curve fitting utilized a non linear least squares routine using mixed Gaussian Lorentzian peak shape and a linear base line [141].

The surface exhibits presence of Ti and O as the main elements with. Ti_{2p} peaks are divided into two levels by electronic spin-orbit coupling. The main charge state of titanium recorded in XPS spectra corresponds to titanium dioxide. Ti suboxides are recorded at smaller concentrations.

3.3.2 Transmission electron microscopy (TEM)

Transmission electron microscopy (TEM) is a method to obtain the structural information of thin layers by transmitting a beam of electrons through the layer. The sample to be imaged is prepared by focused ion milling that thins the sample thickness. The thinning is needed in order to obtain electron transparent region of the sample. These electrons interact with the layer to provide its structure image. This technique provides information in two modes; image mode and the electron diffraction mode.

The TEM image in Figure 3.3 exhibits the TiO_2 as deposited on top and c-silicon on the bottom with the visibility of the interface between the layers. The TiO_2 in as deposited sample shows no grain formation in the bulk material. The underlying silicon layer shows atomic resolution.

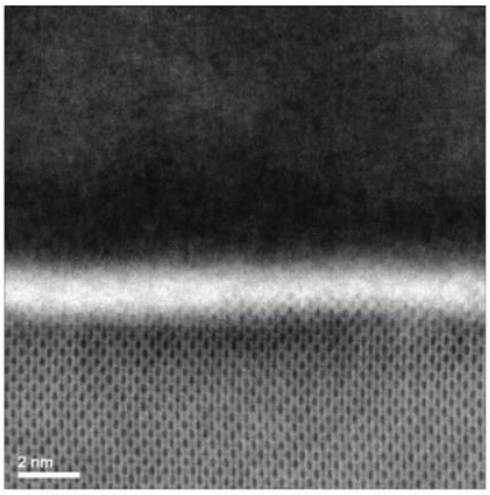

Figure 3.3 TEM image of TiO_2 (top) on silicon (bottom) substrate. It also shows the interface layer between TiO_2 and silicon [120].

The electron diffraction pattern, known as Selected Area Diffraction Pattern (SAED) shows crystallographic state of the material such as amorphous, single crystal or polycrystalline. It allows for identification of material type, phase, orientation and

defects. The real planes with atoms are equal to the real lattice and these correspond to the dots in the reciprocal lattice. The distance between the rings and the distance between the spots can be used to obtain the lattice parameters of the polycrystalline material. TEM is very advantageous to observe the amorphous and crystalline layer having structure with grain growth.

Amorphous material does not have any long range order so the obtained rings due to diffraction will have broad diffused intensity. Their appearance is halo. With the increase of crystallization of the amorphous phase, when sparsed small crystals develop, the material become polycrystalline and these rings acquire specific diameters, corresponding to the interplanar distance (related to Miller indices h,k,l). Therefore identification of the material will be more precise. Further increase of crystallinity results in formation of spotted rings that will indicate the type of crystal lattice developed and orientation. So from the image of selected area electron diffraction, from the rings and the spots in the reciprocal lattice, we can identify growth of even very small crystals

3.3.3 X-ray Diffraction (XRD)

The x-ray diffraction from crystalline substance or from powder provides signature structural information. The x rays diffracted from the crystalline material exhibits detailed composition and crystallographic structure. Crystals have crystallographic planes, depending on crystal lattice type that have specific interplanar distance. Incident x rays at θ angle are reflected back at a characteristics angle and intensity. If θ is the reflection angle, the constructive interference will take place and it will be recorded on a detection screen. Using Bragg law we can calculate interplanar distance with the equation given below.

$$n\lambda = 2 * d * sin\theta, \qquad \text{Equation 3.4}$$

where λ = x-ray wavelength, d = atomic spacing and θ is the angle of diffraction.

To identify the crystallographic composition and orientations, θ is scanned so that the peaks corresponding to different grains' orientations for the specific material can be recorded. The x ray detector measures the intensity of the peaks (on Y axis) and diffracted angle (on X axis). The peak position, width and intensity give information of the crystalline element.

3.3.4 Atomic Force Microscopy (AFM)

The atomic force microscopy comprises of a cantilever having a sharp tip that is used to scan over the specimen to be imaged (Figure 3.4). The scanning can be done in two modes, tapping mode and contact mode. In the tapping mode the tip is oscillated at or near the tip resonant frequency as mentioned in its specifications. Thus, the tapping mode scans the surface with intermittent contact of the tip on it. The tapping mode causes less damage to the tip as well as the sample surface as compared to the contact mode. The silicon nitride tip has a conical shape with a nanometer radius of curvature. A laser spot focused on the tip of the cantilever is reflected back to a position sensitive photodetector. As the tip approaches the surface, it becomes deflected due to the forces between the tip and the surface. This deflection of the tip shifts the laser spot on the detector and measures the differential voltage. This differential voltage is processed by the computer to provide a topographical image of the substrate. The forces between the tip and sample include van der Waals forces, chemical bonding, electrostatic forces, etc. The tip and sample surface might get damaged if the tip is scanned at a constant height. Hence, a

feedback mechanism is utilized that adjusts the tip and sample distance based on the force between them.

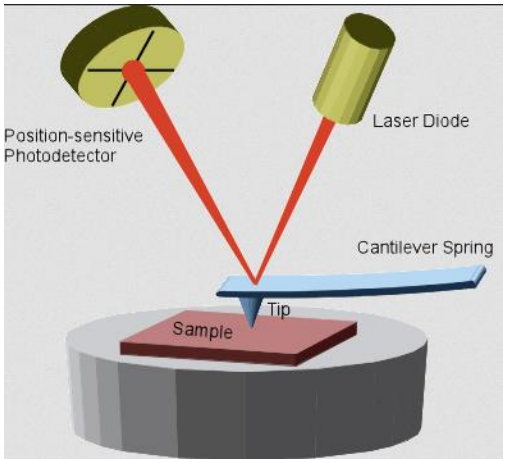

Figure 3.4 Atomic Force Microscopy equipment [145]

The AFM also provides force distance curves. These curves provide information on forces between the sample and the tip with respect to the distance between them. Various surface properties such as adhesion force and Young's modulus can be calculated from these force distance curves. Since the surface of materials may be modified by various processes as seen in annealing induced roughness, AFM is a tool of choice. Atomic force microscopy of as deposited samples showed a smooth surface morphology while the annealed samples had an increase in the surface roughness due to crystallization and grain formation [146].

The TAD (Ti as deposited) sample had no grain formation and had a mild roughness of 0.73 nm indicating a smooth surface (Figure 3.5). The Ti sample annealed at 800 C for 4 h in the presence of nitrogen gas had a sharp increase in roughness (2.74 nm) and grain formation of primary crystallite size of 26.6 nm. The annealing causes recrystallization and increase in the surface roughness of the sample.

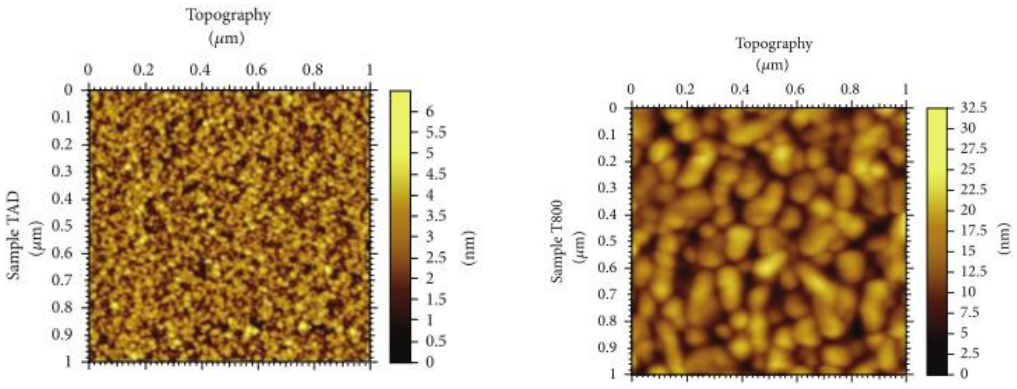

Figure 3.5 AFM topography of TAD and T800 (Ti annealed at 800 K for 4 h in nitrogen gas environment)

3.4 Project Goal

The microcellular environment plays a very critical role in controlling the cell behavior and function. Researchers have utilized proteins abundantly present in the extra cellular matrix (ECM) of the cellular microenvironment such as lamilin, collagen, fibronection and proteoglycan. However, there has also been enormous research of obtaining synthetic/ artificial materials that would be biocompatible for cell culturing and tissue engineering. Titanium and its alloys have been the best biocompatible materials and development of more such metallic biomaterials are in progress. Our project focuses on testing, titanium diboride (TiB_2), as a possible biomaterial with various cell types (HUVEC, MSC and Islet of Langerhans) for studying conditions for rapidly enhancing vascularization of implanted islets. Prolonged viability of EC, MSC and Islets of Langerhans on this material might pose TiB_2 as a possible material for in vitro cell culturing applications for prosthetic devices. Other application may be where wear and corrosion resistance in load bearing implant are important or in stents where endothelial cells are required to prevent thrombosis. Karagkiozaki et al. [147] studied the biocompatibility of materials such as amorphous carbon, carbon nano tubes, TiBN and

titanium diboride. All these thin film materials showed good cytocompatibility with suitable roughness and surface free energy. Makau et al.[239] studied the viability of titanium-titanium boride composite and its prospect to be used as a biomaterial. The presence of boron had enhanced the hardness and gave suitable reinforcement of Ti both chemically and mechanically stable.

TiB_2 has been known to undergo oxidation in a self-binding reaction, thus forming a potential passivation on the surface, similar to titanium. TiB_2 has been tested in microelectronics industry as gate electrodes in integrated circuits due to its high temperature stability that preserves its composition and interface with the dielectric layer beneath it during subsequent high temperature integrated circuit processes. It also has a high work function compatible with PMOS devices. Annealing processes conducted on amorphous layers induced grain growth, decreased the resistivity and modified the work function of TiB_2, but still maintained high work function required for gate electrodes [148]. It has been used for formation of contacts for ultra-shallow junctions for deep submicron devices such as PMOS devices in integrated circuits [149]. Electrical characterization was conducted for measurement of specific contact resistivity, I-V and C-V measurements of annealed and non annealed samples.

Other mechanical properties of TiB_2 are its high hardness (25 GPa), elastic modulus of 565 GPa and good corrosion resistance. These parameters may vary depending on the deposition processes used [150]. Since high corrosion resistance and hardness are the desired properties for prosthetic's for load bearing implantation, TiB_2 can be added as a coating of Ti material for improvement. One can expect that TiB_2 will show good biocompatibility, as reported for TiO_2, since oxide formation will take place

at its surface. The hardness can be improved by using compatible alloys such as TiB_2 at the surface. The passivation of TiB_2 by native oxide increases its biocompatibility [128].

Chapter 4: Experimental methods

This chapter will discuss the experimental procedures conducted for accomplishing the project goals of designing a Biological Micro Electro Mechanical System (BIOMEMS) device in order to have controlled cell growth that provides mechanical support and specific patterns. The development of the BIOMEMS device utilized silicon technologies used in Integrated Circuit (IC) fabrication. Deposition of various materials such as silicon nitride, titanium diboride and formation of silicon dioxide on silicon substrate was followed by UV light lithography for patterning specific designs and etching the material from non-pattern areas. The titanium diboride patterned substrates were used for cell culturing of Human Umbilical Vascular Endothelial Cells (HUVEC), Mesenchymal Stem cells (MSC) and Islets of Langerhans in vitro. Titanium diboride surface was characterized by X-Ray photo spectroscopy (XPS), Atomic Force Microscopy (AFM), nanoindentation, BioAFM and contact angle measurements. The cells were characterized in Confocal microscopy with fluorescent staining dyes, Bio Atomic Force Microscopy (BioAFM), and Scanning Electron Microscopy (SEM).

4.1 Design of circle and line network pattern

Micro design mimicking the vascular network in the form of circle and line patterns is incorporated into array structures that will facilitate repetition of such patterns. Different line width dimensions used in the arrays (5-50 μm) for HUVEC and MSC and circular configuration for Islets of Langerhans (diameter: 100-500 μm) as shown in Figure 4.1. The smallest dimensions of lines were used to mimic the sizes of capillaries. L-Edit Pro V8 (layout editor) and AUTOCAD software was used to design two separate files (.tdb format) of two different line array pattern and five different files for each

circle of diameter 100-500 µm using µm dimension rules. These files were used to make two masks: one with combination of both line patterns and the other mask with combination of circles patterns of 5 dimensions. The line mask has an array of 36 patterns with line width ranging from 5 µm to 50 µm (every 5 µm). One of the line pattern have straight grid design while the other has curved lines in order to observe the influence of pattern dimension and design on cells (Figure 4.2 - a and b). The other mask comprises of array of only circles ranging from 100 µm to 500 µm (every 100 µm) as seen in Figure 4.2 - c and d. Both the masks have division lines of 150 µm width. The alignment marks on the mask were used during lithography to align the circles on the line pattern.

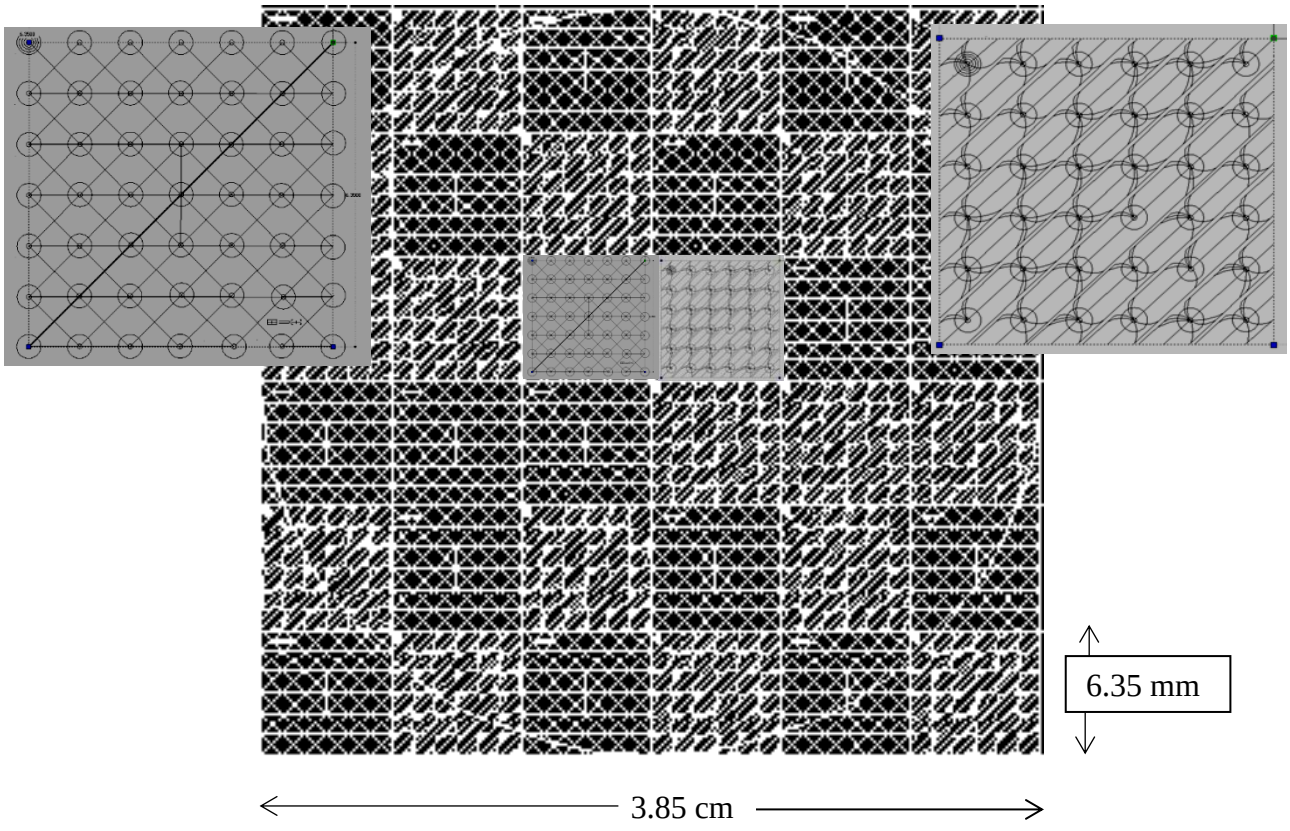

Figure 4.1 Mask for circle and line network pattern.

The masks were fabricated with chromium pattern on a glass plate. The masks were used for patterning TiB_2 to study only HUVEC (on lines pattern) or Islets (on circles). Lithography technique allows for multiple exposure of photo resist such that the two designs could be overlapped on one layer in order to study interaction of HUVEC on line structures with islets on the circles connected to these lines.

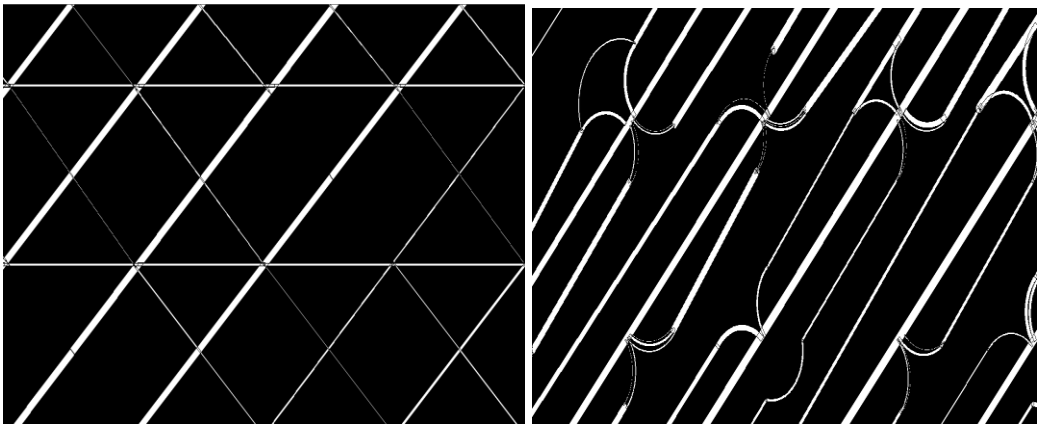

(a) (b)

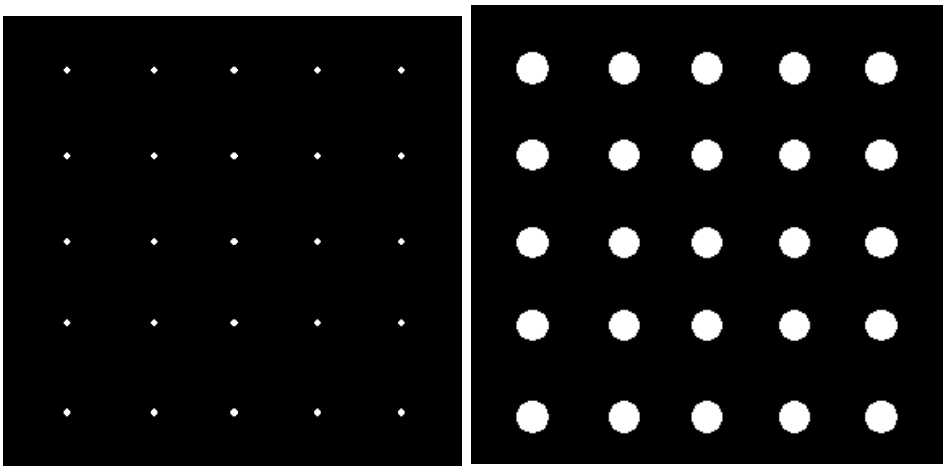

(c) (d)

Figure 4.2 L-Edit images of circle and line network pattern with (a) and (b) line widths varying from 5 µm to 50 µm (c) and (d) and circles ranging from diameter 100 µm to 500 µm.

4.2 Fabrication processes

The fabrication of the substrate for cell studies was implemented using silicon and Micro Electro Mechanical Systems (MEMS) technology. In order to study the effect of material on cell viability, material layers of silicon oxide, silicon nitride and titanium diboride on silicon substrate were implemented.

4.2.1 Material deposition

4.2.1.1 Titanium diboride (TiB_2) deposition

The titanium diboride was deposited in an electron beam evaporator present in the University of Houston facility. Silicon wafers (100), n and p type, either with thin SiO2 (2 nm to 60 nm) or without oxide were cleaned using RCA clean and HF etch. The cleaning process was important as it removes contaminants that could decrease adhesion of deposited layers. TiB_2 chunks loaded into the graphite crucible were used as source for the e beam evaporation. The electron beam at 8 kV melts the TiB_2 chunks at a melting point of 3215 °C. Several runs were used to outgas with the shutter closed in order to have no contamination during deposition. The power was increased progressively in each melting run. The first run was begun at 4% soak for 5 min and then ramping to 5% for 3 mins keeping the pressure 10^{-6} torr. During the second run pressure increased to $2*10^{-6}$ torr with a 5% soak for 3 min and ramp to 6% for 3 min. At the third run the soaking was 6% for 3 min and in the fourth run power was ramped to 7% for 4 min. In the consecutive runs the base pressure had to be maintained as low as $1*10^{-6}$ torr to $2*10^{-6}$ torr to out diffuse contaminants. At 8% power, open shutter when pressure as low as about $9*10^{-7}$ torr, giving a deposition rate of 5-10 A/sec. The power could be increased further to have quicker deposition and thickness of 20 to 70 nm. The thickness of the

deposited layer is measured in situ using quartz crystals based on the density (4.5 g/ cm^3) and the Z –ratio (0.8) of the film that is deposited. In case of acoustic mismatch between the deposited layer and crystal, the Z ratio corrects the change in the frequency to the transfer function of thickness. The thickness of the crystal affects the resonant frequency of the oscillation of quartz crystal. With deposition of material on the crystal surface, increases the crystal thickness and decreases the resonant frequency of the crystal. This frequency change is correlated to the change in the mass and thickness of the deposited material.

4.2.1.2 Silicon Nitride deposition

Chemical Vapor deposited silicon nitride layers of thickness 66 nm were obtained from Texas Instruments for cell culturing. Previous researches have mentioned this material to have no toxic effect on cells cultured on them [120]. They observed that the fibroblast cell morphology on silicon nitride ceramic samples were similar to the cells on titanium. Ni et al. [223] concluded that the suitability of cell culture on silicon nitride is due to the presence of NH_2 groups on its surface. However, there have been contradictory results observed in the literature regarding the biocompatibility of silicon nitride [120].

4.2.1.3 Silicon dioxide formation

The thermal oxidation process forms layer of silicon dioxide on the silicon surface. Thermal oxidation takes place by the diffusion of oxygen to the SiO_2/ Si interface to retain the oxidation reaction. The oxidation was performed in furnace in dry oxygen ambient conditions with varying time and temperature to grow silicon dioxide of up to 60 nm thickness. Silicon dioxide layer has a stable composition; the bulk composition is same as the surface composition. Clean silicon dioxide in aqueous

environment have OH^- termination and is hydrophilic. It is negatively charged resulting in adsorption of air borne contaminants making the surface hydrophobic.

4.2.2 Optical photolithography

The fabrication of the circle and line network patterns was done in two steps of lithography utilizing two separate chromium masks with chromium pattern on transparent glass. Kasper (Optical contact mask printer with Hg lamp) was used to conduct optical lithography with negative photoresist NR9-3000P (Futurrex) and developer RD6 (Futurrex). The negative photoresist was spin coated on the substrates with TiB_2 in two steps starting with 300 RPM for 10 s for uniform spreading and then at 4000 RPM for 50 s to obtain a 2-3 μm photoresist thickness. The substrate was prebaked for 120 s at 150° C to outgas solvents and was exposed for 70 s.

For studies of interaction between HUVEC and islets we used both masks with lines and circles in consecutive exposures to pattern our layers (TiB_2 and Si_3N_4) on the same layer. The first exposure of 70 s was conducted with the lines pattern mask and baked for 60 s at 100° C. The mask was then changed to the circle pattern mask and alignment marks are utilized to align the lines and circles. The same resist was exposed again for 70 s and the substrate was baked for 60 s at 100° C. Next, the photoresist was developed in RD6 for 40 s and quenched in DI water. The developer was used to remove the unexposed photoresist from the background (non-patterned) area and to retain the photoresist on the pattern area. The patterned resist was then used as a mask in wet etching of the film. We also used single masks (either lines or circles) to explore behavior of individual cell types, HUVEC and Islets.

4.2.3 Wet etching

The lithography was followed by wet etching of the silicon nitride (with oxide on top as a ahrd mask) and titanium boride using hot phosphoric acid (Temperature 160 °C) and 30% hydrogen peroxide, respectively, to remove unprotected (by photoresist) layers and produce the pattern. Wafers were rinsed in DI water for ~ 5 mins. After wet etching, the photoresist mask was removed with acetone and immediately followed by IPA rinse and then by running deionized water rinse. Finally, they were N_2 dried and stored for experimental purposes.

4.3 Material characterization

Based on the various factors affecting cell culturing on materials, the TiB_2 was characterized for its surface composition, roughness, hardness, Young's modulus and surface energy (hydrophilicity / hydrophobicity). The surface chemical composition provides surface elements of different functional groups that cause adherence of cell on the material. The initial contact of cell adhesion on a material is affected by the material surface characteristics. The nano scale roughness possibly provides adhesion sites for the focal adhesion complexes of cells during attachment. The hardness or stiffness of the material acts as physical cues affecting adherence and growth of cells.

4.3.1 X-Ray Photoelectron Spectroscopy

X-ray photoelectron spectra (XPS) were obtained at room temperature with a base pressure below $3*10\text{-}^{9}$ torr on a PHI 5700 X-ray photoelectron spectrometer equipped with a monochromatic AlKa X-ray source. The substrate was introduced at atmospheric pressure of 10^{-8} to 10^{-9} torr and after closing the chamber is pumped for about 5 to 10 minutes to have the chamber under vacuum. If the pressure inside the chamber suddenly drops below 10^{-7} torr, the control system will automatically shut down. The substrate is

irradiated with a photon source of energy and photo electrons are emitted. The XPS provides the elemental details of the material surface.

4.3.2 Hardness measurement-nanoindentation

The hardness and Young's Modulus of titanium diboride (maximum thickness 60 nm) was measured in MTS nanoindenter XP at the University of Houston, Mechanical Engineering Department facility. The Berkovich tip with a spring stiffness of 80 N/m, resonant frequency of 180 Hz and load of 0.3 nN was used for the measurements. The TiB_2 samples used for analysis were as deposited layers and after using annealing conditions of 950 °C for 5 s, 1000 °C for 1 s and 1100 °C for 5 s. The Berkovich probe tip diameter was 20 nm in diameter and is indented to 50 nm depth of TiB_2 (Maximum thickness of TiB_2 layer is 60 nm). The record of the penetration depth gives the load displacement curve that can be used to interpret mechanical properties of material such as hardness and Young's modulus.

4.3.3 Surface roughness

Atomic Force Microscopy (AFM) was used to analyze the surface characteristics of titanium diboride. The substrate was scanned with an Asylum Research AFM in tapping mode with a silicon probe (AC240TS) of 2 N/m force and resonant frequency of 70 kHz. The scan rate was 1 Hz and sampled/ line at 256. The silicon cantilever probe was calibrated until the resonant frequency was obtained and the laser beam spots on the tip of the cantilever. The tip was engaged as it approached the surface and began the tapping mode scanning. The AFM images provided the surface topography and roughness. Cross section of the AFM images can also be used to provide the surface roughness of the material.

4.3.4 Peak force mode BioAFM

Complimentary AFM was aimed at acquiring information on mechanical properties of the material. The goal was to identify the difference in the material characteristics of silicon background area and patterned TiB_2 that the HUVEC experience when in culture on the substrates. The BioAFM measurements were conducted with Bruker AFM Multimode8 in the Methodist Hospital Research Institute labs at Texas Medical Center. A silicon nitride probe (SCANASYST-AIR) having resonant frequency of 70 KHz, force of 0.4 N and spring constant of 0.5 – 0.8 N/m in tapping mode was used for the Young's modulus, adhesion force and also roughness measurements. The AFM tip was calibrated using the thermal drift capability and ramping the tip for the resonant frequency, deflection sensitivity and spring constant. The BioAFM was used to quantify the difference in the adhesions and Young's modulus of TiB_2, silicon and cells in case of pattern specific cell growth and non-pattern specific cell growth.

The Peak Force quantitative nanomechanical property mapping (QNM) tapping mode applies at every pixel controlled force curve on the substrate. These continuous force curves at each pixel of a single image can be used to quantify a number of material properties like Young's modulus (based on Sneddon model) of the material surface as well as the cell surface and adhesion force of material surface as seen in Figure 4.3. The Young's modulus in Sneddon model is calculated as given below

$$F = 2 * E * d^2/\pi(1 - v2)tan\ \emptyset, \qquad \text{Equation 4.1}$$

where F is force, E is Young's modulus, d is indentation depth, $\emptyset$ is conical tips half angle and v is Poisson's ratio. The Sneddon model is based on the contact theory of a rigid conical tip and an elastic half space [152].

The red curve in Figure 4.3 is the extending curve (approach curve) while the blue curve is the retracting curve (unloading curve) after the tip makes contact with the surface. The minimum force on the approach curve is at the instance of tip making the first contact with the surface and the maximum force is obtained when the tip is completely indented into the surface. The minimum force on the unloading curve is when the tip has reached the top of surface after indentation. Both the curves stabilize at the baseline force value. The slope of the retracting curves is used to calculate the Young's modulus of surface using Sneddon model and batch processing.

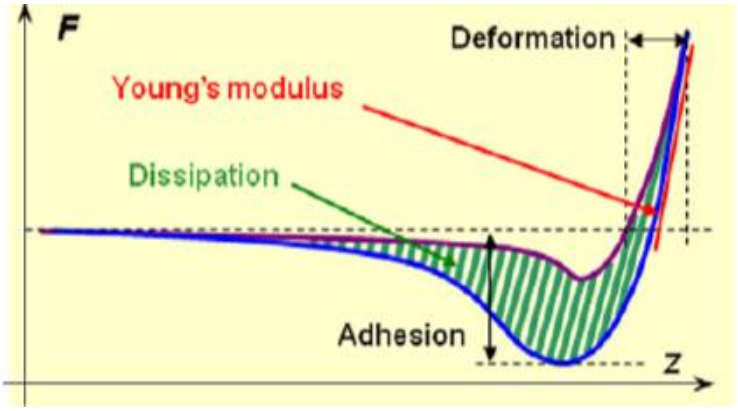

Figure 4.3: Force distance curve of PeakForce tapping mode AFM [153].

The presence of linear unloading indicates consistent tip radius throughout the scan. Linear regression is performed on the points of the retracting curve (linear range of unloading curve) to obtain the slope of each curve [154] in the batch processing. The batch process saves the Young's modulus and the coefficient of determination (R^2) value in an excel sheet. R^2 of greater than 0.98 indicates a good fitting of the Young's modulus using the Sneddon model. Adhesion force values are obtained from the baseline to the minimum force of the retracting curve [153].

4.3.5 Water contact angle measurement

Contact angle measurement were performed with double distilled water on Matrix Technologies 8300 Eletrapette Programmable piper instrument at University of Houston, Department of Chemistry. The VWR pipette was filled with 20 µl of double distilled water by the programmable piper. 5 µl of double distilled water was dropped on the substrate and the contact angle was viewed from the microscope. The contact angle in three regions on silicon and TiB_2 substrate was used for the contact angle measurement. The images of contact angle were recorded with a digital camera.

4.4 Cleaning and sterilization protocol

The substrates with TiB_2 patterns were cleaned in a heated ultrasonic cleaner. The fabricated substrates were first rinsed and cleaned in heated (temperature 45 °C) acetone for 5 min. They were then cleaned in heated (temperature 45 °C) Isopropyl Alcohol for 5 min, rinsed in deionized water (DI) for 5 min and N_2 dried. The cleanliness of the substrate was observed under a microscope and in spotlight. The substrates were sterilized in 70% ethanol for 15 min in the sterile hood and N_2 dried and used for the cell

4.5 Cell culturing

4.5.1 Human Umbilical Vein Endothelial Cells

HUVECs obtained from Lonza (Passage 1 to Passage 10) / ATCC (Passage 1 to Passage 9) were cultured in GIBCO Medium 199 supplemented with 10% of Fetal Bovine calf serum (heat inactivated), 10% of Bovine calf serum (heat inactivated), 1% of fungizone, 1% of Penicclin/ Streptomycin, 1% of Heparin, 1% of HEPES and 1% of ECGF (Endothelial Cell Growth Factor)/ VEGF (Vascular Endothelial Growth Factor). The ECGF/VEGF is good for two weeks and needs to be added freshly. The cells were

grown on 0.2% gelatin coated flasks in incubators at 37° C and 5% CO_2 environment. After every passage, the first culture media change is done after 24 hours of splitting and then every second day.

The initial experiments were conducted with two different media with two different amount of Vascular Endothelial Growth Factor (VEGF). The culture media with low VEGF had 1% of VEGF added to GIBCO Medium199 supplemented media while the high VEGF comprised of 1.6% of VEGF. The high VEGF culture media gave a prolonged viability and better growth kinetics of HUVECs on TiB_2 substrates as compared to the low VEGF culture media.

4.5.2 Islets of Langerhans

Islets of Langerhans extracted from cadavers, post isolation were kept in suspension flasks in incubators at 23° C and 5% CO_2 environment. Media (20 Liters GIBCO CMRL 1066 with 100mg/dl glucose, 23.4 ml of 10 N Sodium Hydroxide, 107.1 gm HEPES buffer, 1 each of Gelman Micro Culture Capsules 0.22um, 100 mg of ZnSO4-7H2O, 10 ml/L ITS+ Premix, 10 ml/L Antibiotic/Antimycotic, 10 ml/L L-Glutamine) was replaced twice the first week post extraction and then once every week from the second week onwards.

4.5.3 Mesenchymal Stem cells (MSC)

These cells form an integral part of tissue engineering due to its expansion and differentiation capability. The MSCs possibly provide vascular maturation [34, 35]. Sorrell et al. demonstrated that HUVEC-MSC vessels were stable for about 4 months in vivo. They suggested that the interaction between endothelial cells and MSC's provided

long survival of the vasculature formed. MSC's supposedly provide matrix molecules for formation and stabilization of tubular structures.

The human bone marrow MSCs obtained from Methodist Hospital were cultured in flasks in DMEM High glucose-D5648 (Sigma Aldrich) (supplemented with 3.7g/ L Sodium bicarbonate for pH 7.4) supplemented with 10% Fetal Bovine Serum at 37° C and 5% CO_2 environment. The culture media was changed every day and used for experiments till Passage 10.

4.6 Cell culturing on titanium diboride patterned substrates

The viability tests of HUVECs were done on silicon, silicon dioxide, silicon nitride and titanium diboride surfaces. The cells were not growing on silicon and silicon dioxide. Cells grew on silicon nitride but this material is controversial (Section 4.2.1.2). They are used for other application such as orthopedics. Prolonged and better HUVEC culturing on TiB_2 patterned substrates as compared to Si_3N_4 patterned substrates suggested better biocompatibility of TiB_2. After identifying titanium diboride causing no toxic effect to cells, all experiments were done on TiB_2 patterned substrates.

4.6.1 Seeding HUVECs

HUVECs were cultured at a seeding density of 30,000 cells per substrate on two different TiB_2 patterned substrates to observe the morphology, growth and orientation of cells as a function of time. One was circles of 450 µm diameter and the other was TiB_2 line patterns, as shown in Figure 4.2, of width 5 µm - 50 µm (every 5 µm) and 150 µm Initial set of experiments were conducted using 1% VEGF culture media and another set of experiment was conducted with 1.6% VEGF culture media. The substrates were imaged in an optical stereoscope microscope every alternate day after culture media

change. Also live samples were stained with Acridine Orange (5 µl) for 5 min and imaged in confocal microscope while fixed cells were stained with Platelet Endothelial Cell adhesion Molecule (PECAM) as per the protocol provided in Appendix A. Day 8 substrates were stained for actin filaments/ cytoskeleton (Phalloidin) and focal adhesions (Vinculin) for observing the attachment and shape of HUVECs on TiB_2 patterns. Staining protocol is provided in Appendix A.

4.6.2 Seeding MSC

MSCs were seeded at a density of 30,000 cells per substrate on TiB_2 lines and circle pattern (Figure 4.2) with circles of 300 µm and 500 µm diameter to observe the influence of pattern and material on the morphology of cells over time. The substrates were imaged in an optical stereoscope microscope every alternate day.

4.6.3 Seeding HUVEC and MSC

Previous researches have shown proliferation capability of cell types in HUVEC-MSC co- culture [50]. No fixed ratio were provided for co-culture, however a lower proportion of the MSC, being more proliferative, was considered for the co-culture [54]. We cultured HUVEC and MSCs of 2:1 ratio at a seeding density of 30,000 cells per substrate (20,000 HUVEC and 10,000 MSC) on the TiB_2 circle and line patterned substrates as shown in Figure 4.2. The substrates were imaged in an optical stereoscope microscope every alternate day. Substrates were stained on day 8 for Actin filaments / cytoskeleton and focal adhesions (vinculin) to observe the attachment and shape of HUEVCs and MSCs on the TiB_2 patterns.

4.6.4 Seeding HUVEC, MSC and Islets

In order to observe the influence of combination of HUVEC and MSC cells on viability of Islets of Langerhans, its morphology and function, Day 1 and Day 9 old Islets of Langerhans were seeded on confluent patterned layer of HUVEC and MSC co-culture. HUVEC and MSC's in the ratio of 2:1 were cultured at a seeding density of 30,000 cells per substrate on TiB_2 line and circle patterned substrates (Figure 4.2). After 2 days of HUVEC and MSC culturing, islets were seeded on these co-cultured substrates and were allowed to settle for an hour before putting the excess HUVEC media in the dish/well and the HUVEC media was changed carefully every day. These substrates were cultured for 21 days (3 weeks) and then were stained for confocal florescence imaging. The primary antibody used for HUVEC and Islet staining were CD31/Platelet Endothelial Cell Adhesion Molecule-PECAM (ab28364-Rabbit), Insulin (ab7842-Guine Pig), Glucagon (ab10988-Mouse) and Somatostatin (ARP13-2366-Sheep) and the secondary antibodies were Alexa Flour 594 (anti Rabbit), Alexa Flour 488 (anti Guinea Pig), Dylight 405 (anti Mouse) and Alexa Flour 647 (anti Sheep) respectively.

4.7 Cell imaging of live and fixed samples

4.7.1 Optical stereoscope microscope

The substrates for all the experiments were imaged on a regular basis in optical microscope (Olympus SZX7) to observe the morphology and behavior of the cells (HUVEC, MSC and Islets). These images were used to analyze the HUVEC growth, elongation and orientation.

4.7.2 Live Confocal imaging of HUVEC

Acridine Orange (5 µl in 2 ml culture media for 5 minutes) was used for staining the live cells to observe the cell viability and cell morphology on the titanium diboride pattern. The substrates are imaged in Olympus Fluoview 1000 Confocal microscope.

4.7.3 Fixed confocal imaging of HUVECs, MSCs and Islets

The cell cultured substrates were fixed (Appendix A) and imaged in the Olympus Fluoview 1000 Confocal microscope. Excitation wavelength of 405 nm, 543 nm and 635 nm were used for secondary antibody excitation of AF405 (Glucagon), AF488 (Insulin), AF594 (PECAM-CD31), AF647 (Somatostatin), DAPI (Nulei), Phalloidin (Cytoskeleton) and vinculin (focal adhesions).

4.7.4 BioAFM Cell imaging: Fixed HUVEC

The HUVEC cultured substrates were cultured and fixed as per the protocol provided in Appendix A. The fixed substrates were placed on the Multimode8 stage by an adhesive tape. The location of imaging on the substrate was observed on the optical microscope. The cantilever was placed in the AFM holder and adjusted for its position on silicon, TiB_2 or cell. The tip was engaged to approach the surface and force curves (.pfc file format) were obtained for calculating surface characteristics of silicon, TiB_2 and cells.

4.7.5 SEM imaging of fixed HUVEC, MSC and islets

The fixing protocol is provided in Appendix A. After fixing, a 6 nm thickness platinum layer is coated on the substrate before imaging in Nova NanoSEM 230 equipment present in the Methodist Research Institute facility. The SEM equipment had a horizontal field working distance of 4 mm with a resolution of 1.6 nm at 1 kV.

4.8 Statistical analysis

The optical and confocal images were analyzed by ImageJ software to measure the % cell coverage area, orientation and Length/Width ratio for each design pattern. Equivalence test was utilized for interpretation of equal mean and student t test along with ANOVA was used for analyzing significantly different mean.

4.8.1 Measurement of percentage cell coverage area

The Acridine Orange stained Confocal images were opened in ImageJ software and converted to 8 bit grayscale images. These images were then threshold (threshold method Huang) and filtered (Median filter to remove < 2 pixels) appropriately such that only the Acridine Orange stained green florescence is accurately selected. This threshold area with respect to complete circular area provides the % cell coverage area on each circle (Figure 4.4).

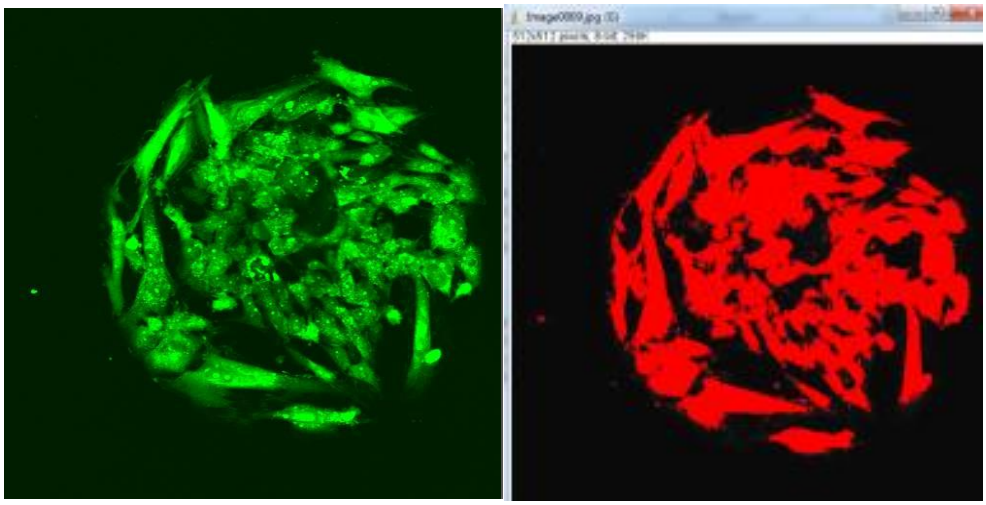

Figure 4.4 HUVEC coverage area on TiB2 circles (Diameter 450 µm). The green is the Acridine Orange stained image while the red is the threshold image from ImageJ. Analysis done in ImageJ software.

4.8.2 Percentage cell coverage area from cell count

Cell count was conducted on the optical images of HUVECs growing on TiB_2 patterned substrates (circles of diameter 450 µm). Maximum cells / mm^2 were taken as 700 to calculate the percentage cell coverage area of HUVEC on the pattern.

4.8.3 Orientation measurement

The orientation was analyzed by drawing a line along the major axis of the cell. On hitting the Control+ M buttons, the orientation of the cell with respect to the horizontal 0° axis is displayed. These angles are then collected on an excel sheet, where it is converted to an angle with respect to the length axis of the pattern line.

4.8.4 Measurement of Length/ Width ratio of HUVECs

The optical images of cells were analyzed in ImageJ for Length/ Width ratio measurement. The line feature was used to measure the length, width and orientation of each cell on different width lines, 5 µm – 50 µm (every 5 µm) and 150 µm. A value of Length / Width ratio greater than 1 indicates the elongation of the cells on the different width lines.

4.8.5 Analysis of Confocal images of Islets

An ImageJ macro was utilized to quantify the total count of Glucagon, Insulin, Somatostatin and endothelial cells (PECAM) inside the islets. The macro provided the total volume of the hormones secreted by the islets cultured on the substrates and the control islets on petri dishes. This macro calculated the normalized hormone secreted value based on the size and the volume of the islet.

Chapter 5: Results and Discussions: Material characterization

5.1 Material characterization

The TiB_2 material used in this work was characterized for its surface composition, roughness, hardness and Young's modulus as described in the following sections. Various parameters affect the *in vitro* cell culturing on materials such as chemical surface composition, surface topography, surface rigidity and elasticity. The cell-materials interface has been hypothesized to be highly dependent on the surface properties of the material [155]. The interaction of the cell surface receptors with the biomaterial surface affects the subsequent cell behavior such as adhesion, growth and proliferation. The TiB_2 material were deposited by electron beam evaporator to form layers of 30 – 100 nm (Section 4.2.1.1) and these layers were patterned using optical photo lithography to have two different patterns; lines and circle design as seen in Figure 4.2 and circles of diameter 450 μm.

5.1.1 Surface chemical composition analysis

Several characterization techniques were used to analyze properties of TiB_2 layers after e-beam deposition processes and after subsequent RTP annealing in various thermal conditions. All annealing processes were done in the nitrogen ambient to limit oxidation of the layers.

5.1.1.1 X-ray Photoelectron Spectroscopy

X-ray Photoelectron Spectroscopy (XPS) was used to acquire complete information about elemental and molecular composition of the TiB_2 layers and the chemical bonding of the atoms such as titanium, boron, oxygen, carbon, and nitrogen.

This analysis allows for surface not bulk characterization due to small escape depths of the emitted photoelectrons; those are typically limited to the single nm range. However, XPS can be also used for depth profiling to observe the layer composition from the surface to bulk when in-situ ion sputtering is implemented. Each element has a characteristic binding energy, which includes binding energy in constituent atoms, effects of bonding with neighboring atoms (chemical shift), as well as electrostatic and relaxation effects. A set of peaks at characteristic binding energies and intensities detected by XPS can be used to identify the electronic state of the surface material. The intensity of the peak corresponds to the concentration of the element in the substrate. It helps to identify presence of any contaminants on the surface, if any.

Surface composition and speciation of TiB_2 layers both as deposited and annealed in RTP were measured using two instruments. One was Physical Electronics 5700 XPS instrument. Photoelectrons were generated via monochromatic Al K_α x-ray sources operated at 350 W. Binding energy scales were calibrated using the Ag-$3d_{5/2}$ photo-electron peaks. Quantification is carried out using a Shirley background subtraction routine and appropriate sensitivity factors.

Another instrument used for XPS was Kratos, Axis Ultra. Background pressure was below 2x10E-9 Torr. monochromatic Al k alpha X rays (15kV, 14 mA). The X-ray spot was about 0.8 mm in diameter. The analyzer was a hemisphere. The pass energy was 160 eV for the wide scans (1100-0 eV) and 20 eV for the narrow scans. Similarly, gold standards were used for analyzer energies. The depth profiling was done using 3 keV Ar+ ions with about 0.8 uA current over approx. 3 mm^2 area. Built-in Kratos sensitivity factors were used for evaluation. As expected the major constituents of TiB_2 (Ti and B)

are identified but several other elements are also detected (adsorbed contaminants or process induced/ reacted elements) in Figure 5.1

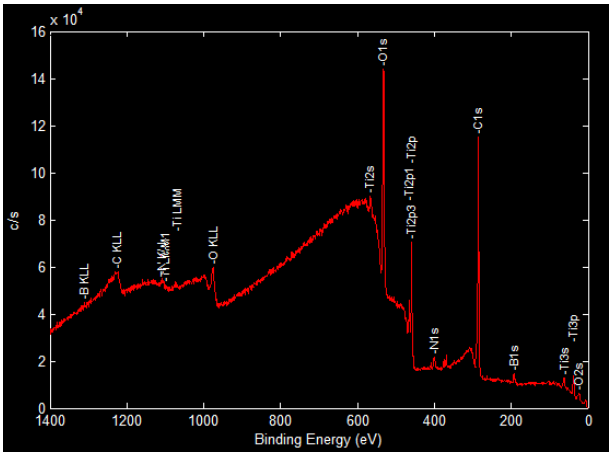

Figure 5.1 Wide scan survey scan obtained for a TiB_2 sample annealed in RTP at 1050°C/1s in N_2 gas.

Depth profiling plots of unannealed and annealed samples were obtained with in situ Ar sputter etch at 5 keV. They are shown in Figure 5.2. These depth profiles for both the as-deposited (a) and annealed samples (b) plotted for all elements show layer uniformity with stoichiometric TiB_2 in the bulk regions except for surface of the films. The plots indicate that annealing in neutral N_2 gas ambient, did not cause compositional changes of TiB_2 within the bulk of the layers. Similar results were obtained for other thermal conditions i.e. temperature and time. That confirms high thermal stability of molecular compositions of TiB_2 during annealing (1050°C for 1 s) but also propensity to formation of boron and titanium oxides at the surface.

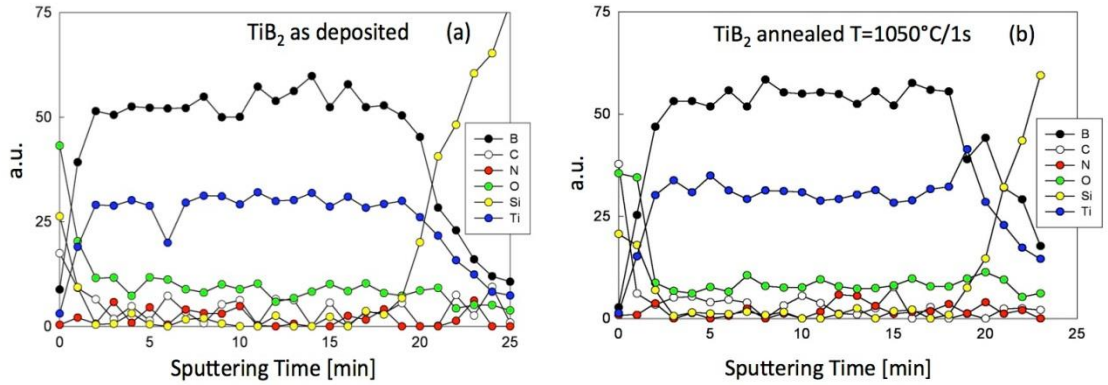

Figure 5.2 Depth profiling XPS of Titanium diboride obtained for as-deposited and annealed RTP at 1050°C for 1s in the nitrogen ambient. [156, 149]

Affinity of titanium to oxygen and resulting titanium oxides is well documented and its biomedical applications relays on these oxides. Oxidation of TiB_2 is also well documented [157, 158], [159, 160]. Ti reacts with oxygen instantaneously and forms oxides in air even at room temperature TiO, Ti_3O_5 [161]. At elevated temperatures Ti^{4+} state is more predominant and TiO_2 is frequently formed [162]. The layer is stable due to limited diffusion though the oxide and the oxide passivates the surface.

To identify surface composition of TiB_2 from the surface to the bulk of the layer we used depth profiles plots for Ti 2p, B 1s, and O 1s. Ti spectrum is plotted for 2p levels and includes 2 p3/2 and 2 p1/2 splits (Figure 5.3).

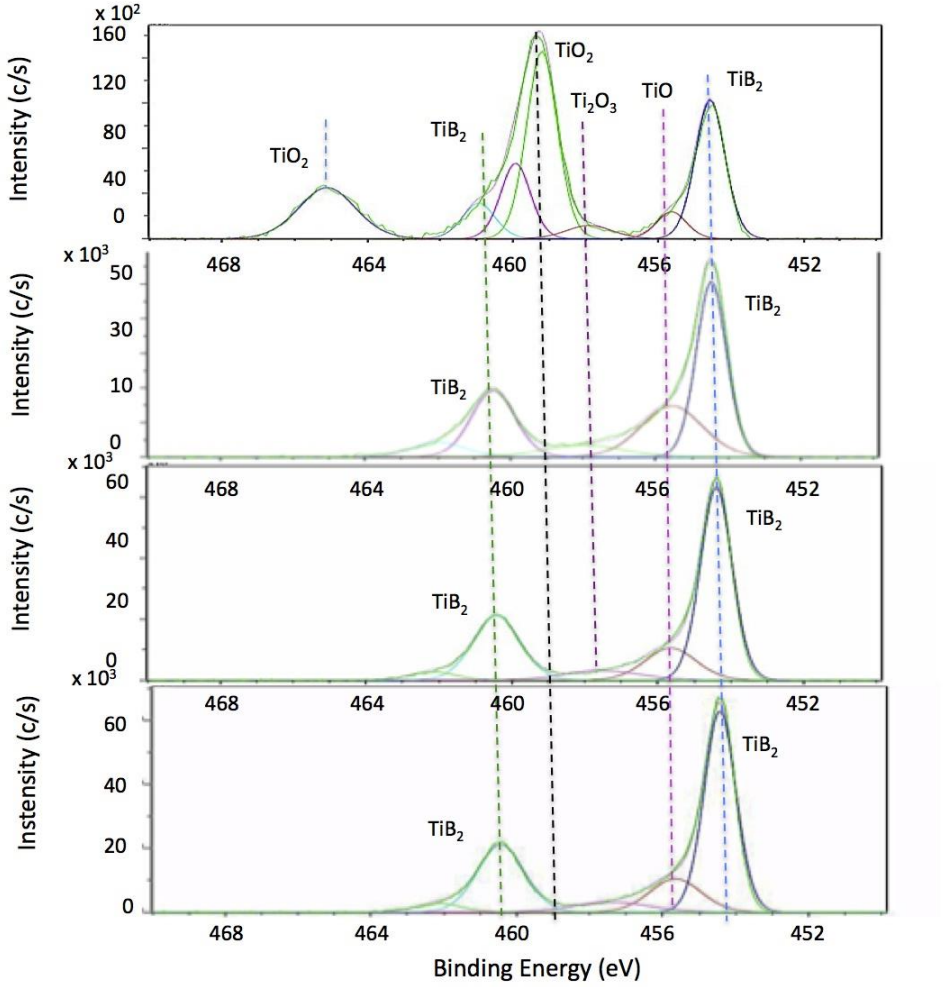

Figure 5.3 Depth profiles for Ti 2p using in situ Ar sputtering of RTP annealed sample at 1050°C/1s. Figure 3a) shows the surface, while sputtering is used for 300 s in b), 210s in c), 3900 s in d) [167].

The depth profiles obtained for B 1s and O 1s complement the characterizations by XPS and are shown in Figure 5.4. Quantitative information on concentrations is included in the Table 5.1.

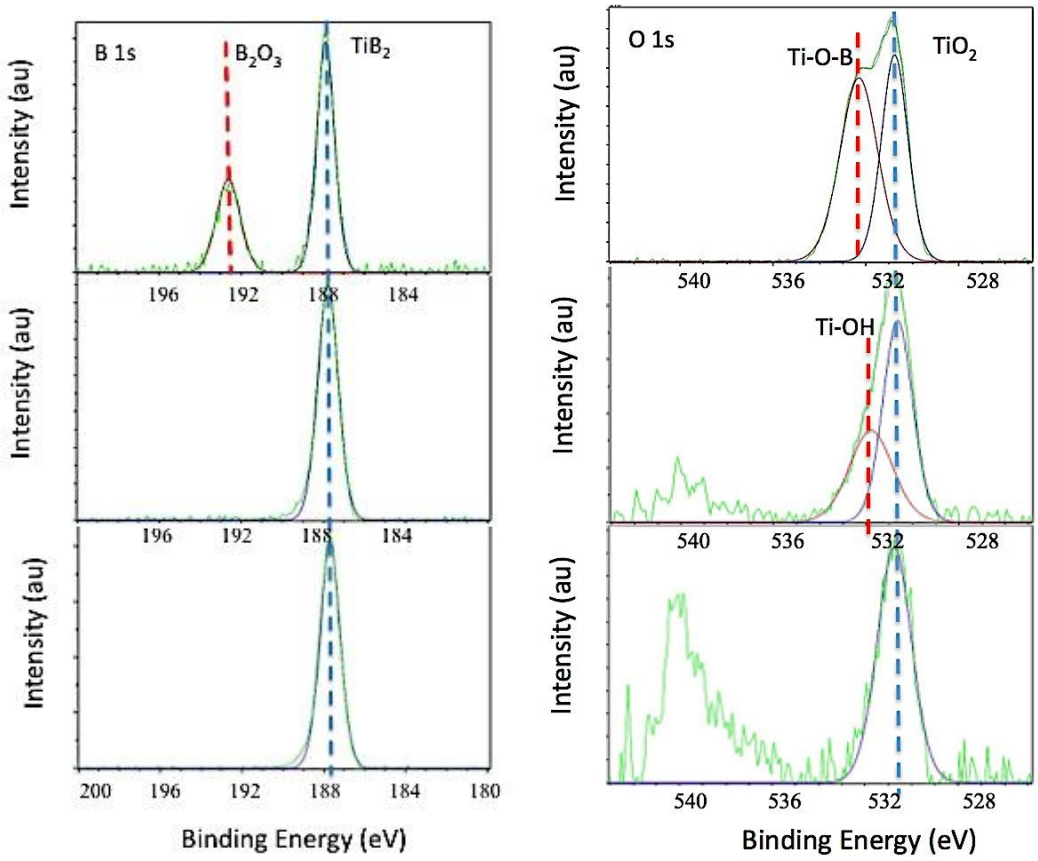

Figure 5.4 Depth profiles for B 1s (4a) and O 1s (4b) using in situ Ar sputtering of RTP annealed sample at 1050°C/1s. The top plots show the surface region. Subsequent plots were obtained with Ar sputtering for 300 s and for 2100 s. [167]

From the Ti 2p spectra it is evident that the oxide formation takes place at the surface not in the bulk of the film. In addition, despite annealing in RTP in the neutral N_2 ambient, concentrations of nitrogen are very low i.e. below 0.4 atomic %; There is no formation of nitrides BN. Fast oxidation of TiB_2 leads to titanium oxides formation at the surface and the concentration of TiB_2 is smaller compared with Ti-O. TiB_2 was identified by binding energies 454.5 eV (Ti 2p3/2) and 460 eV (Ti 2p1/2). Oxides included TiO_2 with 459.2 eV (Ti 2p3/2) and 465.2 eV (Ti 2p1/2). The most stable of all oxides Ti-O is TiO_2. There were also suboxides present in the surface region such as Ti_2O_3 corresponding to Ti^{3+} and TiO – to Ti^{2+} states, respectively. The oxides are confined to the surface layer due to their low permeability, which limits the oxidation process.

Table 5.1 Percentage Atomic concentration of B 1s, Ti 2p, O 1s, and C 1s on unannealed titanium diboride surface, sputter etched for 300 s, 2100 , and 3900 s surface [167].

	B 1s Atomic concentration %	Ti 2p Atomic concentration %	O 1s Atomic concentration %	C 1s Atomic concentration %
Surface	17.17	10.8	40.1	27.4
Sputter etch 300 s	47.9	32.6	12.8	4.2
Sputter etch 2100 s	59.8	33.7	3.1	2.7
Sputter etch 3900 s	60.3	33.1	3.1	2.8

The spectrum of O 1s confirms TiO_2 presence in the surface region (530 eV), Ti-O-B bonds (532.7 eV) and Ti-OH (531.7 eV) [163]. Depth profiles confirmed that boron oxide (Ti-O-B) is located only at the surface. It was easily removed in sputter etching together with titanium hydroxide. The remaining TiO_2 peak should in fact be scaled down as it corresponds to very low oxygen concentration (see table). From the spectrum of B 1s we can confirm that TiB_2 has reacted with oxygen at the surface and B-O (B_2O_3) oxides were formed. Typically, oxide formation even on well known material such as titanium may have nonuniform (layered) composition where more stoichiometric TiO_2 is close the Ti surface and oxygen deficient ex. Ti_2O_3 is at the surface. In the case of TiB_2 oxidation the B_2O_3 layer is typically at the top surface and if high temperature process is

used it may evaporate because low its melting temperature. This oxide is present at the surface only.

5.1.1.2 X-ray Diffraction

X-ray diffraction (XRD) gives the structural information of the material from the scattering x-rays from crystalline surface. Crystalline materials have a number of planes that have interplanar distance which causes x rays to be scattered at a characteristics angle depending on the lattice plane. XRD was conducted to determine crystallographic structure of the deposited and annealed layers. Crystallographic structure has an influence on electrical properties i.e. since it affects carrier transport and can result in higher conductivity. It may also affect work function since it might depend on crystal orientation [164, 165]. That will contribute to surface charges and will have an influence on cell culture. Finally, crystallographic structure of layers with large size grains, may change also planarity of the surface causing roughness of various degree that then can lead to cell growth modification.

In our experiments we used the reference peaks for TiB_2 obtained from ingot chunks used as a target material in e-beam deposition (Figure 5.5). As-deposited layers were amorphous therefore XRD did not show any diffraction peaks [149]. However, the annealing processes lead to recrystallization where grain growth was controlled by the thermal conditions (temperature and time) and was also affected by the substrate used for boride layer deposition (oxide vs. silicon). Figure 5.5 illustrates grain growth in various conditions of thermal budget.

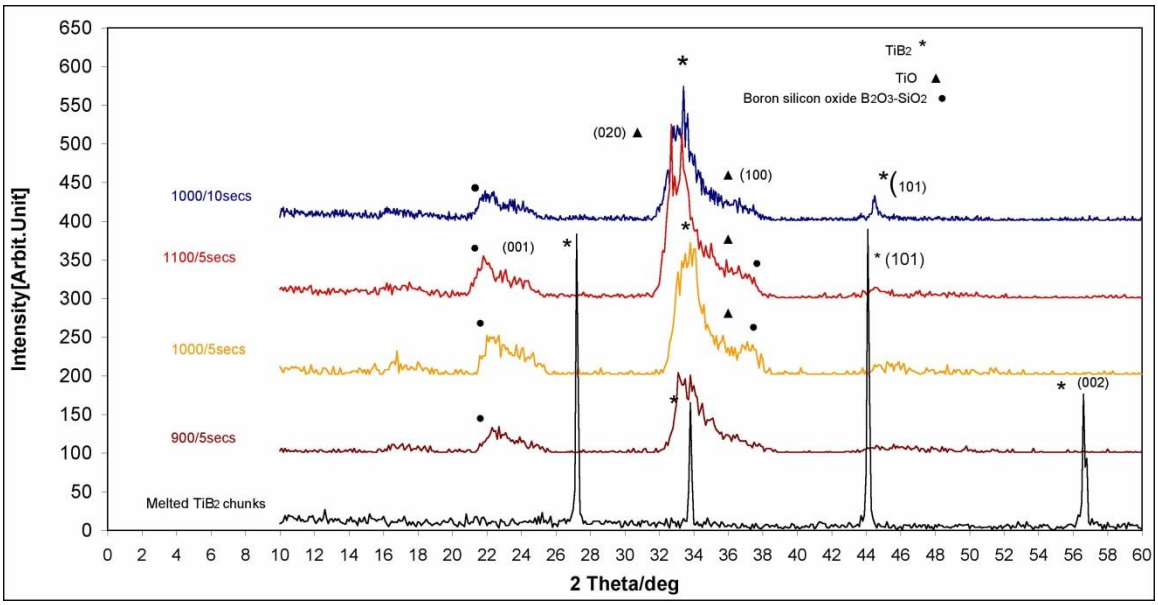

Figure 5.5 XRD results obtained from the RTP annealed TiB2 layer processed using various thermal budget [149].

We could identify the grain growth of TiB2 phase. However, since the RTP processes are short only small grain sizes are typically observed. We did not detect any crystalline form of TiO_2 such as rutile or anatase phase. In general, recrystallization can be also modified or degraded if contaminants are present within a layer. Our process of e-beam deposition typically performed at about 10^{-6} torr has introduced small concentrations of oxygen contaminants (typically below 2 atomic %) that would limit the grain growth.

5.1.1.3 Transmission Electron Microscopy (TEM)

Cross section TEM was done for films that were either deposited only and for films that were annealed in RTP in various thermal conditions. Low magnification micrographs obtained in TEM allow to evaluate planarity of the films, interface of TiB_2 with the substrate and the surface layer within larger distance. High resolution micrographs of such films allow for nm range imaging to inspect crystallographic structure at atomic resolution therefore monitor grain growth and changes in surface layer.

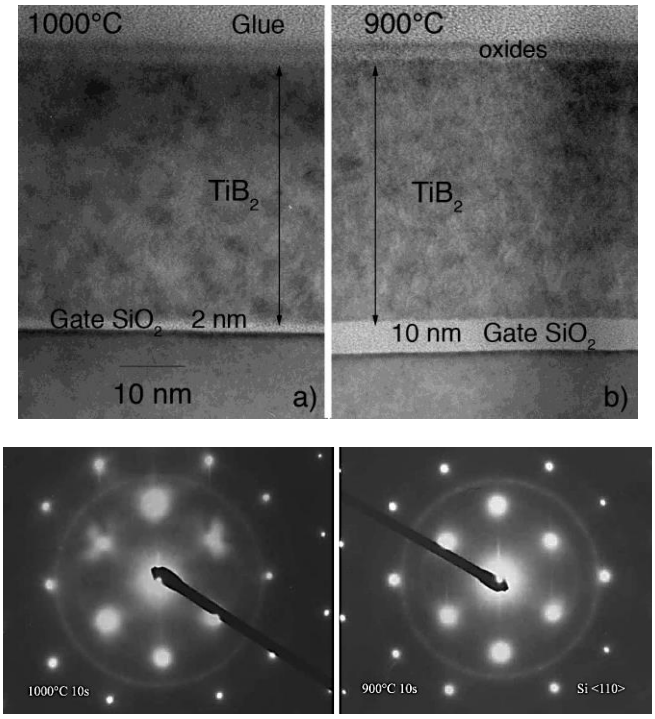

Figure 5.6 TEM cross section at high resolution for TiB2 deposited on thin oxides and annealed in RTP. high resolution images of a TiB2 film deposited on oxide layer and annealed at 900 °C and 1000 °C for 10 sec Below we include SAED images for identification of TiB2 nanocrystals [166].

Important here is the confirmation that thin oxide layers that were detected by XPS are clearly visible on the TEM micrographs. The selected area diffraction patterns (SADP) included in the figure indicate that original amorphous layers (not shown here) undergo crystallization but the grains' sizes are small i.e. limited to about 5 nm. Hexagonal structure of TiB2 was identified by the radii of the diffraction rings.

At higher temperatures (1100 °C/1s) much larger grains were formed in TiB_2 deposited directly on Si (Figure 5.7). The corresponding SAED results prove this enhanced recrystallization.

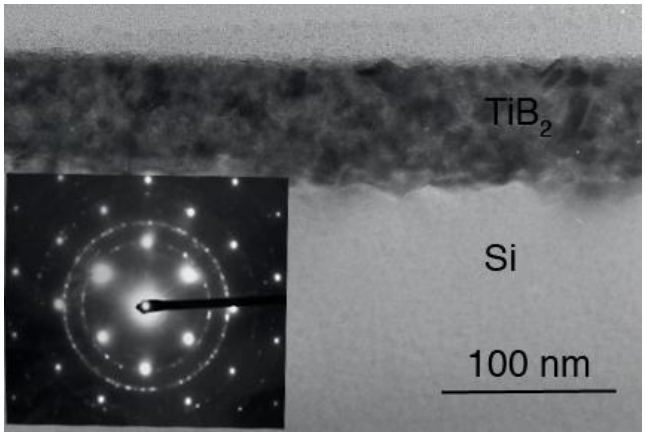

Figure 5.7 Cross section TEM obtained for TiB_2 on Si annealed at 1100 °C/1s with the inset of SAED [166].

Large grains of the order of 10-20 nm coincided with roughing of the Si/TiB_2 interface. This would result in degradation of the surface planarity by introducing the roughness of at most the same order as the grain sizes in such thin films. We will discuss later the influence of material properties related to chemical composition and structure on adsorption and mobility of cells during culturing.

5.1.2 Surface roughness

The surface roughness of TiB_2 non-annealed and annealed samples were measured in AFM in tapping mode. The surface roughness of non annealed layers were observed to be about average 3.77 nm indicating that the TiB_2 surface is relatively smooth surface with mild roughness as seen in Figure 5.8. TiB_2 substrate samples that were annealed at 1000 °C for 5 s in the N_2 ambient have an increase in surface roughness of the range of 6 nm to 8 nm with the formation of grains in the bulk of the films. Presence of surface roughness of the material provides increase in material surface area as compared to a completely smooth substrate [146].

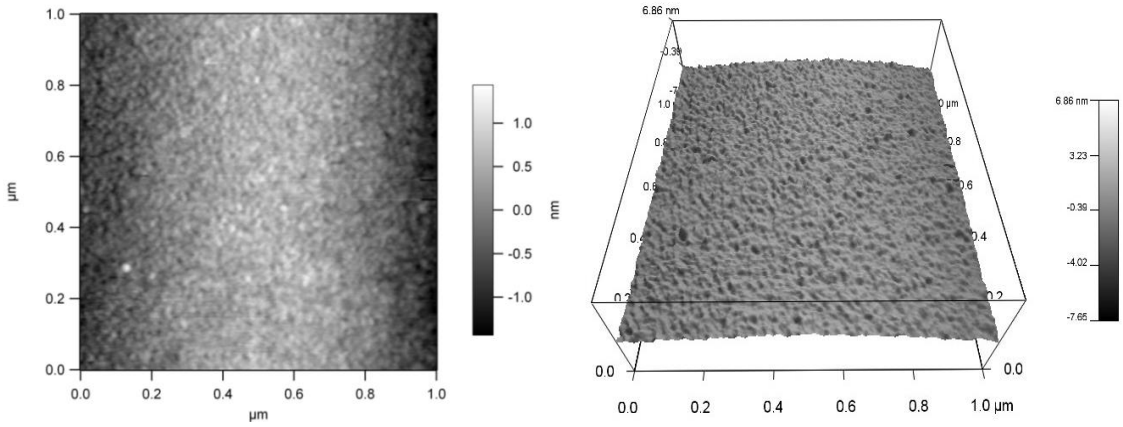

(a) (b)

Figure 5.8 AFM images for surface roughness of non annealed TiB_2 substrate (a) 2D AFM image (b) 3D AFM image.

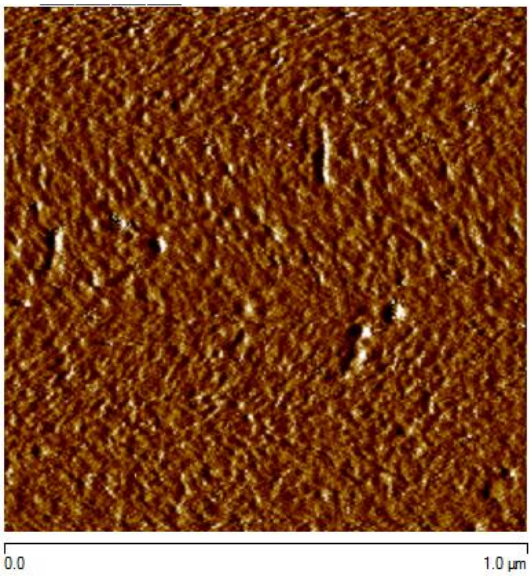

Figure 5.9 Average surface roughness of non annealed TiB_2 is 3.77 nm.

Amorphous material is deposited and depending on the substrate type and thermal budget, recrystallization will occur by solid phase epitaxy or by growth of grains which follow crystal nucleation formation at high temperatures. Grains from the recrystallization will grow to minimize surface energy of the grains to reduce grain boundaries. Longer annealing process performed at high temperatures lead to growth of

these grains in the bulk layer as seen in Figure 5.7. The cells cultured on our non-annealed TiB_2 had a cell area of 1132 ± 357 μm^2 and the annealed TiB_2 had cell area 1528 ± 254 μm^2. Annealing affects surface composition of materials along with roughness. Native oxide formed on TiB_2 comprises B_2O_3 and TiO_2 with its suboxides. TiO_2 thin layer have excellent mechanical stability and chemical stability. It is known that in as deposited film these oxides are amorphous. TiO_2 exist also in rutile and anatase phases depending on technology and at typically higher temperature, α phase is transformed into rutile. The transformation of anatase to rutile depends largely on high temperature and time. Yoo et al. [168] studied the effect of annealed temperature using conventional thermal annealing (CTA) in nitrogen atmosphere and rapid thermal processing (RTP). The RTP is short duration (in seconds) while the CTA is longer duration (in hours). CTA annealing above 800 °C exhibited rutile TiO_2 structure on the surface and the RTP at the similar temperature showed weak brookite structure of TiO_2. Aziz et al. [169] observed that anatase to rutile transformation occurred at annealing temperature above 650 °C for 1 h where 100 percentage of TiO_2 anatase is transformed to rutile phase.

Petersson et al.[170] studied that the surface roughness of titanium dioxide obtained from sandblasting followed with hydrofluoric acid wet etching caused a decrease in resistivity and an increase in conductivity leading to the increase in number of charge carriers and possibly increase in protein adsorption when the material is used for *in vitro* cell culture.

Our results show recrystallization of the films that increases with thermal budget. Annealing of TiB_2 decreases its specific contact resistivity. Ranjit et al. [149] examined

the current- voltage characteristics of non-annealed and RTP annealed TiB_2 sample showing decreased resistivity with increase in temperature. Recrystallization on annealing caused increase in grain growth and decrease in grain boundary lead to less scattering and trapping of carriers. The decrease in grain boundary improves electron transport thus decreasing the resistance. They reported decrease in resistivity of the annealed TiB_2 sample up to 3 times as compared to the non-annealed sample (150 μΩcm). The grain growth may result in the change in the metal work function due to crystal orientation effect [171].

5.1.2.1 Effect of surface roughness on cell behavior

Cell attachment to the substrate material in *in vitro* culture requires protein adsorption from the culture medium on the material surface. The protein adsorption on material takes place due to electrostatic and hydrophobic/hydrophilic interactions. Bakir et al. [136] mentioned that the electron transfer that possibly takes place during the protein and the material interaction facilitates conformal protein layer formation. Rechendorff et al. [172] used the quartz crystal microbalance with dissipation and ellipsometry to conclude that fibrinogen protein adsorption on the evaporated tantalum film surface increases by about 70% with increase in the nanometer scale roughness (2 nm to 32.9 nm) and surface area (increase of approximately 20%). They also studied the attachment of bovine serum albumin on nanometer scale rough surface which exhibited less protein adsorption as compared to fibrinogen [173].

Surface roughness is an important factor in cell attachment and proliferation. Cell focal adhesion complex are able to sense the surface mechanical properties and respond by adhering and growing on the material surface [121]. Jiang et al. [174] studied the

HUVEC cell adherence on three different surfaces; surface with rutile TiO_2 only, surface with anatase TiO_2 and surface with both anatase and rutile TiO_2 phases. The surface of anatase and rutile phase combination had smaller roughness (2.67 nm) as compared to the surface with only anatase (3.58 nm) and only rutile (5.56 nm). They concluded that all three surfaces exhibited good biocompatibility, however rutile phase TiO_2 had better HUVEC cell adhesion and growth as compared to the other surfaces. The reason being that the rutile phase of TiO_2 surface had certain surface roughness that was suitable as adhesion and growth sites for HUVEC culture. The nanorough surface possibly provides better adhesion sites for the formation of focal adhesion complexes of HUVECs on its attachment to the material. The anatase and rutile have the same properties such as hardness, density and tetragonal crystal structure but anatase has higher volume of unit cell as compared to rutile. Rutile has a denser crystal structure and is more closely packed as compared to anatase and thus have fewer paths for metal ion release. In the case of our metallic TiB_2 we also have TiO_2 and suboxides on the surface and similarly to Ti, this material seems to be biocompatible.

Contradictory results of HUVEC on nano rough surfaces have also been reported. Gentile et al. [78] performed HUVEC culturing on electrochemically etched silicon substrates of roughness 2.33 nm to 101.47 nm. They showed better cell growth on substrates with medium roughness of 10 nm to 45 nm and attributed it to the increased surface energy. Hence, the cell biomaterial interactions are influenced by the range of nanoscale roughness of the biomaterial. Cai et al. [175] had observed no significant effect on cell growth based on different nanometer scale surface roughness on titanium. They increased the surface roughness of titanium by increasing the deposition rate which in

turn increased the thickness, roughness and the grain size of the biomaterial.. Another research group [140] justified contradictory results showing better HUVEC growth on crystalline Ti-O (smooth surface – 2 nm) as compared to amorphous Ti-O surface of roughness 56.2 nm [176]. Their Ti-O films were made with deposition along with plasma immersion ion implantation technique in the presence of oxygen. They confirmed their results of HUVEC adherence and growth on smoother crystalline Ti-O surface was better as compared to rough Ti-O surface where the rough Ti-O surface was obtained by 5 min to 60 min etching by Ar ion [177]. The Ti-O crystalline smooth surface showed normal cell adherence and attachment while amorphous Ti-O showed moderate spider shaped morphology.

5.1.3 Hardness of biomaterial TiB_2

The hardness of the 60 nm TiB_2 layer on silicon substrate was measured with MTS nanoindenter XP equipment. The nanoindentation measurement needs to be done with a sharp tip of 20 nm diameter with an indentation depth such that the tip does not reach the soft substrate (silicon) 60 nm beneath the hard material (TiB_2). The thickness of the complete layer is 30 nm – 100 nm. Hardness represents the plastic deformation that takes place on the material as the tip is indented into it.

The Figure 5.10 indicates the hardness and modulus of the TiB_2 material measured in the nanoindenter. The standard deviation is for ten separate indentations. Young's modulus is calculated from the load displacement curves using Oliver and Pharr model [186]. It allows calculating the hardness and Young's modulus from the slope of the unloading curve fitted with Oliver-Pharr nonlinear curve (not shown here).

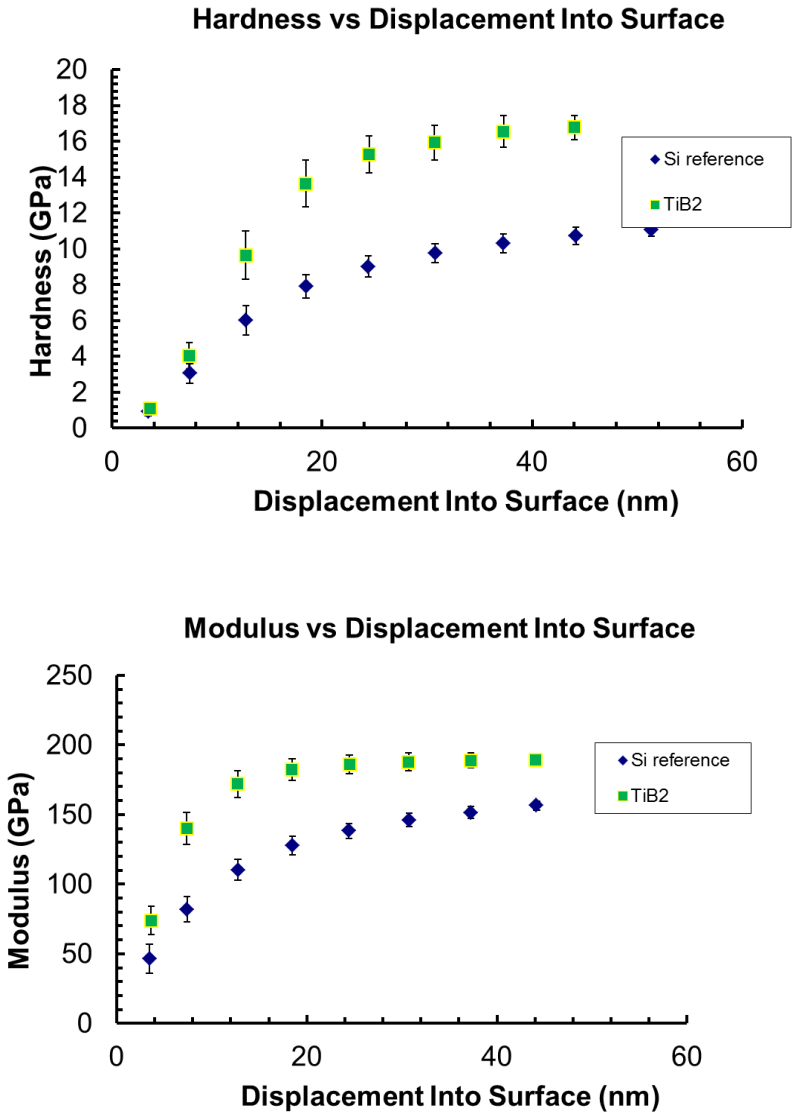

Figure 5.10 Hardness and modulus measurement of TiB_2 and silicon (10 indentations for each material at each indentation depth).

The TiB_2 material has thin native oxides with Ti-O, B-O layer of about 2 nm thickness on the surface. The initial low values of hardness and modulus possibly is due to the roundness of the indenter tip and the plastic region of TiB_2 during indentation [178, 179]. The hardness and modulus value reach stable value after about 30% indentation (20 nm) into film thickness. Han et al. [180] used model formulated by Yu et al. [181] to account for the mismatch in measurement due to presence of hard material (W) on top of

a soft material (silicon or glass). They studied the substrate effect by comparing the stiffness of thin layer with the stiffness of same material homogenous layer (S/Sh). For a hard thin (640 nm) layer on a compliant substrate the substrate effect decreased i.e. the stiffness of hard thin layer was less than the stiffness of homogenous hard layer. The thin soft substrate was silicon or glass and hard layer was tungsten. Our experiments show a value of 14 GPa for the TiB_2 material after an indentation depth of 30 nm for hardness measurement and 180 GPa for the modulus measurement at 15 nm depth (Figure 5.10). The book value of hardness and Young's modulus of thick titanium diboride layer is 25 GPa and 565 GPa [150]. Our value of hardness and Young's modulus are in close approximation to the measurement of 100 nm TiB_2 with a sharp Berkovich tip at 27 % and 17% film thickness depth (Hardness 18 GPa and Young's modulus 190 GPa) from literature [178]. The underlying silicon, when measured as a reference substrate, indicates hardness of 10 GPa and Young's modulus of 150 GPa. The book value of hardness and Young's modulus of silicon is 12 GPa and 170 GPa, respectively.

One of the factors that possibly affects the hardness and the modulus measurement is the pile up effect after the indenter is unloaded from the substrate [133]. Pile up causes sample material piling up at the edges of the indent, which in turn underestimates the contact area and provides a higher hardness and modulus value [182, 183]. The TiB_2 alloy exhibits an enhancement in the hardness as compared to that of titanium. The hardness and Young's modulus of titanium is reported to be 12 GPa and 188 GPa, respectively [151]. Addition of boron to titanium enhanced the strength and stiffness properties of this alloy [131, 132]. TiB_2 shows a hexagonal structure with boron atoms forming a covalent bond network in the titanium matrix structure [184]. Other Ti-B

compounds (less stable) are available in various processing of deposition but TiB_2 can be evaporated by e-beam since the phase diagram shows congruent melting [185].

Measurement of hardness of a thinner material layer is more complicated than that of a thicker material layer. For a thicker layer the indenter tip remains within the bulk material and provides the intrinsic material properties. However, thin layer measurement will show substrate effect [178, 180, 186, 187]. Therefore, the indentation of the tip should not exceed the thickness of the thin layer thickness [179]. Ideally, 10 % indentation depth is used for thin film hardness and Young's modulus measurement [188].

Endothelial cells respond well i.e. adhere, migrate, proliferate and differentiate on stiffer materials [87, 189]. The substrate hardness is one of the physical properties that control cell behavior both *in vivo* and *in vitro*. In culture, the cell spread area determines sensing of the substrate rigidity and accordingly changing of the cells shape [190]. Cells migrate towards stiff regions away from the softer ones. This is termed durotaxis. They also might become stiffer on a stiffer and hard matrix compared to the compliant substrates. Their adhesion mediated signaling results from sensing mechanical forces induced by stiff substrate material and generation of opposite reactive cell forces.

Grevesse et al. [191] studied effect of three different matrix rigidity of polyacrylamide hydrogel (2.5 kPa, 8.5 kPa and 25 kPa) on HUVECs. The single cell was seeded on a rectangular shaped micropattern coated with fibronectin having an area of 1200 μm^2. The cytoskeleton on the rigid substrate is more aligned as compared to the softer substrate.

To identify the hardness effect on HUVEC culturing, Bruni's group [119] used untreated titanium alloy Ti-6Al-4V and glow/ plasma discharge treated Ti-6Al-4V alloy at 10^3 Pa pressure using plain air for 2 h at 700 °C. The treated Ti-6Al-4V layer exhibited higher hardness (694 HK) and thicker layer as compared to untreated Ti-6Al-4V layer (353 HK). The higher hardness treated layer seems to provide better biocompatibility with HUVECs as compared to untreated samples.

5.1.4 BioAFM of HUVEC cultured on TiB_2 patterned substrates.

Peak Force Quantitative NanoMechanical property mapping (PF-QNM) mode of AFM was utilized for the measurement of surface adhesion and Young's modulus of the TiB_2, silicon and HUVEC cultured on TiB_2 patterned substrates. Two different sets of TiB_2 patterned on Si (or SiO_2/Si) were evaluated. One of the TiB_2 patterned substrates had cells growing selectively on only TiB_2 not on silicon (or silicon dioxide) (selective cell growth) and the other one had cells growing non-selectively on the TiB_2 patterned substrate (non-selective cell growth). The chips cultured with cells were fixed with glutaraldehyde (fixing protocol : Appenndix A) and analyzed using force distance curves obtained from the BioAFM. For reference measurement, a clean TiB_2 patterned substrate and a clean TiB_2 patterned substrate with glutaraldehyde fixative were used.

The Peak Force tapping mode works similarly to tapping mode and the only difference is its operation in non-resonant mode. The tapping oscillation is well below the cantilever frequency, hence avoiding the filtering effect. The piezo z-position during imaging in air is regulated by sinusoidal wave that drives the cantilever tip. The separation between tip and sample is calculated from the piezo z position and the cantilever deflection. The extension of z piezo is adjusted, as the tip scans the surface,

based on the feedback loop. The triggering at peak force allows extraction of data from noisy backgrounds. The ScanAsyst algorithm provides automatic control of optimizing the minimum force needed to track the substrate surface and also the feedback gain depending on the current condition of substrate at various locations [192, 193]. The BioAFM uses force curves to calculate the surface properties such as adhesion and Young's modulus of TiB_2 and silicon to observe their effect on the growth and adherence of HUVECs on the patterned substrates. The adhesion force obtained from the force curves indicate the influence of surface forces on the attraction of the AFM tip during the retracting (unloading force curve) cycle. The Young's modulus is obtained from the retracting force curves using Sneddon model. The other models available for Young's modulus calculation are Hertz and Derjaguin-Muller-Toporov (DMT) model [194, 195]. The Sneddon model is based on the contact theory of a rigid conical tip on an elastic half space. The Hertz model is based on the contact mechanism of a flat tip on an elastic half surface without considering adhesion force while the DMT model considers the adhesion force with the same flat tip. The Sneddon model also does not account for the adhesion force between the tip and the sample, hence providing a better estimation of the Young's modulus of the material. The Young's modulus in Sneddon model is calculated as given below

$$\mathrm{F}= 2 * E * d^2/\pi(1 - v2)tan\ \emptyset, \qquad \text{Equation 5.1}$$

where F is force, E is Young's modulus, d is indentation depth, $\emptyset$ is conical tips half angle and v is Poisson's ratio [152]. The rigid conical tip is used for our measurement of surface properties of material and the fixed cells. The Young's modulus depends on the

indentation depth (approximately 3 nm), force, Poisson's ratio (0.3) and the angle (10°) between the surface of indenter and the material surface plane.

5.1.4.1. BioAFM on clean TiB_2 patterned substrate and clean with glutaraldehyde fixative TiB_2 patterned substrate

Clean TiB_2 patterned substrate and clean substrate with fixative was used as reference for analyzing the presence of glutaraldehyde fixative and its effect on the measurements of Young's Modulus and adhesion on the substrate surface. Figure 5.11 indicates the presence of glutaraldehyde on the substrate surface after the AFM fixing protocol. The surface on the right side (Figure 5.11) had the fixative while the surface on the left side is with fixative partially removed with deionized water and Q-tip.

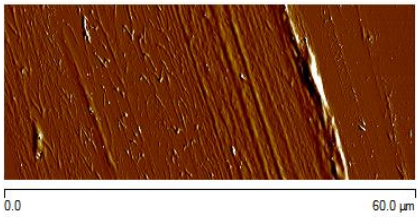

Figure 5.11 Glutaraldehyde fixative after fixing protocol. Fixative removed from titanium diboride surface with DI water and Q-tip.

The measurement of the Young's modulus and adhesion force is obtained from batch processing of 900 force curves for each measurement image. Due to plastic deformation on TiB_2, the retract curve traces below the approach curve as seen in Figure 5.12.

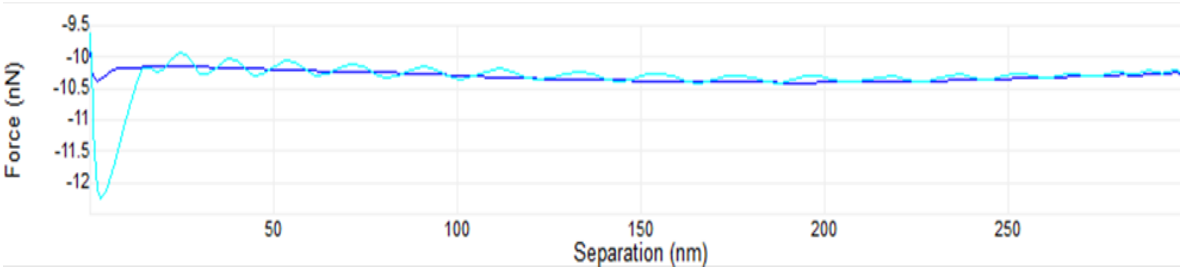

Figure 5.12: Force distance curve of TiB_2 surface. The dark blue is the approach curve and the light blue is the retract curve.

The frequency distribution of Young's modulus on clean TiB_2 and silicon with and without fixative layer was obtained from the 900 curves (for each frequency distribution graph) that were analyzed (Figure 5.13). TiB_2 shows an almost normal distribution of the Young's modulus while the silicon distribution is slightly skewed. This skew possibly is due to artifacts of the cantilever tip or presence of particles on the silicon/ SiO_2 surface.

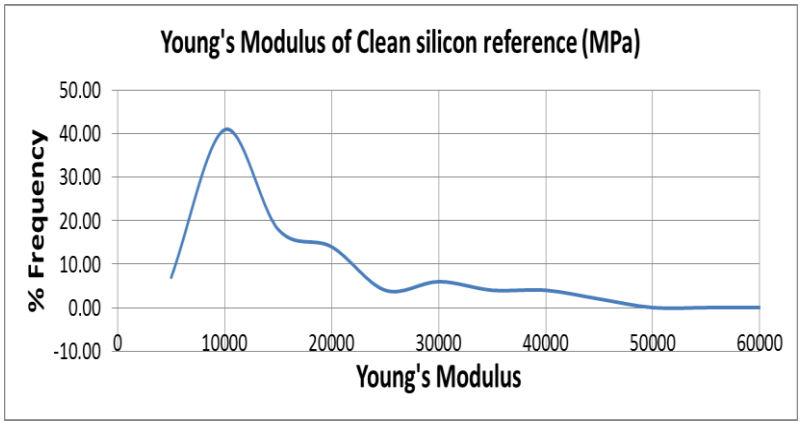

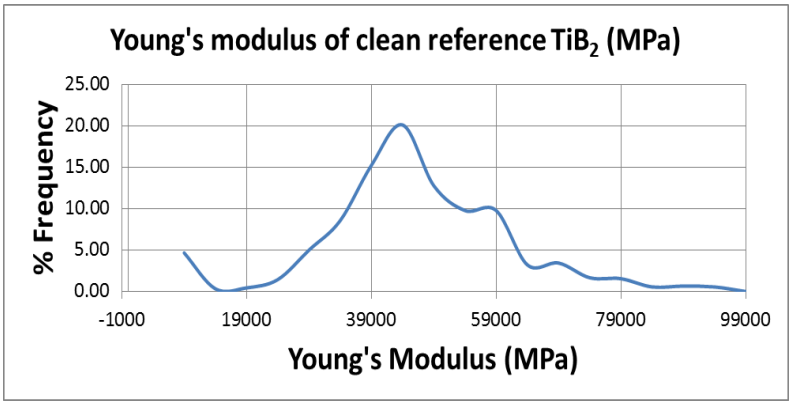

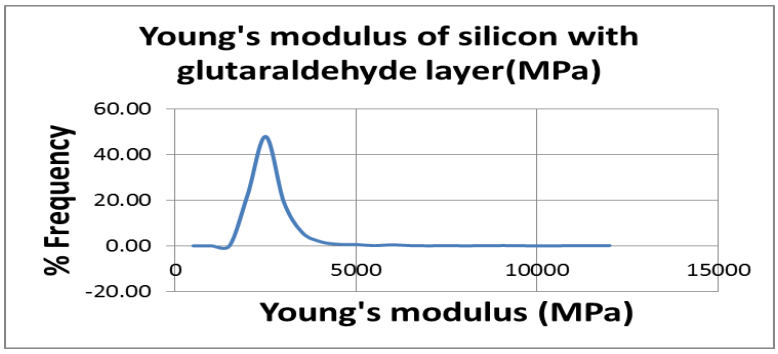

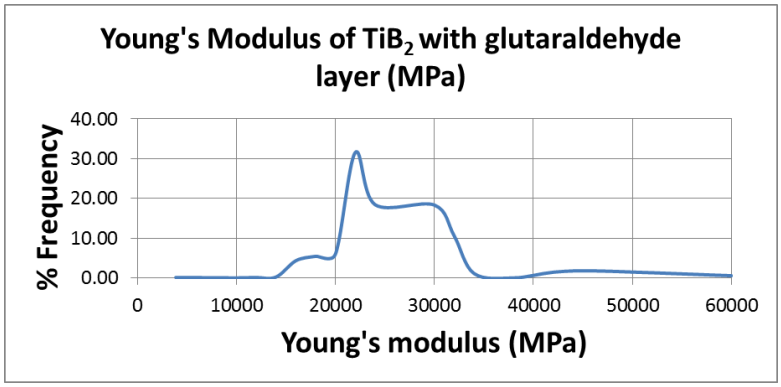

Figure 5.13: Frequency distribution of Young's modulus on clean silicon, clean titanium diboride, clean silicon with glutaraldehyde layer and clean titanium diboride with glutaraldehyde layer.

This distribution graph provided the mean/ median value of the Young's modulus and adhesion force with standard deviation. The Young's modulus and the adhesion force are enlisted in Table 5.2. The clean substrate without fixing layer indicate a higher Young's modulus and higher adhesion force for both TiB_2 and silicon as compared to substrates with the fixed layer. Even though the presence of glutaraldehyde decreases the Young's modulus and adhesion force values on silicon and TiB_2 as compared to the clean substrate, the values for TiB_2 are higher than that for silicon in both the cases (clean and clean with fixing layer substrate). The cells cultured on these substrates experiences different stiffness of these two substrates as seen in Table 5.3.

Table 5.2 Young's modulus, adhesion force and roughness measurement of silicon and TiB_2 on clean TiB_2 patterned substrate and clean with glutaraldehyde fixative TiB_2 patterned substrate.

Substrate	Silicon	TiB_2
Young's Modulus of Clean substrate in MPa (Reference)	Mean= 13,894 Median= 10,592 Mode= NA Stdev= 989	Mean=43,413 Median=42,835 Mode=41,898 Stdev=15,721
Adhesion (nN)	Mean= 38. 13 Median= 39.59 Stdev= 15.49	Mean=Median= 92.78 Stdev = 7.49
Roughness (nm)	2.50 to 4.00	2.00 to 3.50
Young's Modulus of Clean glutaraldeyde fixed substrate (Reference)	Mean=2,403 Median=2,278 Mode=2,068 Stdev=681	Mean=24,134 Median=22,397 Mode=22,397 Stdev=5,921
Adhesion (nN)	Mean=2.50 Median=2.89	Mean=4.53 Median=4.53
Roughness (nm)	3.00 to 4.00	2.00 to 3.00

Table 5.3. Young's modulus and adhesion force of silicon and TiB_2 on clean TiB_2 patterned substrate and clean patterned substrate with glutaraldehyde fixing layer.

Material	Silicon	TiB_2
Young's Modulus of Clean substrate in MPa (Reference)	10,592	42,835
Adhesion force (nN)	39.59	92.78
Young's Modulus of Clean glutaraldeyde fixed substrate (Reference)	2,278	22,397
Adhesion force (nN)	2.89	4.53

The roughness of 2 nm to 4 nm in Table 5.2 is comparable to the roughness of titanium diboride of 2 nm to 6 nm. Hence, the glutaradehyde fixative does not affect the roughness measurement of the surface but decreases the adhesion and Young's modulus values of the substrates with fixing layer. Chtcheglova et al. [196] mentioned more about the effect of fixing layer on cells and substrates. They detected the presence of globular large features on the cell surface that were formed due to fixing in glutaraldehyde. Their fixed cells showed an increase in stiffness after the glutaraldehyde fixation due to collapse of the membrane during the dehydration step of the fixing protocol.

The results of mechanical parameters obtained here by AFM do not match those from nanoindentation. AFM is a surface analysis where the indentation depth of the tip is approximately 3 nm while for a nanoindenter, the maximum indentation depth is 50 nm. AFM facilitates capturing of force distance curves of substrate and cell at the nanometer scale resolution. The Young's modulus of TiB_2 in BioAFM is comparable to the modulus of nanoindenter (Figure 5.10) at an indentation depth of 4 nm. AFM force curves provide

better nanomechanical property values since it measures surface properties of the material that the cell experiences during culturing [194].

5.1.4.2. BioAFM on fixed TiB_2 patterned substrate with specific cell growth

PeakForce allowed us to measure cells grown selectively on TiB_2 layers. There were no cells growing in the silicon substrate. The TiB_2 patterned substrate having cell growth only on TiB_2 were fixed and analyzed. The Young's modulus and adhesion force of silicon, TiB_2 and cells were calculated from force curves. The frequency distribution of Young's modulus TiB_2, silicon and cell growing on TiB_2 pattern only were analyzed from 900 curves for each distribution curve as seen in Figure 5.14. The Figure 5.14 (a) shows the optical image of cell attached to TiB_2 pattern and the Figure 5.14 (b) is the AFM height image of the respective cell nucleus region.

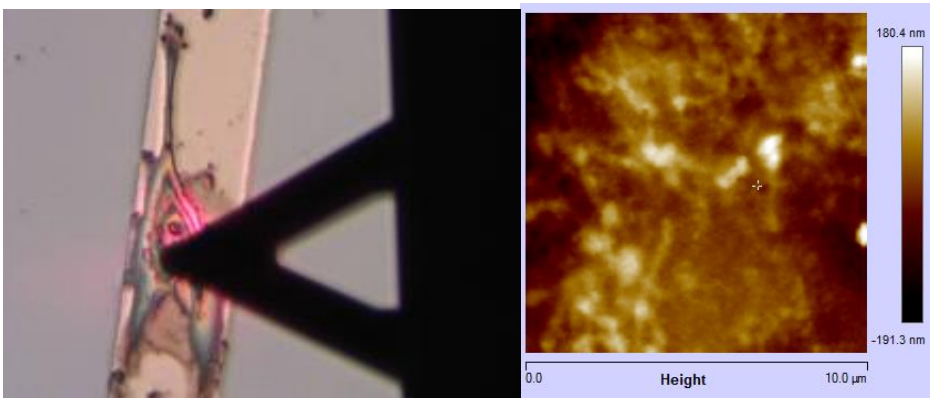

(a) (b)

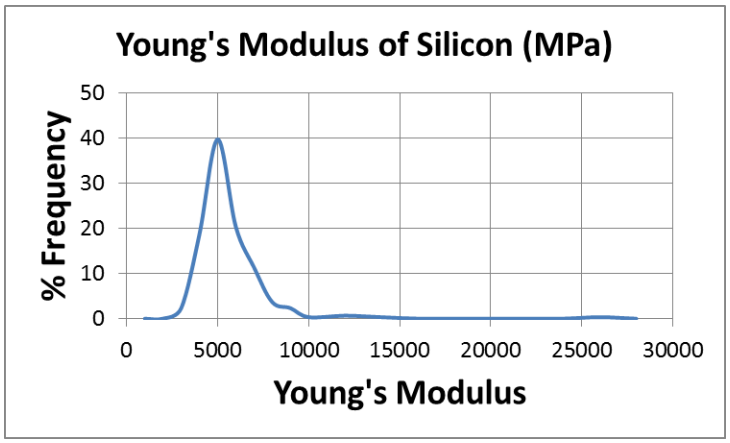

(c)

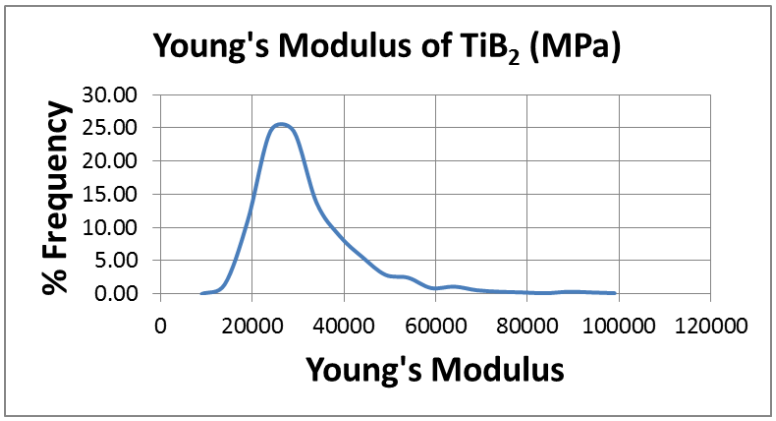

(d)

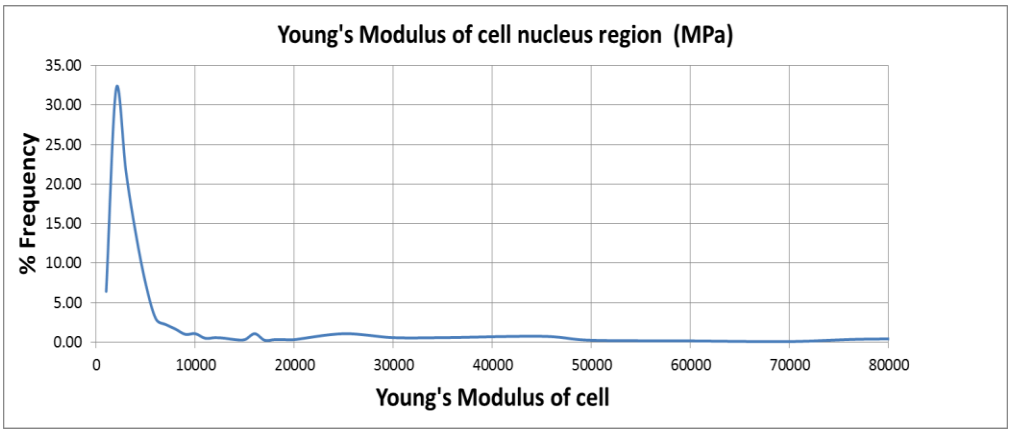

(e)

Figure 5.14 Frequency distribution of fixed and cell cultured (a) silicon (b) titanium diboride (c) cell optical on TiB_2 pattern. (d) Optical image of cell on TiB_2 pattern (e) AFM image of cell on TiB_2 pattern.

The Young's modulus, adhesion force and roughness of TiB_2, silicon and the cell are enlisted in the Table 5.4. The table provides the Mean/Median values along with the standard deviation. Both mean and median values are mentioned since the frequency distribution is not completely a normal distribution.

Table 5.4. Young's modulus, adhesion force and roughness measurement of silicon, TiB_2 and cell from fixed TiB_2 patterned substrate with specific cell growth

Substrate	Silicon	TiB_2	Cell
Young's Modulus in MPa (Sneddon model) Selective cell growth on TiB_2 only	Mean=5,039 Median=4,700 Mode=4,053 Stdev=1,787	Mean=29,545 Median=26,545 Mode=26,623 Stdev=3,617	Mean=2,679 Median=2,184 Mode=2,383 Stdev=1,806
Adhesion (nN)	Mean=1.298 Stdev=0.86	Mean=4.43 Stdev=0.21	-
Roughness (nm)	3.50 to 5.00	2.50 to 4.00	-

In selective cell growth, mechanical properties of materials used as substrate had difference in stiffness i.e. silicon stiffness 4,700 MPa and TiB_2 29,545 MPa. That corresponded to the adhesion forces which showed much larger value on TiB_2 4.43 nN as compared with Si 1.298 nN. Adding fixing layer of glutaraldehyde decreased the Young's modulus and adhesion force values indicating residual layer but maintained larger differences between TiB_2 and silicon. The Young's modulus and adhesion force of TiB_2 is larger than that of silicon. This is similar to our data from clean and clean substrate with fixing layer. The increase of Young's modulus of silicon from 2,278 MPa on substrate with fixing layer to 4,700 MPa for substrate cultured with cells and fixed

possibly might be due to presence of the cell on TiB_2 and protein secreted from the cell surface on entire material surface [197].

5.1.4.3. BioAFM results of cell stiffness on TiB_2 patterned substrate

Force curves on the fixed cell attached to TiB_2 patterned substrate were obtained. The cell stretched to a length of approximately 120 µm on a 50 µm width line (optical image in Figure 5.15). It is well documented that stiffness of micropattern and adhesion play an important role in growth and cell spread. From our results, where we have a harder TiB_2 material (Young's modulus ~ 26 GPa) and a constrained area (pattern), the cell stretching is restricted within the pattern. The Young's modulus of cell (nucleus region) has a wide distribution with a median value of 2,184 MPa. The cell Young's modulus is higher than that of a living cell due to the glutaraldehyde fixative effect. The gentle fixing is done to increase the hardness and to be able to have good resolution images as seen in Chtcheglova et al. [196]. Their Young's modulus of cell had increased to about 10 to 16 fold as compared to live cell imaging. The fixation enables the visibility of cytoskeleton as well [198]. The wide distribution of cell elasticity of cell is partly due to inhomogenous cytoskeleton structure in the cytoplasm [199]. Figure 5.15 (a) is the highest resolution peak force error image that shows the HUVEC adherence and growth only on TiB_2 pattern. The peak force (in the force curve Figure 5.12) is the vertical distance from the base straight line (starting point of the tip) to the maximum peak force point (indentation of the tip on the sample). The feedback of the peak force value from the force distance curves gives the peak force error image. In Figure 5.15 (b), the height profile shows the stretched cell on TiB_2 pattern with a height of 1.7 µm at the nucleus

region and Figure 5.15 (c) shows the 3D image. Figure 5.16 provides the adhesion force mapping of the TiB_2 (TiB_2 more adhesive as compared to silicon) and silicon.

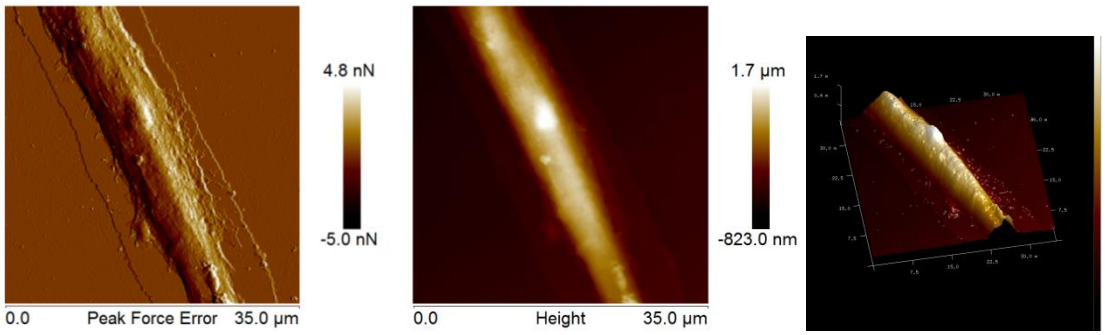

(a) (b) (c)

Figure 5.15 HUVECs were cultured on TiB_2 patterned substrate for 4 days and fixed with glutaraldehyde for BioAFM imaging. BioAFM fixed substrate of HUVEC cultured on TiB_2 pattern (a) Peak force error image, (b) Height AFM image and (c) 3D Height AFM image.

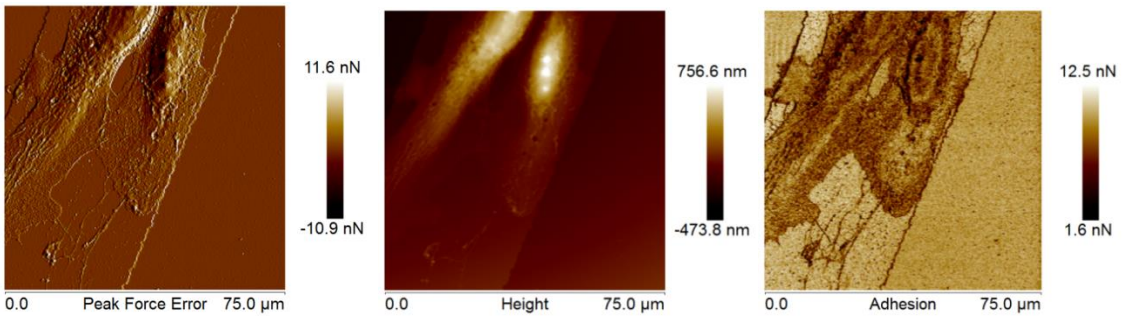

Figure 5.16 BioAFM fixed substrate of HUVEC cultured on TiB_2 pattern on day 4 (a) Peak force error image, (b) Height AFM image and (c) Adhesion AFM image.

The height profile in Figure 5.17 indicates the flattening of HUVEC on titanium diboride patterned substrates. The HUVEC edge (Figure 5.17 (b)) is flattened and exhibits the presence of cytoskeleton that has the highest height in the image.

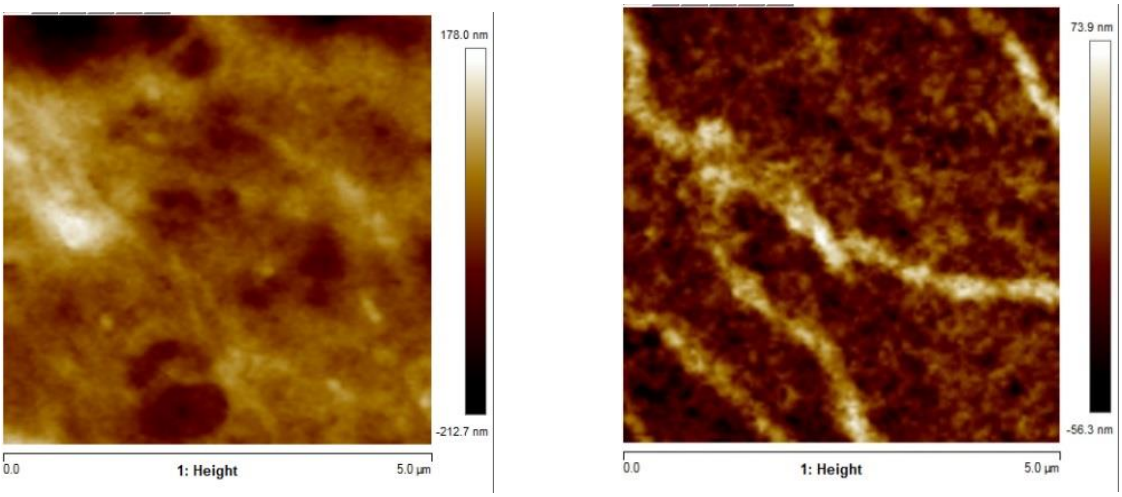

(a) (b)

Figure 5.17 BioAFM on fixed f HUVEC cultured on TiB_2 pattern on day 4 (a) Height profile of HUVEC nucleus, (b) Height profile of HUVEC edge.

The physiochemical properties of the artificial biomaterial control the protein adsorption contributing to cell survival and growth [118, 119]. Our AFM results show that TiB_2 has a more adhesive and stiffer surface than background silicon that possibly facilitates more protein adsorption on TiB_2. In studies of proteins adsorption conducted in the Fetal Bovine Serum (FBS) as the culture medium mainly albumin, vitronectin, fibrinogen and fibronectin [200, 201] were used. Horie et al. [202] studied the adsorption of proteins from cell culture medium with 10 % Fetal Bovine Serum (FBS) on TiO_2 particles. Albumin and fibronectin was observed to have adsorbed on the metallic oxide surface. The presence of divalent ions such as calcium and magnesium facilitated the adsorption of the proteins.

5.1.4.4. BioAFM on fixed TiB_2 patterned substrate with non-selective cell growth

TiB_2 patterned substrate with cell growing on silicon and titanium diboride were fixed. This substrate was analyzed to measure the Young's modulus and adhesion of silicon and TiB_2 to identify possible reason for the non-selective cell growth. The Figure

5.18 provides the frequency distribution of Young's modulus of Silicon, TiB_2, and cell on both silicon and TiB_2 obtained from analyses of 900 force curve for each frequency distribution graph.

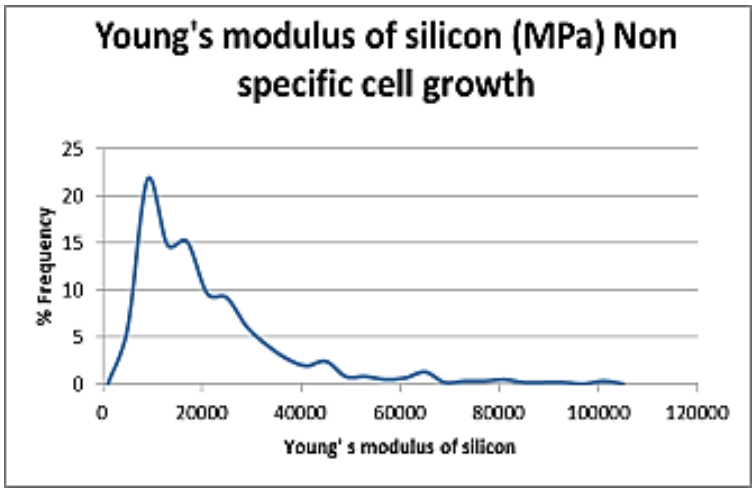

(a)

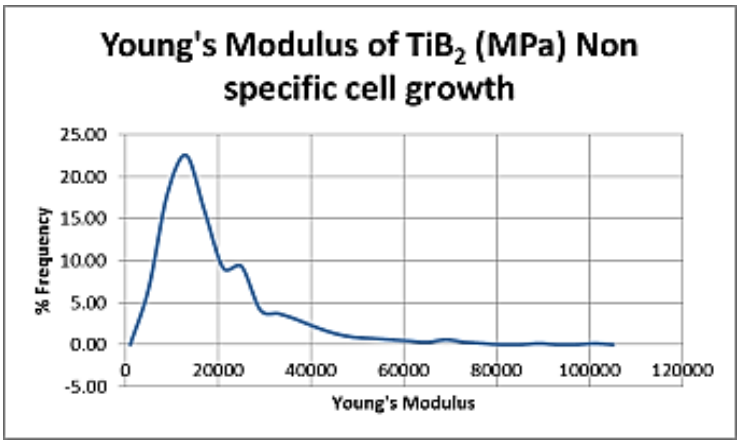

(b)

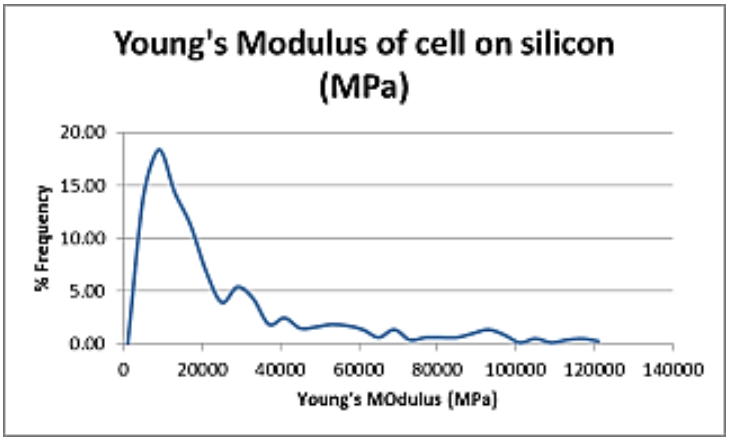

(c)

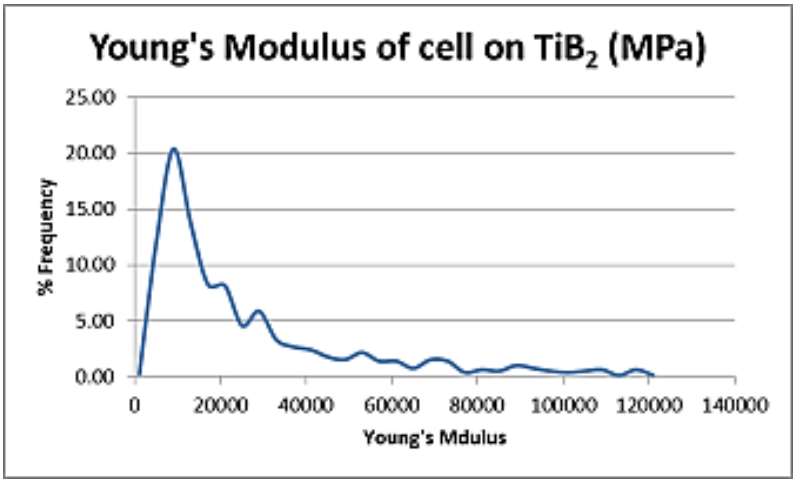

(d)

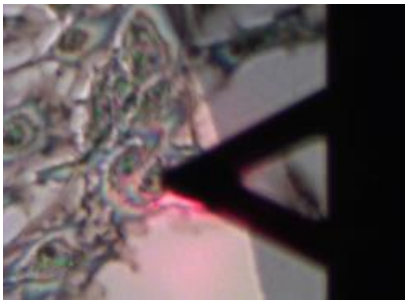

(e)

Figure 5.18 Frequency distribution of fixed and cell cultured (a) silicon (b) titanium diboride (c) cell silicon (d) cell on TiB_2 pattern (e) Optical image of cells on TiB_2 pattern.

The Table 5.5 enlists the Young's modulus, adhesion force and roughness of the TiB_2 and silicon surface that had cells growing over the entire substrate. The fixed sample

with non-selective cell growth does not show any significant difference in the modulus and adhesion force values of TiB_2 and silicon. The cell's Young's modulus on TiB_2 and silicon is also provided.

Table 5.5. Young's modulus, adhesion force and roughness measurement of silicon, TiB_2 and cells from fixed TiB_2 patterned substrate with non-selective cell growth

Substrate	Silicon	TiB_2	Cell
Young's Modulus in MPa (Sneddon model) Non selective cell growth	Mean=19,282 Median=14,820 Mode=13,113	Mean=18,978 Median=13,830 Mode=5,236	Cell on silicon Mean=123,907 Median=15,697 Mode=10,267 Cell on TiB2 Mean=93,571 Median=18,471 Mode=27,143
Adhesion (nN)	4.48 ± 2.59	4.28 ± 2.46	-
Roughness (nm)	4.00 to 5.50	3.50 to 5.00	

In the case of non-selective cell growth both parameters, Young's modulus and adhesion force, are comparable. Interestingly, Young's modulus of silicon is increased significantly while for TiB_2 the values are smaller. That indicates deposition of layer on the patterned substrate surface. Substrate preparation before seeding used simple cleaning processes (acetone, Isopropyl alcohol in ultrasound at 50 °C) followed by DI water that should not leave residual layers. However, storage of silicon wafers with patterns in air in boxes and changes in time due to various reasons (laboratory handling) typically results

in organic depositions that changes surface properties manifested by a contact angle change. Hydrophobic surfaces (> 90 °) with large contact angle become more hydrophilic and superhydrophilic surfaces (0 °) become much less hydrophilic (30 °) [203]. Standard RCA cleaning processes used in Si processing could not be used in our samples because H_2O_2 included in all RCA steps etch TiB_2.

To determine all individual mechanisms responsible for force curve repulsion requires quite involved characterization and subsequent modeling. In the case of our results, most probably there were surface contaminants that did not appear to change hydrophilic/ hydrophobic behavior but might have influenced mechanical parameters after cell growth.

The presence of contaminant might have caused non-selective cell growth. The cells growing non-selectively have neighboring cells signaling that restricts its stretching on the substrate. The broad range of the measured cell stiffness corresponded to the region of sharp tip AFM scan such as on the nuclei (on the bulge) or on the lamellopodia (cells stretched perimeter area) and on the extent of cell stretching. The Young's modulus of the fixed cell periphery on silicon was approximately 15,697 MPa and that on TiB_2 was 18,471 MPa. The stiffness of cells on silicon and titanium diboride is similar since they are attached to the substrate having similar Young's modulus

Cell density and cell to cell interaction on biomaterial substrate possibly affects the measured mechanical properties of cell as reviewed by Mason et al. [204] and C.S. Chen et al. [205]. Chiou et al. [206] revealed that the presence of surrounding cells at confluency on the substrate increases the individual cell stiffness. Elongated stretched cell shape indicates highly organized cytoskeleton while spindle shaped cell morphology

has a randomly oriented cytoskeleton. The lampellopodia edge region has lower stiffness. However, Sato et. al showed results that cell stiffness is larger at the edges as compared to the nuclear region which is contradictory to what was demonstrated by Chiou et. al [206]. Also, since the lamellopodia edges are thinner (about 200 nm) their measurement might be affected by the substrate present beneath it. Mathur et al. [208] demonstrated that the Young's modulus of live cells were 7 KPa, 3 KPa and 1 KPa at the nucleus, cell body and edge, respectively. The cell elongation or stretching takes place by the edges of the lamellopodia, thus the lamellopodias form weak adhesion as compared to the nucleus region [207]. In addition cell stiffness will depend on the size of the micropatterned area, the substrate rigidity and the presence of neighboring cells.

We cannot exclude that after HUVEC adhesion there may be extra cellular matrix secretion by HUVEC, which could possibly cause lower value of Young's modulus of the TiB_2 and higher on Si material surface. The natural EC secreted ECM is complex and dynamic comprising of biologically active components. Xue et al. [209, 210] studied the ECM secreted from EC on pure titanium and characterized the ECM morphology and its chemical composition. The initial cell adhesion takes place due to surface properties of the material and the later interaction takes place with the biological adhesive molecules that are secreted by EC. They determined that the ECM secreted by EC comprised of fibronectin, laminin and type IV collagen facilitates adhesion and proliferation of the cells and inhibits platelet adhesion.

Other report showed that ECM secreted (collagen and fibronectin mainly) by EC have varied stiffness based on the protein density secreted. Tu et al. [210] reported ECM secretion from HUVECs cultured *in vitro* on titanium that enhanced its cytocompatibility

and haemetocytobility. These titanium substrates after 6 months implantation in canine arteries exhibited confluent monolayer of cobblestone type morphology of endothelial cells. Lavigne et al. [211] conducted HUVEC culturing on aluminum spots functionalized with silica groups to characterize the ECM deposited by the HUVEC on the substrates using mass spectroscopy. After 7 days of culturing till cell confluency on substrates, the mass spectroscopy of the substrates after cell removal showed the presence of fibronectin and fibrillin in the HUVEC synthesized ECM on the silica functionalized aluminum spots. The exact ECM components were not identified but the main components, fibronectin and fibrillin, was identified in the mass spectroscopy. ECM secreted by HUVEC on the substrates facilitates better cell growth and proliferation. This secreted ECM replicates the natural ECM of HUVEC to which it is adhered/ attached.

5.1.5 Water contact angle measurement

The sessile drop technique was used to measure the contact angle silicon and titanium diboride to identify its hydrophilicty/ hydrophobicity. The contact angle measurement indicated the hydrophilic nature of our TiB_2 material giving a contact angle value of 20° (Figure 5.19). An unclean substrate (67°) still showed a hydrophilic nature but lesser hydrophilic than an ultrasound cleaned substrate. Wettability of a surface is due to surface tension of the substrate, surface tension of the liquid and the interfacial tension. The force between the liquid and solid, also known as the interfacial tension, counteracts the surface tension of the substrate. With more attractive forces between the liquid and substrate, the interfacial tension is lower and tends to spread the liquid over the substrate surface [74].

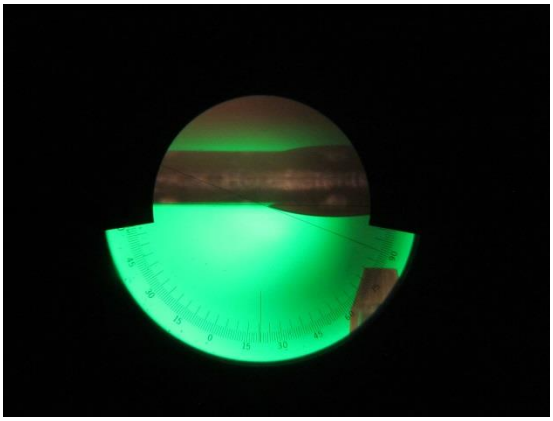

Figure 5.19 Contact angle of cleaned TiB_2 substrate.

The contact angle measurements can be used to calculate the surface energy of the substrate from the equation given below [213].

$$E_s = E_{lv} * \cos \theta, \qquad \text{Equation 5.1}$$

where E_s is the surface energy of contacting surface, E_{lv} is the surface energy between liquid (water) and vapor (air) is 72.8 mJ/ m^2 (with dispersive component as 21.8 and polar component as 51 mJ/ m^2) at 20 °C and θ is the static contact angle. For the cleaned TiB_2 substrate having static contact angle of 20 ° (hydrophilic), the surface energy is calculated as 68.41 mJ/ m^2 from equation 5.2 The unclean TiB_2 substrate with a contact angle of 67 ° had surface energy of 28.44 mJ/ m^2. Thus, the surface energy increases from 28.44 mJ / m^2 to 68.41 mJ / m^2 with hydrophillicity change from 67 ° to 20 ° as the substrate is cleaned with ultrasound cleaner. The surface energy of a substrate is comprised of dispersive (non polar) and polar components. The non polar component is affected by surface roughness while polar component is due to the presence of polar groups and electric charges on the substrate surface [212].

Surface energy of a biomaterial depends on several characteristics such as surface chemical composition, surface roughness and surface charge. Thus a balance of all physical, mechanical, electrical, and chemical properties provides a suitable biomaterial

surface for endothelization. Obtaining the exact balance of all the properties is not possible since each of them acts as variable during experimentation. Khang et. al [213] showcased that increase in roughness (nanometer and micro roughness) of titanium enhanced the surface energy and in turn increased the endothelial cell adhesion density and aspect ratio of cells as compared to flat titanium surface.

Lu et al. [214] also studied the endothelial cell response on flat titanium, nanorough surface and microrough titanium surface. They concluded better cell attachment and growth on the nano-rough and micro-surface as compared to flat titanium surface over a period of 5 days. The increase in roughness from flat to nanometer and submicron rough surface correspondingly increased the hydrophilicity from 42 ° to 31 ° and 18 ° (decrease in contact angle) of the material surface. Li et al. [215] concluded that increase in nanoroughness increases the hydrophilicity of titanium substrate (contact angle 31 °). The increase in hydrophilicity is possibly due to higher content of hydroxyl group on the material surface.

Titanium show typically hydrophilic properties and has strong affinity to oxygen, so titanium dioxide is naturally formed on its surface. TiO_2 has a high dielectric constant (50 – 170), that's causes strong van der Waal's bonds and electrostatic forces due to polarization effect of titanium making the surface hydrophillic. The adsorption of protein such as albumin, IgG and fibrinogen is maintained when adsorbed on the titanium dioxide surface [216]. Hydrophilic surfaces have a high surface energy while the hydrophobic surfaces have low surface energy. From other research studies it has been observed that the surface wettability probably influences the adsorption of proteins from the culture medium onto the substrates. These substrates then act as the adhesion sites for

endothelial cell attachment. Wachem et al. [217] results showed the less protein adsorption takes place on highly hydrophilic and highly hydrophobic surface and did not necessarily enhance biocompatibility of the material. A highly hydrophobic surface gave less biocompatibility due to increased cell affinity on the substrate and a highly hydrophilic surface hindered the cell to cell interactions [74].

Results of AFM obtained by Choi et al. [218] have shown reduction of adhesion force on hydrophobic silicon surface after hydrofluoric acid (HF) etch compared to traditionally cleaned silicon surface with silicon dioxide termination. They attributed these results to reduction in capillary force between the sample and the tip. Xi et al. [219] also characterized adhesion forces on hydrophilic/ hydrophobic silicon surface obtained with and without HF etch and recorded larger adhesion forces on hydrophilic than hydrophobic surfaces.

In addition, the dependence on humidity in atmosphere was strong on hydrophilic surfaces but much smaller on hydrophobic surfaces. However, the roughness of the surface that developed during cleaning process could have played additional role. Such roughness dependence of hydrophilic/ hydrophobic have been recorded on various materials by Maghsoudy et al. [220]. Here again dependence on humidity was recorded on several hydrophilic graphite but not on hydrophobic materials. Wenzel effect [109] explains the effect of roughness on hydrophilic/ hydropbhobic surface. The hydrophilic surface becomes more hydrophilic and the hydrophobic surface becomes more hydrophobic.

Chen et. al [79] had modified the roughness of the Ti-O film surface by Ar plasma etching. The etching process over time of 5 mins to 60 mins gave reduced roughness of

1.1 nm from 1.9 nm along with increased hydrophillicity. They concluded that the reduced roughness and hydrophillic nature of the surface had enhanced the biocompatibility of the film surface with the endothelial cells. This was in agreement to the behavior of cells on our patterned TiB_2 substrates. The latest trend is to develop tiatanium alloys with desired biocompatible characteristics for HUVEC and HUVEC-MSC co-culture that includes mild roughness surfaces with hydrophillic properties as well as Young's modulus in the range of 7 – 25 GPa. Examples of tested titanium alloys areTi-6Al-4V, Ti-6AL-7Nb, Ti-12Mo-6Zr-2Fe and Ti-13Nb-13Zr with Young's modulus in the range of 55 – 85 GPa [221, 222].

5.1.6 Effect of surface charges

Surface charge also plays a critical role in protein adsorption and subsequent cell adhesion and growth. The surface properties of the passive oxide layer formed on titanium and its alloys used as implants were examined for the presence of surface charge [128]. Zeta potential provides the potential on the surface of a substrate material. The presence of chemical groups on the material surface produces the surface charge. The most effective technique for zeta potential measurement is to apply an electric field to a suspension with particles made of this material in the electrolyte and by measuring the motion of the particles across the electrodes. The particles will travel faster if they are highly charged. This method is known as electro-phoresis [223].

When a material is placed in an electrolyte solution, an electrical double layer occurs on the solid material surface. The double layer comprises of two layers of charges, one of the layer (on solid material) is the surface charge caused from the adsorption of ions from electrolyte on the material based on the materials chemical functional

composition. The second layer in the electrolyte is made up of ions that are electrostatically attracted to the surface (known as Stern layer) and is a broader surrounding diffuse layer.

Titanium oxide in water forms hydroxyl groups on the surface. Since titanium oxide is amphoteric, these hydroxyl groups might be either positively charged on negatively charged based on the surrounding fluids pH. In case of an acidic environment, the surface obtains a positive charge inhibiting adsorption of positively charged proteins. In a basic solutions, the titanium oxide surface becomes negatively charged [170]. Based on the nature of oxide, at a particular pH the surface will have zero charge and this pH is called point of zero charge (pzc). The pzc of titanium oxide is 6.2 and at physiological pH titanium oxide surface has a negative charge. [224, 225]. Zeta potential for TiO_2 and SiO_2 is shown in Figure 5.20, where TiO_2 acquires positive charges at pH below 6.2 while SiO_2 has negative charges in any relevant pH solutions.

Titanium dioxide and silicon dioxide are negatively charged with corresponding zeta potential of -20 and -40 mV at physiological pH [226]. This negative charge facilitates protein adsorption such as albumin from cell culture medium. Guo et al. [122] demonstrated a surface modification method sandblasting to induce negative charge on titanium oxide surface. This negatively charged surface provided better protein adsorption such as albumin and in turn endothelial cell adhesion and growth. Tofail et al. [227] conducted electrical modification of titanium surface to enhance its interaction in biological environment. The cell and solid surface interaction takes place due to the presence of van der Waals and electrostatic charges. Cells and natural biomaterials are

generally negatively charged that causes a repulsive electrostatic energy between the cell and biomaterial surface.

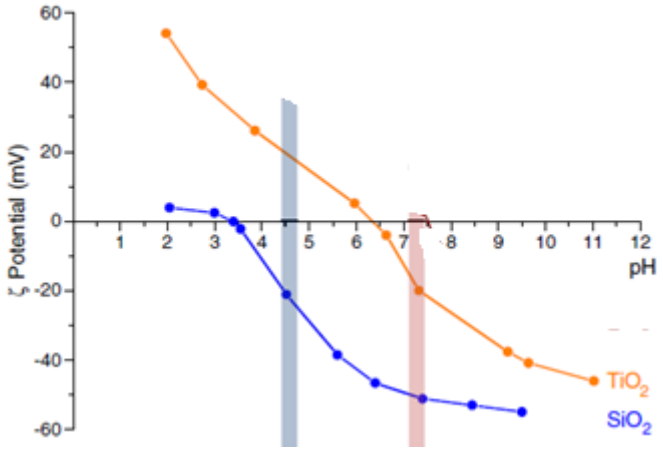

Figure 5.20 Zeta potential of (a) Titanium dioxide (b) Silicon and silicon dioxide [226].

Various factors such as surface roughness, surface hardness, Young's modulus, wettability, surface energy, adhesion force and surface chemical composition affects the final cell adhesion and growth on the substrates. Increase in roughness of TiB_2, depending on the roughness range, increases the surface area of providing decrease in wettability and increase in surface energy. This increased surface energy possibly increases the cell adhesion and cell growth on TiB_2 substrates. Material characteristics of TiB_2 such as mild surface roughness of 2 nm to 4 nm, stable chemical composition with thin native surface oxide layer, high hardness of 14 GPa, Young's modulus of 180 GPa and adhesive force possibly facilitate the adhesion and growth of HUVECs and MSCs on it. A number of titanium alloys are presently used for biomedical applications and surface modification or chemical treatments are incorporated to obtain a suitable material based on the application. The addition of boron to the titanium enabled higher hardness of the material.

The surface characteristics of TiB_2 show inert properties and they depend on surface composition, roughness, surface energy, hardness and charges. It is difficult to differentiate the effect of individual characteristics. The presence of grain boundaries causes increase in surface area and increase in surface energy with energy stored in the grain boundaries. The long term protein adsorption and cell attachment depends on the synergistic material surface characteristics. Important aspects are the cleaning and sterilization processes that affect the wettability of the material. Difference in wettability possibly might have direct effect on the type of protein adsorbed on the surface and eventually the cell attachment [216].

The unsaturated dangling chemical bonds on the material surface form strong bonds with molecules from the environment. Kasemo et al. [228] showed the influence of cleaning and sterilization on titanium implants. The outermost surface of titanium comprised of 2-5 nm TiO2 oxide layer. This oxide layer had hydrocarbons and inorganic impurities on the outer surface. The composition, morphology and topography has been well documented in literature but there is no prediction of the effect of the contaminant layer on the surface. The interaction between the biological systems takes place at this surface interference. The presence of contamination and impurities can be analyzed by surface analysis spectroscopy since both would have different surface chemical composition. Minor changes during the processing, cleaning and sterilization procedures will affect the biological properties of the material [229].

Specific and non-specific cell growth takes place either due to material surface properties or through the type of cell culture medium used. Using UH culture medium,

specific or non-specific cell growth takes place due to surface handling or cleaning processes of the material.

Chapter 6**: Results and Discussion**: Biological Characterization

Various materials such as silicon (Si), silicon dioxide (SiO_2), hafnium boride (HfB_2), silicon nitride (Si_3N_4), and titanium diboride (TiB_2) were evaluated to select a biomaterial for Human Umbilical Vascular Endothelial Cells (HUVEC) and Mesenchymal Stem Cells (MSC) growth. HUVEC growth was observed on silicon nitride, titanium diboride and hafnium boride. Silicon and silicon dioxide, surfaces did not support HUVEC adhesion. The initial cell attachments are favored by the hydrophilic/hydrophobic nature of the material surface and its chemical composition. Since titanium has been traditionally used for stents and implant materials for ages, we selected titanium diboride for our research as a prospective biomaterial. The material characterization of titanium diboride exhibited favorable mechanical and physical properties for cell adhesion, culturing and growth. The rigidity and hydrophilicity (high surface energy seen in contact angle measurement) of TiB_2 patterned substrates of different micropatterns indicated a striking specificity in the cell growth only on the TiB_2 pattern.

6.1 Single cell cultures

TiB_2 layers patterned on Si/SiO_2 substrates were analyzed for biocompatibility with culturing of HUVEC, MSCs and islets of Langerhans. The attachment of these cells on the substrate material over time indicated no cytotoxic effect of the material on cells.

6.1.1. Qualitative analysis

6.1.1.1. Human Umbilical Vein Endothelial Cells (HUVEC)

Single-cell cultures of HUVECs on silicon and SiO_2/Si substrates with titanium diboride patterns were evaluated to test the biocompatibility of this material. The pattern

included squares ranging in size from 50 µm to 200 µm and varying diameter ring shaped pattern of 20 µm width. As seen in Figure 6.1, HUVEC adhered and grew only on the titanium diboride pattern exhibiting a striking preference for TiB_2 and not silicon/silicon dioxide. The silicon and SiO_2/Si background material surface was devoid of cells.

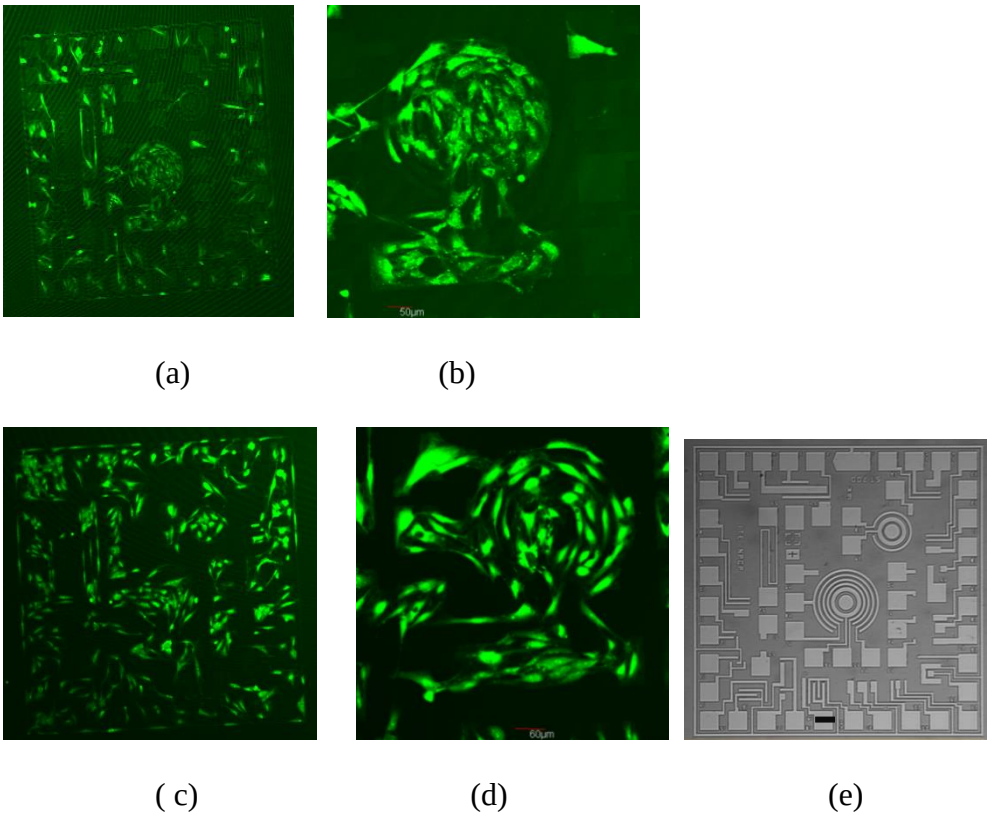

(a) (b)

(c) (d) (e)

Figure 6.1 HUVEC cell adherance on titanium diboride pattern. (a) and (b) are Day 7 Images. (c) and (d) are Day 9 images. HUVEC were seeded on two substrates (0.5 mm*0.5 mm size each) at a seeding density of 50,000 cells per substrate. The substrates were stained with 5 µl Acridince Orange for 20 min on day 7 and day 9 and were imaged using a confocal laser microscope at excitation wavelength of 488 nm. (a) and (c) are images acquired using a 4X objective and images in (b) and (d) are acquired using a 20X objective, (e) Optical image of titanium diboride pattern on silicon. Scale-200 µm.

6.1.1.2. Islets of Langerhans

The attachment of islet of Langerhans on titanium diboride surface was evaluated by seeding them directly on the patterned substrates. In the lines and circles pattern the circle diameters ranged from 100 µm to 500 µm to facilitate to accommodate the

physiological islet size. The islets had to be carefully seeded on the circular pattern and the culture medium was changed every alternate day. Figure 6.2 shows an islet attached on the substrate, on day 4 after initial seeding. The islets are not firmly attached to the surface and wash away easily. The objective was to observe the attachment of the islets in the absence of any other cell type such as HUVEC and MSC.

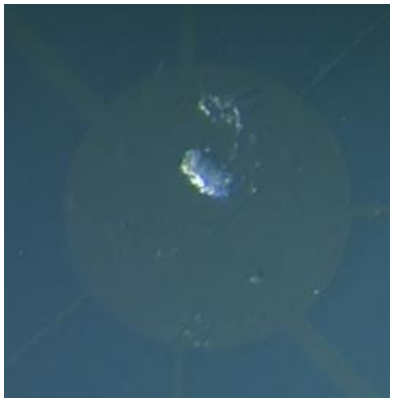

Figure 6.2 Islet attached on titanium diboride circle pattern of 500 µm diamter till day 4. The islets were 12 days old when seeded on the substrate.

6.1.1.3. Mesenchymal Stem Cells (MSC)

TiB_2 patterned substrates were used to evaluate the potential of cellular patterning to control MSC behavior such as adhesion and growth. MSC were cultured in contact with substrates for time periods up to 24 days in MSC culture media. The samples were analyzed for cell adhesion and morphology using optical microscopy. Our results (Figure 6.3) demonstrate that material properties influence MSC behavior in vitro. MSC grow non-pattern specific till Day 6 and eventually start migrating towards the TiB_2 line and circle patterns. From day 9, MSC are only adhering to the circles in the form of 3D spheroids and remain there until Day24 with a decrease in the diameter of the MSC agglomerates. After the MSC migrate to the TiB_2 patterns on the substrates, they agglomerate on the circular patterns to form clusters (Figure 6.4).

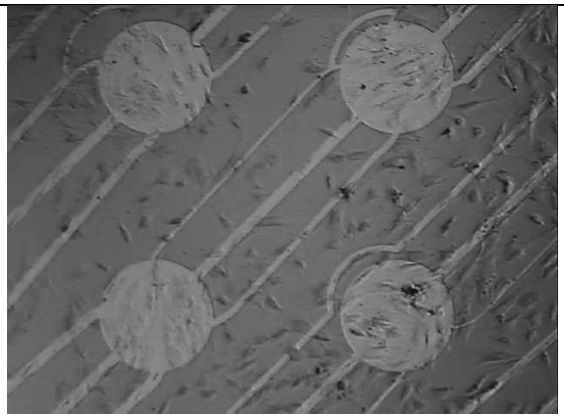 Day1	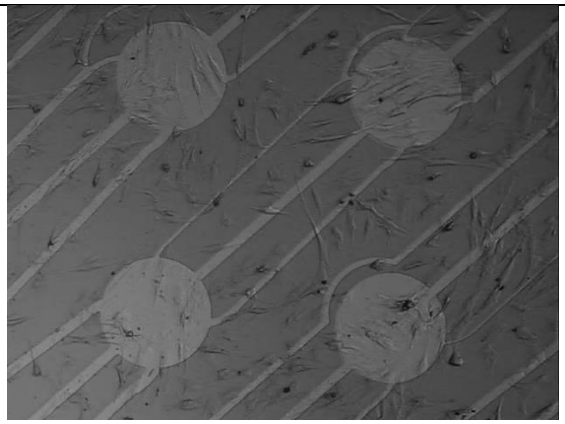 Day2
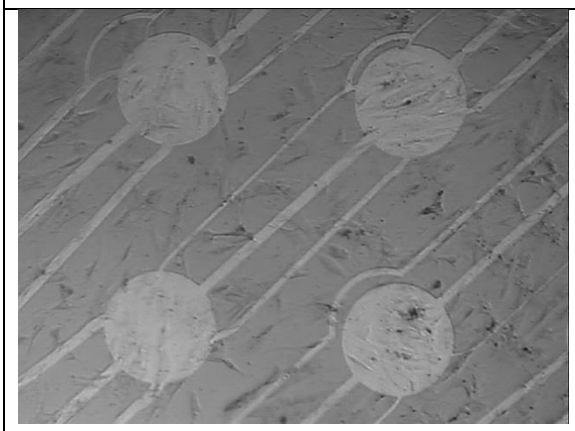 Day3	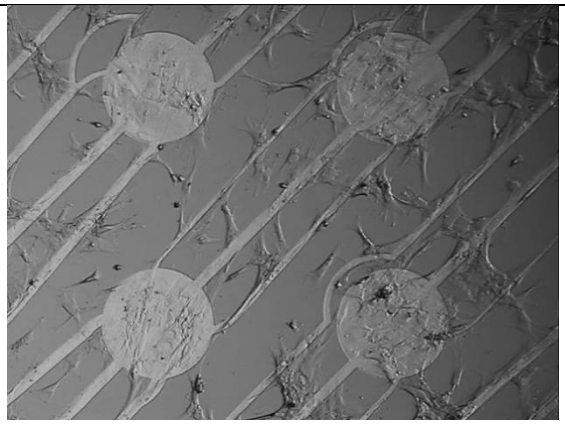 Day4
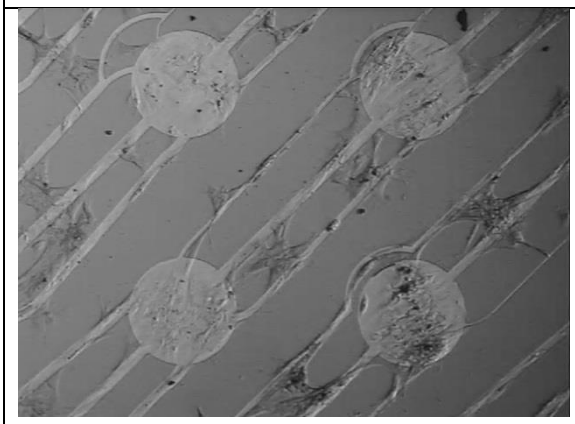 Day6	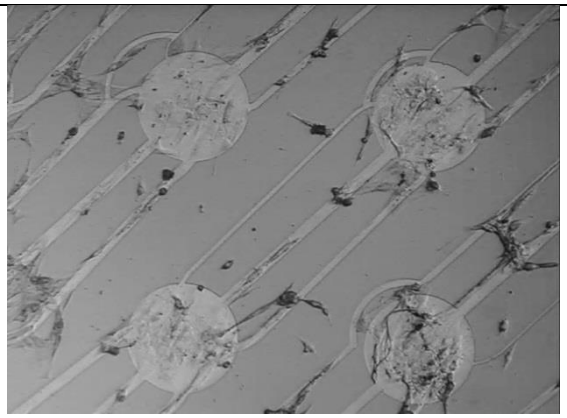 Day7

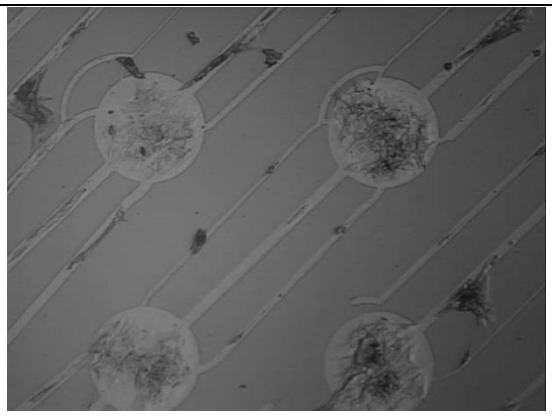

Day9

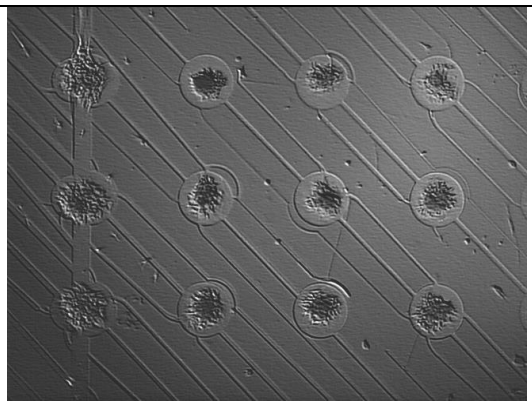

Day13

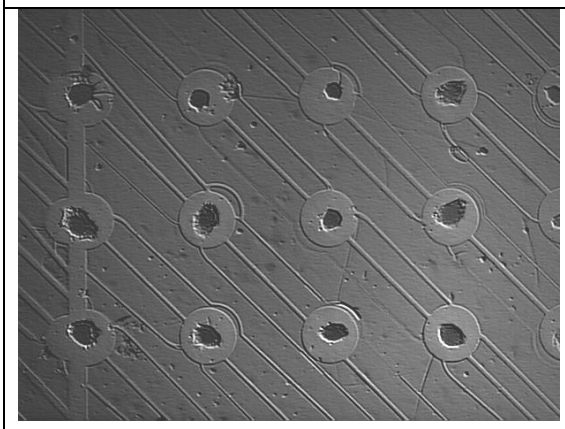

Day17

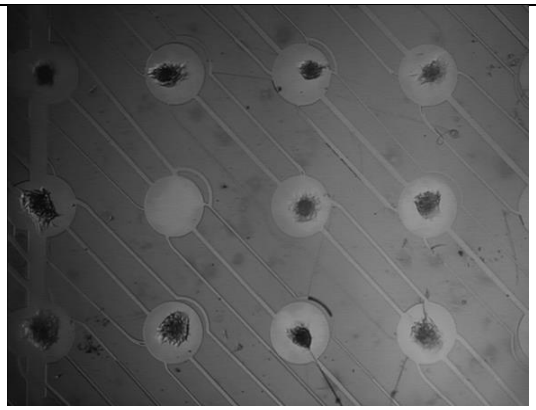

Day22

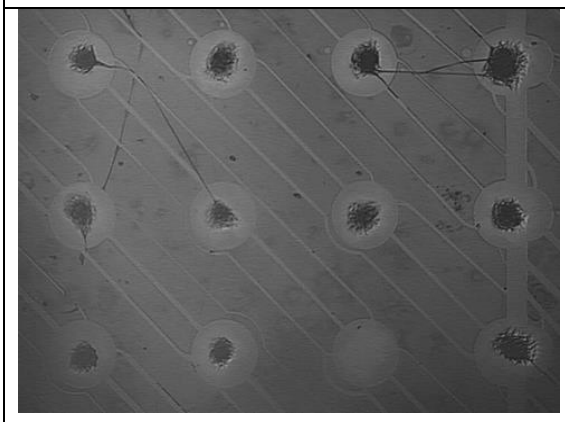

Day24

Figure 6.3 Mesenchymal Stem Cells growth on TiB_2 circle and line patterned substrate over a period of 24 days. The substrates were seeded at a cell density of 30,000 cells per substrate.

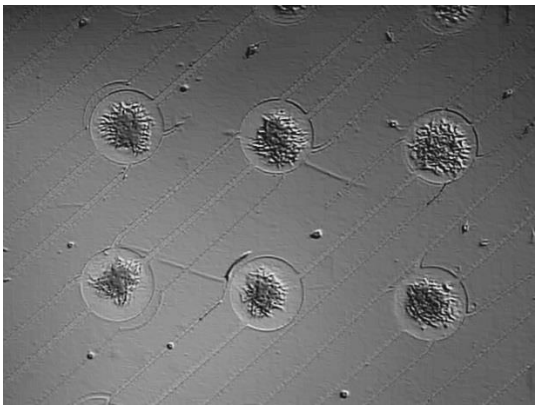

Figure 6.4 Mesenchymal Stem Cell spheroids (3D structure) on TiB_2 circles on day 13.

The results of this study support the idea that certain surface patterns can induce techniques for interesting behavior and possibly can be used further for differentiation [40]. Even though the material properties of silicon and titanium diboride are different such as surface energy, hardness, and chemical composition, the initial MSC adhesion takes place on both the materials. After few days of culturing, the MSCs migrate in response to the stiffness gradient imposed by titanium boride patterns and start aligning and growing along the micropattern design. This behavior of MSCs can be utilized for confining the cells on specific patterns and using them for further differentiation into other cell types. The silicon and titanium diboride surface in exposure to atmosphere forms a thin (2 – 5 nm) native oxide layer. The silicon dioxide and the titanium dioxide formed on silicon and titanium diboride respectively have hydrophilic surface properties which possibly are experienced by MSC at the point of adhesion. After days of culturing, the MSCs experience the surface properties of titanium diboride and begin growing specifically only on the titanium diboride pattern.

Myllymaa et al. [230] shows a reverse behavior of MSCs with cells initially growing specific on titanium patterns squares on silicon substrate and after five days begins to exceed the square area and spreads into the background silicon area. They

attribute this behavior of MSC to the chemical composition difference of the materials. The wettability/surface free energy also plays an important role in the MSC adhesion and growth behaviour. Iskander et al. [231] studied the growth of MSC on titanium patterned substrates. They reported enhanced cell adhesion on small micrometer patterns compared to larger patterns.

6.1.2. Quantitative analysis

6.1.2.1. HUVEC growth and viability

Fluorescence staining of HUVEC with acridine orange was utilized to observe the viability of HUVEC on titanium diboride material and as an in vitro biological assay for cell viability. Cell viability provides a relative measurement of biocompatibility over time. Satisfactory cell growth (lack of rounded cells) on TiB_2 substrates until 13 days of culture indicates lack of toxicity of the material. HUVEC cultured on TiB_2 circle patterns specifically adhered and grew on the TiB_2 pattern. Confocal images of the HUVEC over time demonstrate cell viability on 450µm diameter TiB_2 circles for a period of 13 days. The cells are retained within the circle throughout the culture period thus indicating contact guidance. As the days proceed, cells on the circle boundary stretch along the periphery and center cells tend to stretch randomly as seen in Figure 6.5.

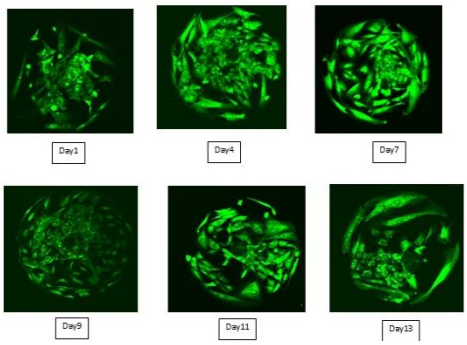

Figure 6.5 Live confocal imaging of HUVEC cultured on TiB_2 circles (diameter 450 µm) at excitation wavelength of 488 nm. Images from different substrates at day 1, 4, 7, 9, 11 and 13 are shown. About 50,000 cells were seeded on each of the substrates (0.75 mm*0.75 mm size each). The substrates each day were stained with 5 µl of ccridine orange dye for 20 minutes prior to imaging.

The percentage cell coverage area of HUVEC on the patterns over time was quantified using ImageJ software as discussed in the Section 4.10.1. The substrates were seeded with 50,000 cells per substrate and stained with 5 µl of Acridine Orange for 20 min on day 1, day 4, day 7, day 11 and day 13 and imaged in the confocal microscope. The experiment was repeated twice, with one substrate for each day in repeat one and a total of five circles imaged per substrate. For repeat 2, two substrates per sampled each day with at least nine circles imaged per day. Quantitative result for experiment one is shown in Figure 6.6. Our results indicate that the HUVEC reach peak growth on day 7 and plateau after 7 days and are viable until thirteen days in culture. The TiB_2 material is non-toxic, since the cells maintain their normal morphology over the time period of 13 days tested in this study.

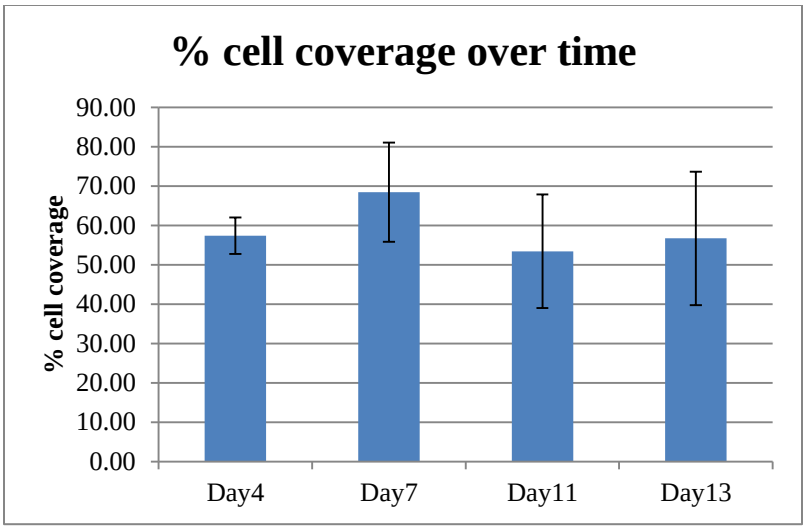

Figure 6.6 Percentage cell coverage area on TiB_2 circles (Diameter 450 µm) from Day 4 to Day 13 from experiment one. One substrate was sampled each day, with a total of five circles imaged per substrate.

Figure 6.6 indicates an increase in the percentage cell coverage area from day 4 to day 7. The cells reach ~70% coverage on day 7 and decrease on day 11 to ~50%. The percentage cell coverage area plateaus over the period of day11 to day13.

HUVECs were also cultured on another different pattern of lines. The line width ranged from 5 µm to 50 µm with width increments of 5 µm. HUVECs grown on the different width TiB_2 patterned lines are confluent by Day 5 indicating cell growth. Figure 6.7 shows the striking specificity in the HUVEC cell adhesion and growth only on the TiB_2 patterns. Figure 6.8 shows the percentage cell coverage increase on TiB_2 patterned line width ranging from 5 µm to 50 µm. The width lines reaches maximum percentage cell coverage area on day7.

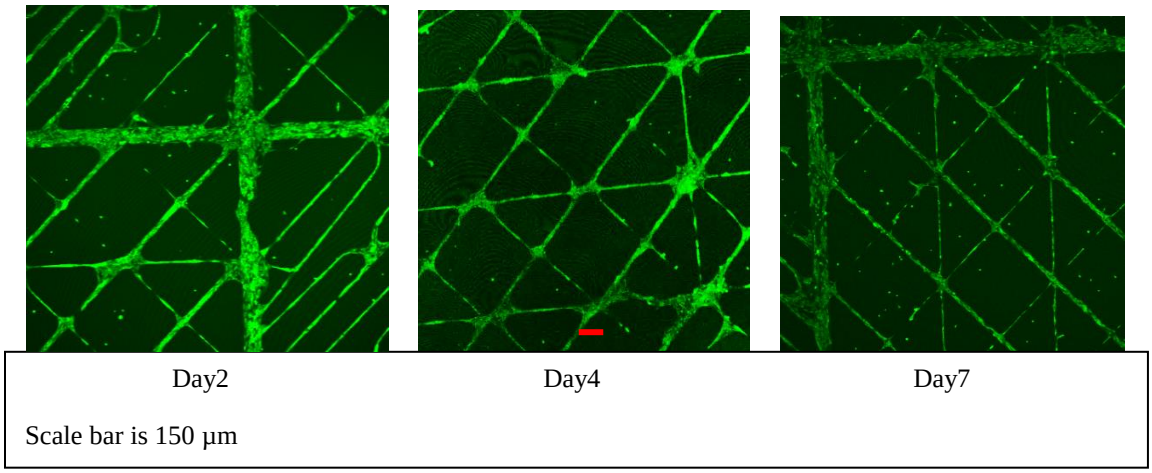

Figure 6.7 HUVEC viability on day 2, day4 and day7 on TiB_2 line patterns. Substrates with line patterns(0.5 mm*0.5 mm size) were seeded at 12,000 cells per substrate. Sample substrates were stained with 5 µl of acridine orange for 20 min on day 2, day 4 and day 5. Representative images show cells on different width lines ranging from 5 µm to 50 µm.

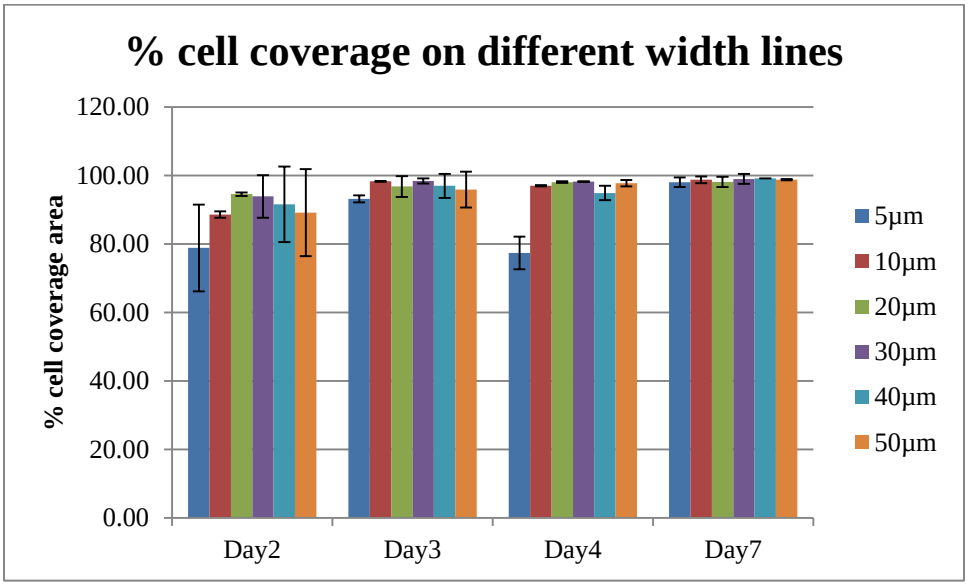

Figure 6.8 Percentage cell coverage area on line patterns on days 2, 3, 4 and 7. Four substrates on day 2, four substrates on day 3, three substrates on day 4, and three substrates on day 7 were imaged. Two to three images each day for each substrate were used to analyze the % cell coverage area on different width lines ranging from 5 µm to 50 µm.

6.1.2.2. HUVEC density

Cell density provides a relative measurement of proliferation over time. Optical imaging was used to study cell growth and morphology on the TiB_2 patterned substrates. HUVEC were confluent in 3 days and over the time the cells were seen stretching along

the periphery of the circle. Cells in the central area of the circle were stretching along both the length and width directions. Growth of the cells on TiB_2 material was tested over a prolonged culturing period of 3 weeks (21 days) (Figure 6.9 and Figure 6.10). The percentage cell coverage area increased from day 2 to day 3 and reached its peak on day 3. It then decreased to plateau over a time of 21 days.

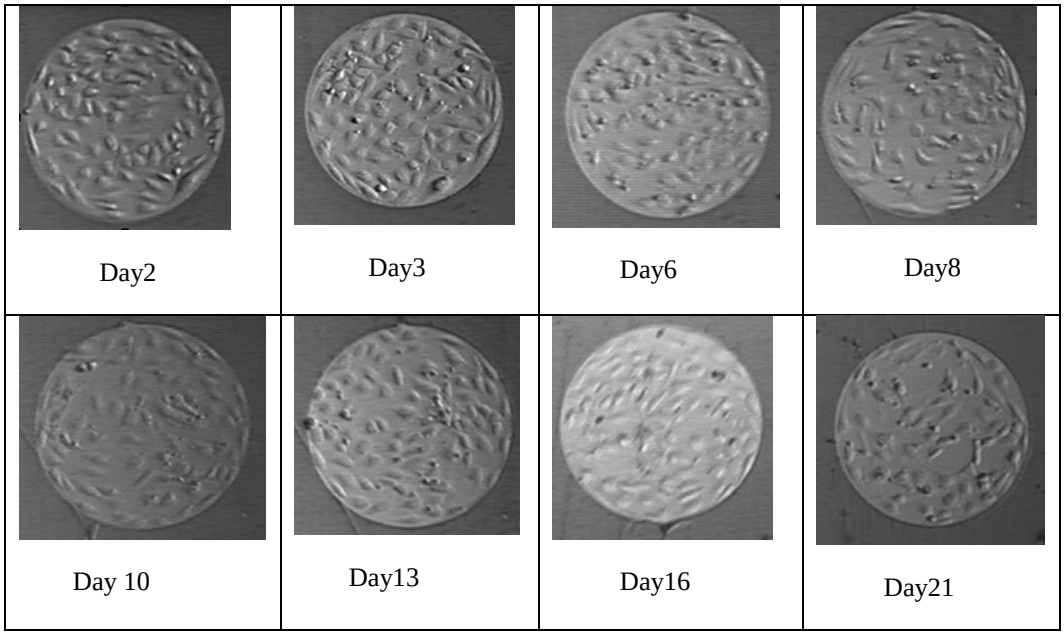

Figure 6.9Cell coverage of HUVEC on TiB_2 circles (diameter 450 µm) from day 2 to day 21. Substrates were seeded with 30,000 cell density per substrate and were optically imaged using stereomicroscopy on day 2, day 3, day 6, day 8, day 10, day 13, day 16 and day 21. Representative images for different days are shown (the same circle is shown on all days, with the exception of day 21).

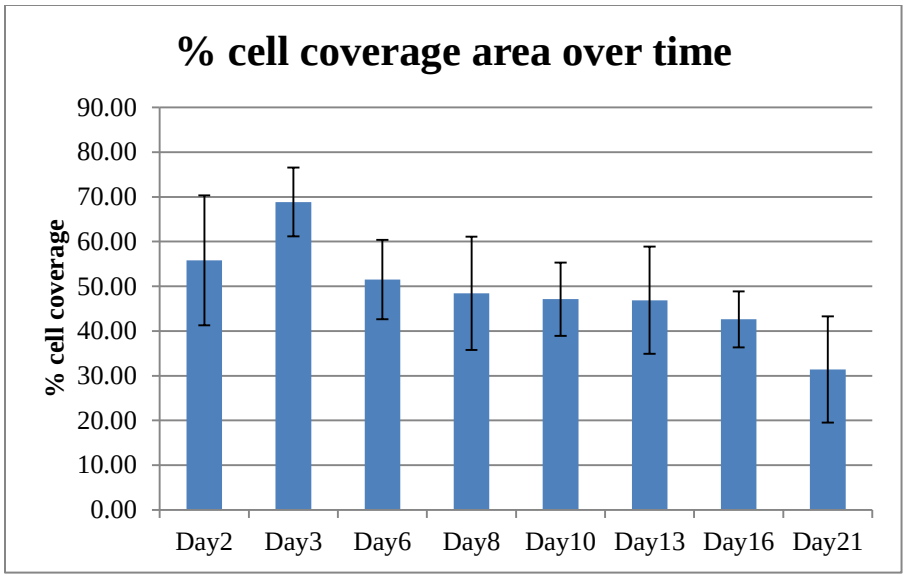

Figure 6.10 Percentage cell coverage area on TiB_2 circles (diameter 450 µm) from Day 2 to Day 21. Mean value of data from two substrates (20 circles) per day is presented.

Similar behavior is seen on circle patterns of larger diameter of 2760 µm (see Figure 6.11), with cells aligning along the perimeters, and displaying random orientation in the central regions.

Figure 6.11. Day 2 optical image of HUVEC on TiB_2 circle (diameter 2760 µm) that was seeded with 30,000 cells. Scale bar-100 µm

HUVEC were also cultured on titanium diboride with another pattern of circles and rectangles until day 21 (Figure 6.12). The cells reach confluency in 10 days and adhered until day twenty-one after seeding. This demonstrates the feasibility of attaining

long-term culture periods of three weeks on the substrates using in this study. Similar trend of orientation is obtained on large areas and alignment at the edges as expected.

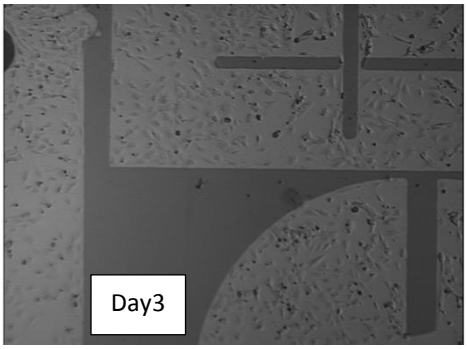

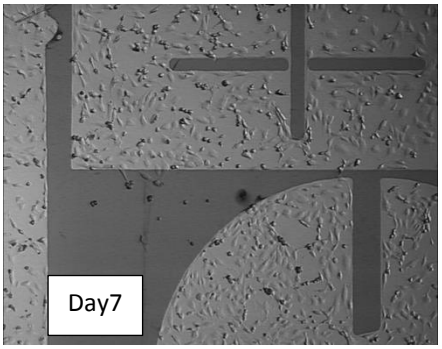

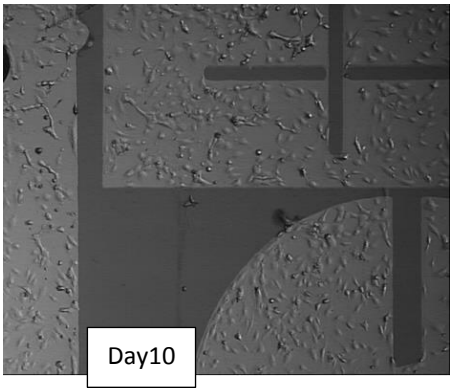

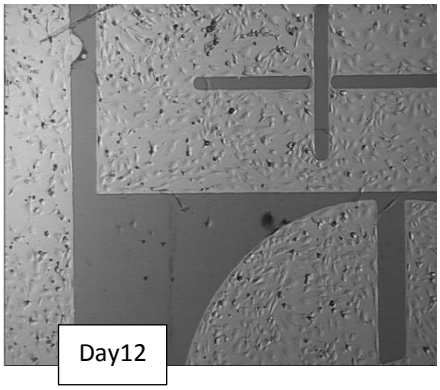

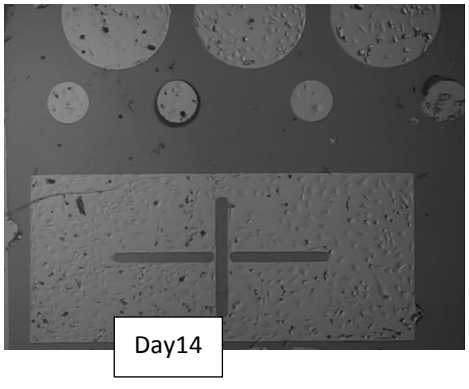

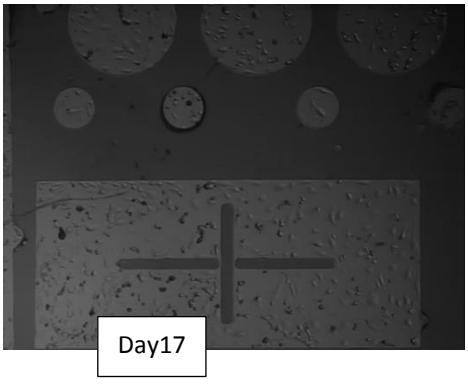

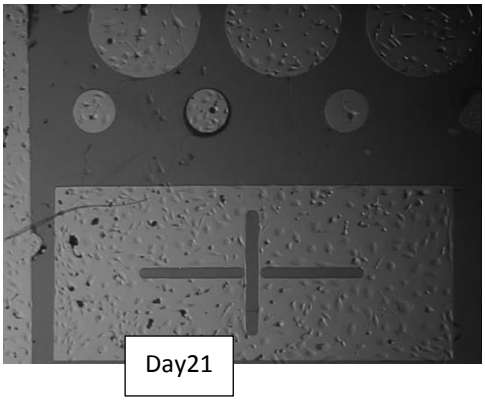

Figure 6.12 Optical images of HUVEC growth on TiB_2 patterned substrates. Cells were seeded on two substrates with 30,000 cells per substrate.

6.1.2.3. HUVEC length/ width ratio

The morphology (elongation) of cells on 5 µm to 50 µm - every 5 µm and 150 µm wide lines was measured with respect to length/width ratio. The cells were cultured on substrates with line patterns of varying widths over a period of 7 days. The 10 µm width lines are covered by single cells along the width while the 40 µm and 150 µm are lined by two or more cells along the width, respectively (Figure 6.13). Patterns of different geometries were studied to determine the effect of line width on cell adhesion and spreading (Figure 6.13 & Figure 6.14).

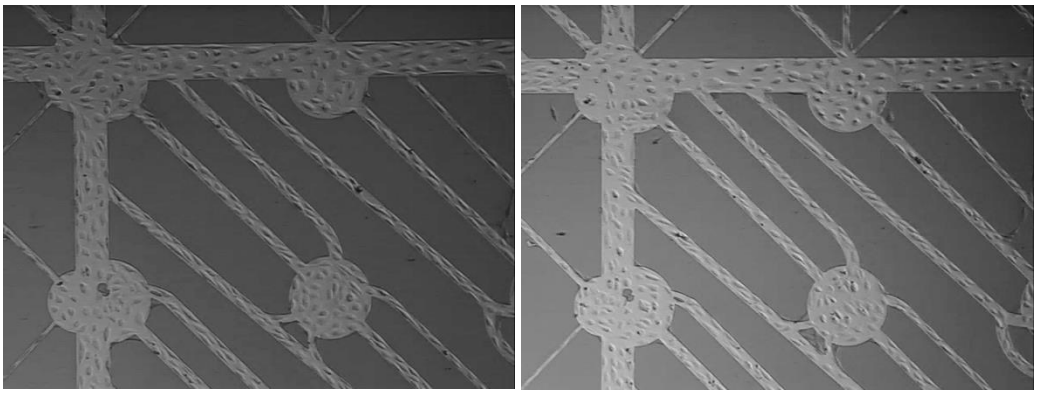

Day4 Day6

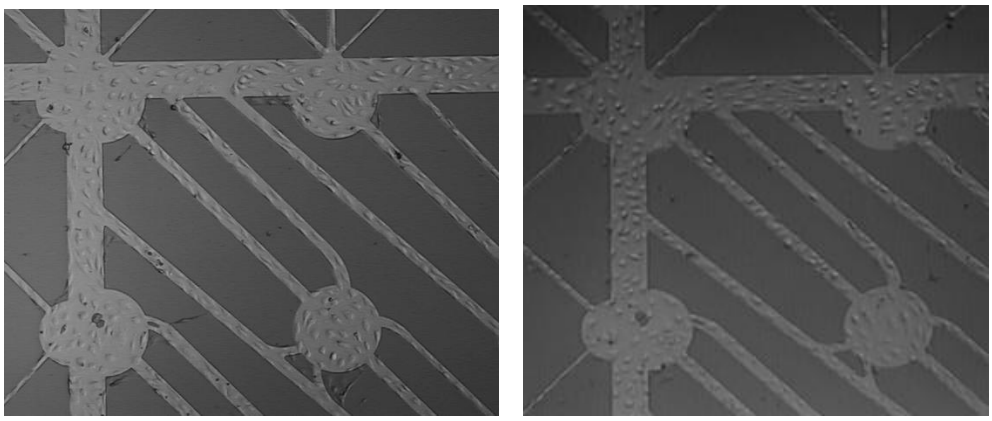

Day11 Day17

Figure 6.13 HUVEC cultured on a substrates of circle and line patterns with a seeding density of 30,000 cells per substrate. Optical images of the same area were obtained on day3, day4, day6, day11 and day17.

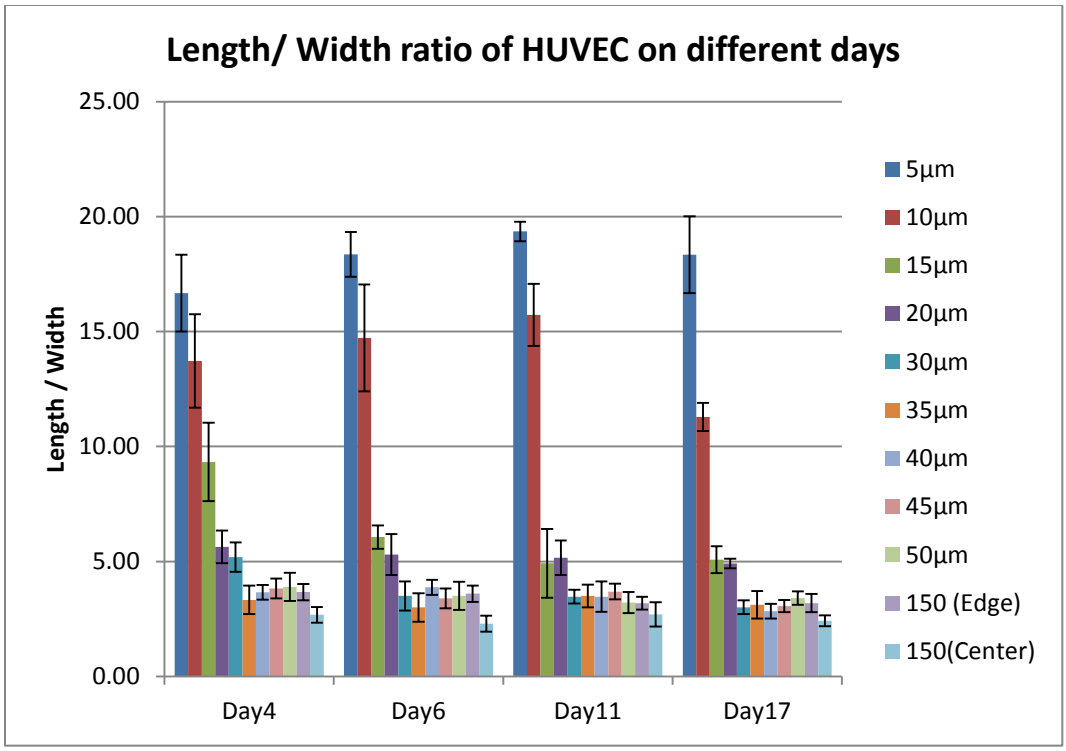

Figure 6.14 Length/ Width ratio of HUVEC cultured on TiB_2 line patterns of line width 5 µm to 50 µm- every 5 µm, and 150 µm on different days. Mean value of data from three substrates (two to three images per substrate) each day were used for image analysis.

For the line patterns tested (see Figure 6.14), for line widths < 30 μm, lines of single cells were obtained. At higher widths of 35 μm, 40 μm, 45 μm and 50 μm, two

cells filled the width of the lines. For the line width of 150 μm multiple lines of single cells were observed along the lines. On the very thin lines, cell elongation was increased along the longitudinal pattern axis. However, the wider line widths allowed the cells to spread in two dimensions.

6.1.2.4. HUVEC orientation

Microtechnology of contact printing has long been used as a versatile tool to design micro patterns of adhesive materials to control the cell activity and orientation on the patterns [**Error! Reference source not found.**]. Orientation of HUVEC to the underlying micro pattern indicates controlled cell growth on patterned area and existence of contact guidance.

Orientation of HUVEC is possibly a preliminary step in advanced tissue engineered devices. The line width influences the orientation and elongation of the cells. Pattern guided orientation of cells was observed on the controlled line dimensions of 5 µm to 50 µm- every 5 µm and the 150 µm wide lines. HUVECs aligned along the longitudinal axis of the lines indicating the influence of contact guidance from the surface topography. Highly elongated cells on the different width line were aligning to the long axis of the line. The orientation of HUVECs was sustained till 17 days of culturing (Figure 6.15).

The distribution of orientation angles in our experiments were observed to be distributed from orientation angle of 0 ° to 35 °. As seen in Figure 6.16, the distribution of orientation angle for 5 µm, 10 µm, and 20 µm width lines is in the range of 0 ° to 10 ° with about 82-90% cells mainly in the 0 ° to 5 ° range. The distribution of orientation angle for 40 µm, 45 µm, and 50 µm width lines is in the range of 0 ° to 15 ° with about

55-80% cells in the 0 ° to 5 ° range, about 10-30% cells in the 5 ° to 10 ° range and about 2-14% cells in the 10 ° to 15 ° range. The 30 µm has cells in the range of 0 ° to 20 °. The orientation angle range of this line is wider as compared to the 20 µm line since at times one cell or two cells are oriented along the longitudinal axis. The distribution of orientation angle for 150 µm (edge) and 150 µm (center) width lines is in the range of 0 ° to 35 °. The 150 µm (edge) has about 75% cells in the 0 ° to 5 ° range, about 15% cells in the 5 ° to 10 ° range and about 10% cells in the 10 ° to 30 ° range. The 150 µm (center) width line has about 48% cells in the 0 ° to 5 ° range and remaining 52% in the 10 ° to 35 ° range

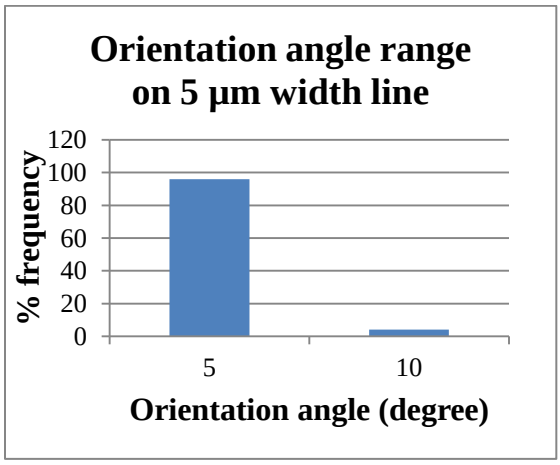

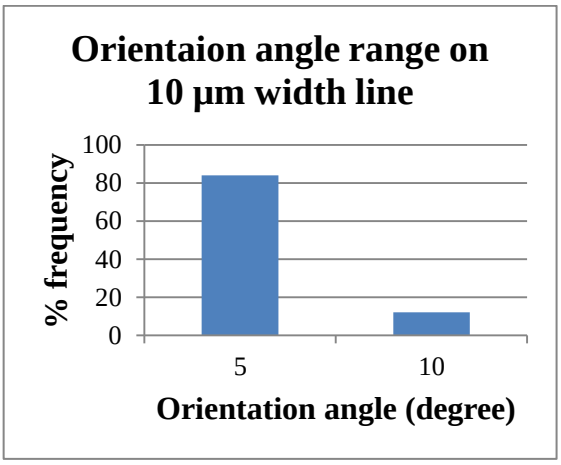

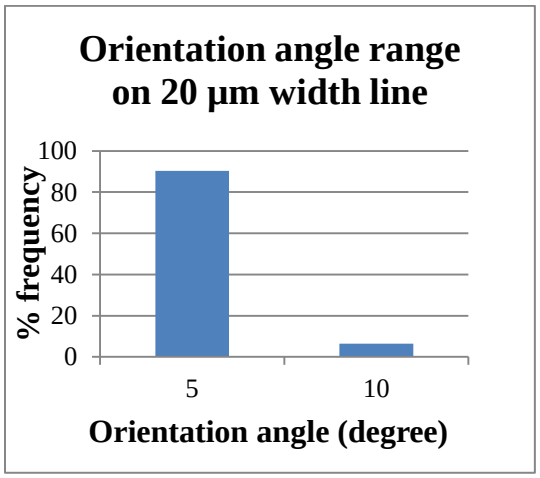

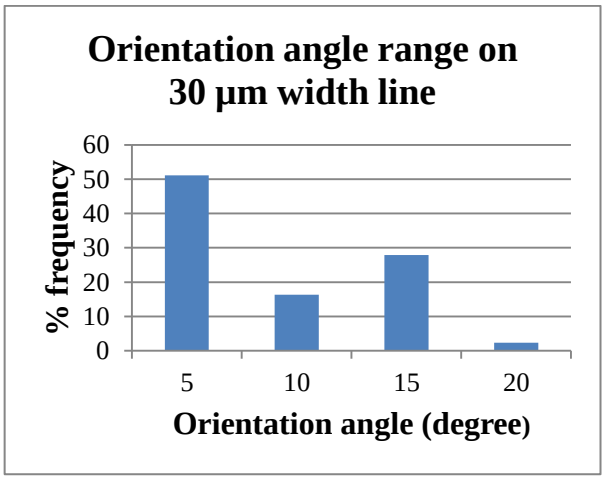

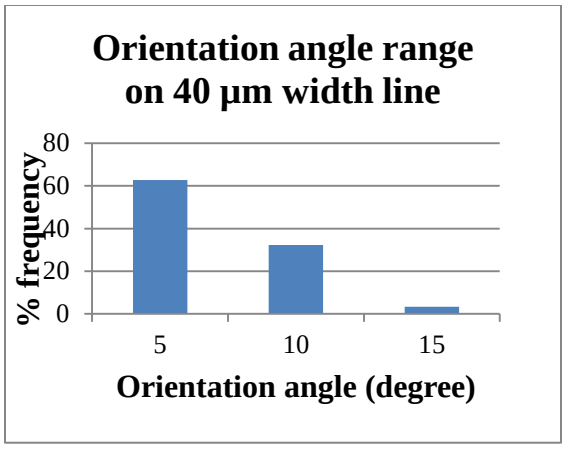
Orientation angle range on 40 µm width line
% frequency
80
60
40
20
0
5
10
15
Orientation angle (degree)

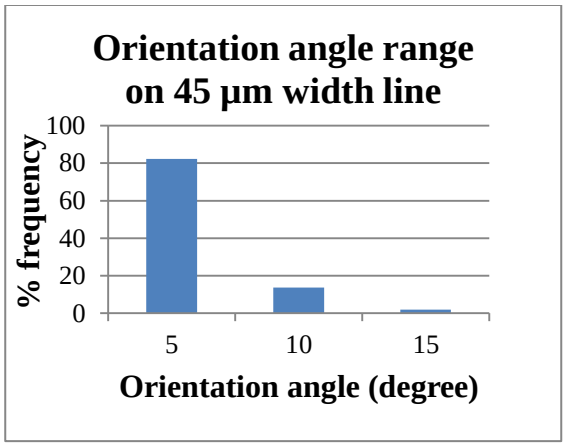
Orientation angle range on 45 µm width line
% frequency
100
80
60
40
20
0
5
10
15
Orientation angle (degree)

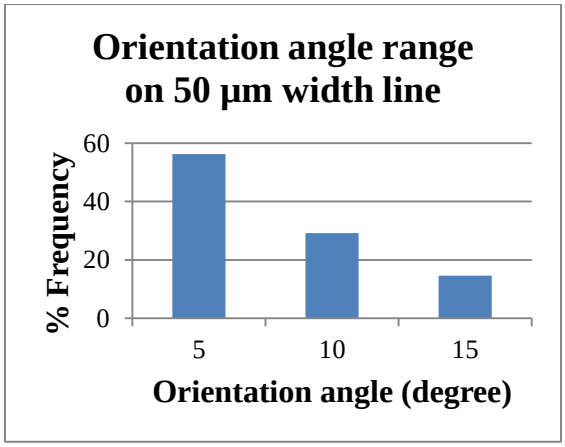
Orientation angle range on 50 µm width line
% Frequency
60
40
20
0
5
10
15
Orientation angle (degree)

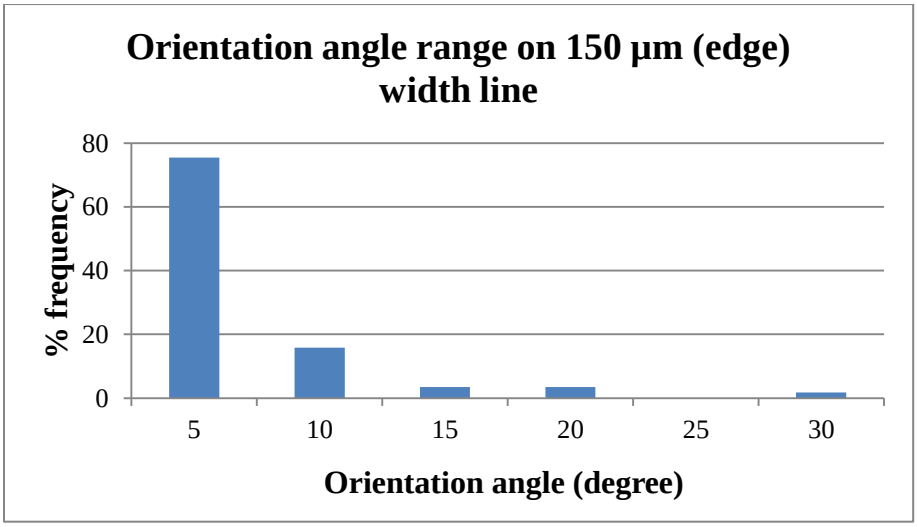
Orientation angle range on 150 µm (edge) width line
% frequency
80
60
40
20
0
5
10
15
20
25
30
Orientation angle (degree)

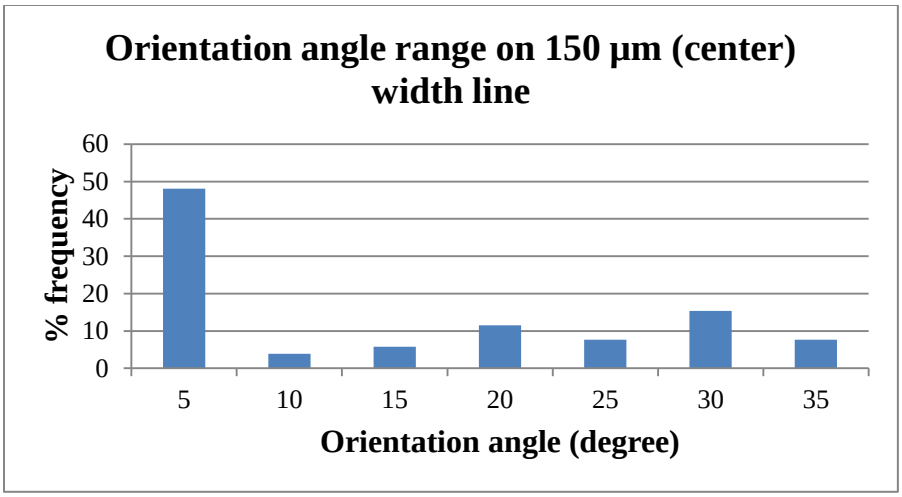

Figure 6.15 % Frequency distribution of HUVEC orientation angles on day 6 on TiB_2 patterned substrates of line width 5 µm, 10 µm, 15 µm, 20 µm, 25 µm, 30 µm, 40 µm, 45 µm, 50 µm and 150 µm (edge and center). Five substrates from two repeats (three images per substrate) were analyzed.

Joie et al. [232] demonstrated that the width of the micro-pattern influences the orientation of the cells on them. They studied the cell orientation on 10 µm, 50 µm, 100 µm and 300 µm micropatterned lines of polymer (PET). The distribution of cells on 100 µm lines were distributed from 0 ° to 20 ° and the ones on the 10 µm and 50 µm were ranging from 0 ° to 10 °. An orientation angle of less than 10 ° was considered good alignment [233].

The cell orientation is also affected by the density of cells attached on the micro-pattern. Cell orientations on thinner lines (5 µm to 50 µm) are aligned irrespective of lower or higher cell density. However, on the 150 µm line, the orientation of cells depends on the cell density attached to the pattern. The cells on the edge and center have a similar orientation if cell density is high (micro-pattern entirely confluent with cells) while for lower cell density the orientation of cells on the edge are along the longitudinal axis of the pattern and the cells at the center are aligned randomly (Figure 6.16).

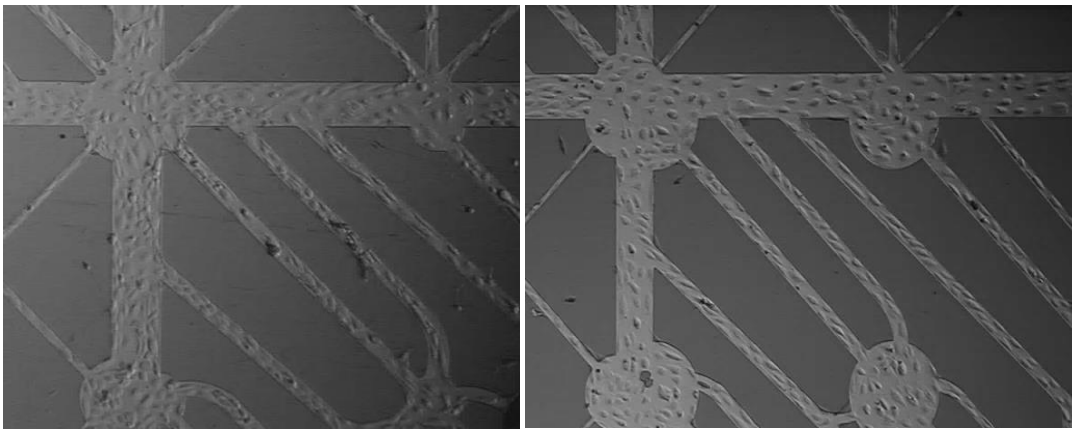

(a) High cell density attached (b) Low cell density attached

Figure 6.16 HUVEC orientation on Day 6 on TiB_2 patterned substrates of line width 5 µm, 10 µm, 15 µm, 20 µm, 25 µm, 30 µm, 35 µm, 40 µm, 45 µm, and 150 µm (edge and center).

6.1.3. Immunocytochemical analysis

6.1.3.1. Platelet Endothelial Cell Adhesion Molecule (PECAM)

Confocal fluorescence imaging of endothelial cells with PECAM and DAPI was performed to observe the cell-to-cell adhesion and cell elongation on different width lines. The degree of expression of adhesion molecules on the surface of human HUVECs depends on the response of the cells against the implanted material. Cenni et al. [234] studied the adhesion molecule expression mechanism on surface modified knitted Dacron surfaces. They fixed the cells after 24 h and observed the expression of PECAM and other adhesion molecules. The expression of PECAM and DAPI shows that HUVECs cultured on TiB_2 patterns maintain their functional phenotype (Figure 6.17).

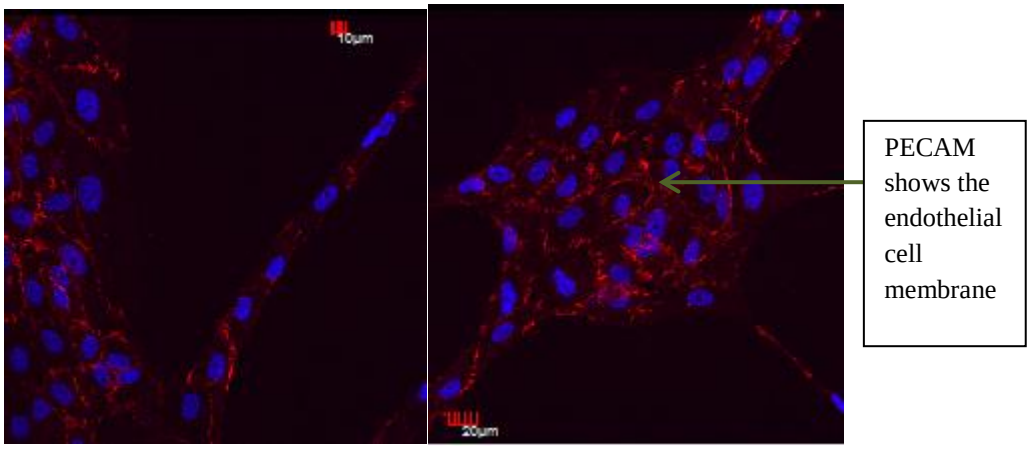

Figure 6.17 HUVECs cultured on TiB_2 patterned substrate till Day3. Three substrates were seeded with 30,000 cells per substrate. Stained with PECAM (Red) and DAPI (Blue) and imaged in a confocal microscope. Staining protocol is described in Appendix A.

CD31 is a glycoprotein that is expressed on the membrane surfaces of endothelial cells. Cultured HUVECs were consistently positive for PECAM-1 (Figure 6.17). The patterns of labeling were varied depending upon the size of the underlying TiB_2 pattern. Laser confocal microscopy at higher magnification showed labeling of the entire cell membrane at sites of cell-to-cell contacts (Figure 6.17). As seen in the figure, the DAPI (Nuclei) staining highlights the stretching of cell, seen as elongated nuclei on the micro patterned lines.

6.1.3.2. Actin filaments and vinculin staing of HUVECs on TiB_2 substrates

HUVEC fixed and stained for actin filaments and focal adhesion protein vinculin on Day 8 were imaged using confocal fluorescence microscopy. The blue, red and the green staining denote nuclei, actin filaments (cytoskeleton) and focal adhesion protein vinculin, respectively (Figure 6.18). The cytoskeleton is organized along the pattern axis on the thinner lines while the actin filaments are randomly oriented in cells in the central regions of the circles.

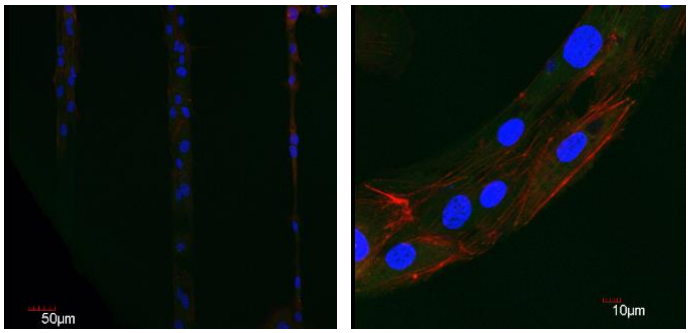

(a) (b)

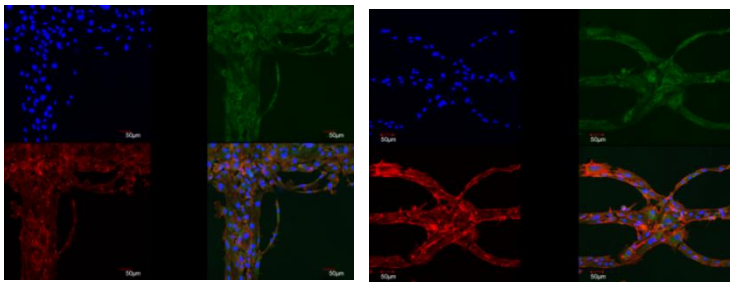

(c) (d)

Figure 6.18 HUVEC were seeded on two TiB_2 patterned substrates with seeding density of 30,000 cells per substrate. HUVEC attachments on the TiB_2 pattern on Day 8 were imaged. Blue-Nuclei (stained with DAPI), Green Focal adhesion (stained for Vinculin) and Red-Actin Filaments/Cytoskeleton (stained with Phalloidin). (a), (c) and (d) are imaged at 20X and (b) is imaged at 60X. The (b) image indicates the alignment of actin filament (red) along the longitudinal axis of the line pattern. Image (a) shows compression of nuclei on different width lines.

The topology of the stiff substrate surface controls the attachment and growth of HUVEC on it [33–35, 235]. Studies have characterized HUVEC adhesion with respect to actin cytoskeleton and focal adhesions. The organization and stretching of actin filaments (cytoskeleton) was observed in the HUVECs cultured on the TiB_2 patterned substrates. The alignment of actin filaments on broader line width 150 µm and on the circular patterns was random, while a very organized alignment was observed on line width ranging from 5 µm to 50 µm. These results indicate that the substrates support the formation of actin filaments-cytoskeleton and focal adhesion points, that are needed for HUVEC attachment and survival.

6.1.3.3. Islet antibody: Insulin

Islets were seeded on titanium diboride patterned substrates to study its attachment. The 12 day old islets were seeded on the patterned substrate and cultured for four days. The circular pattern provides 100 µm to 500 µm area circle specifically to seed the islets. The substrate was fixed on the fourth day and were stained for nuclei (DAPI-blue), insulin (green), and endothelial cell marker (PECAM). Insulin staining indicates the functional viability of islet on the substrate (Figure 6.19).

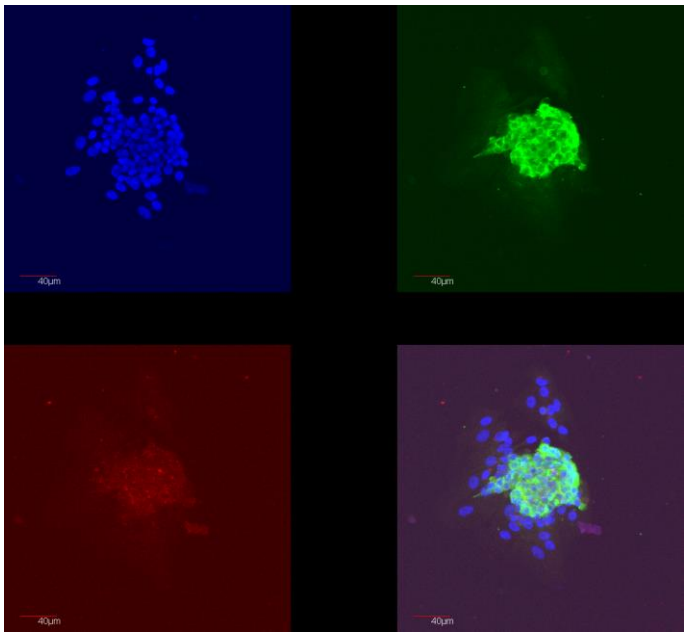

Figure 6.19 Islet attached on titanium diboride circle pattern of 500 µm diamter till day4. The substrates were fixed on day4 and stained. Blue-DAPI, Green-Insulin, Red-PECAM, and overlay image. The islets were 12 days old when seeded.

6.2. Co-cultures

6.2.1. Qualitative analysis

Previous studies have indicated the advantages of co-culture of HUVEC and MSC for tissue engineering applications. The co-culture initiates bidirectional communication

between the cell types and their stable structure. Loffredo et al. [48] exhibited stable structure formation of tube network with co-culture than the single HUVEC cultures.

6.2.1.1. HUVECs and MSCs

For tissue engineering, endothelial cells are often combined with other cell types to attain a prevascular network (Loffredo & Lee, 2008) . It is important to find culture conditions that are suitable for both the organization of both HUVECs and MSCs on the circle and line pattern. The HUVEC and MSC combination was growing specific to the TiB_2 pattern from day1 and was confluent by day 2 as seen in Figure 6.20.

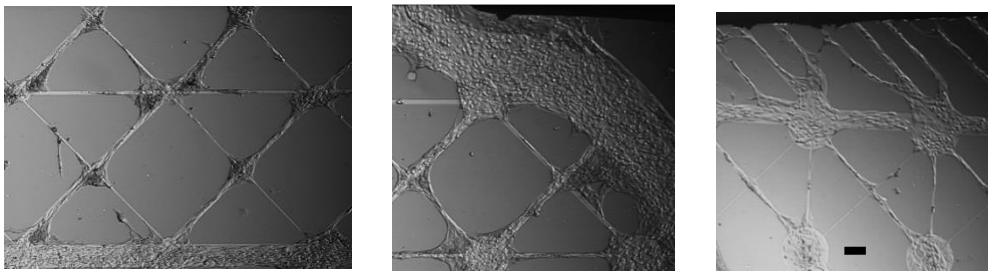

Figure 6.20 Optical images of HUVEC and MSC cultured on TiB_2 patterned substrates on day2. Scale bar 150 µm. Three substartes each in two experiments were seeded with HUVEC and MSC at cell density of 30,000 cells per substrate at the ratio of 2:1.

As the days progressed, the co-culture began to move towards the bigger circular area and gradually agglomerated as spheroids on the circles as seen in Figure 6.21. The co-culture also were retained on the line pattern. Thus the titanium diboride pattern facilitated the growth of HUVEC and MSC co-culture specifically only on the pattern.

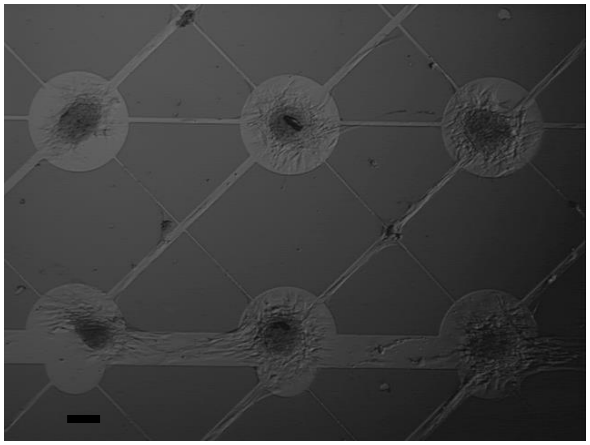

Figure 6.21 Optical images of HUVEC and MSC cultured on TiB_2 line and circle patterned substrates on Day8. Three substartes each in two experiments were seeded with HUVEC and MSC at cell density of 30,000 cells per substrate at the ration of 2:1. Scale bar 150 µm.

6.2.1.2. HUVECs and islets

HUVECs were cultured on titanium diboride line and circles patterned substrate for 9 days and were observed to be growing specifically only to titanium diboride. The islets were then seeded on these HUVEC cultured substrates and were cultured further for 4 more days. The Islets remained attached to the pattern where HUVECs were attached. Thus, the HUVEC provides sites for the islets to attach on its surface. No islets were observed on the silicon surface (Figure 6.22).

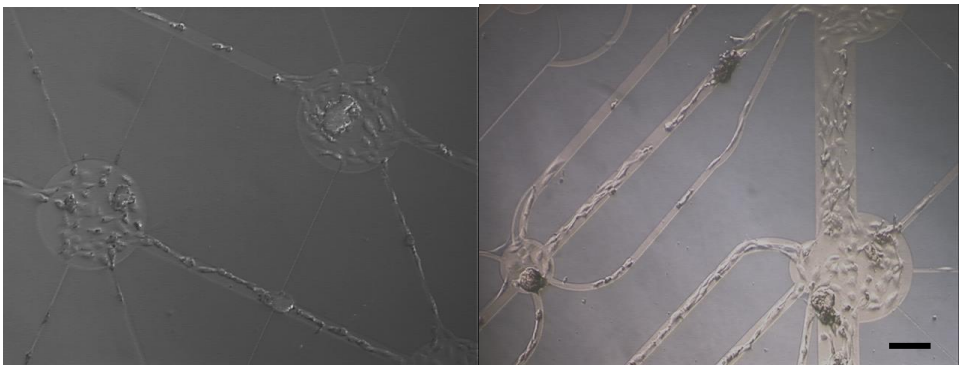

Figure 6.22 Optical images of HUVEC and islet cultured on TiB_2 line and circle patterned substrates on day 13. HUVEC cultured for 9 days and then islets were seeded on these substrates and cultured for 4 more days. Scale bar 150 µm.

The HUVECs were also cultured on titanium diboride patterned circles (450 µm diameter) for four days and were then seeded with islets and cultured for 12 more days with alternate day culture media change. As seen in Figure 6.23, the islets remained attached to the HUVEC cultured pattern over time.

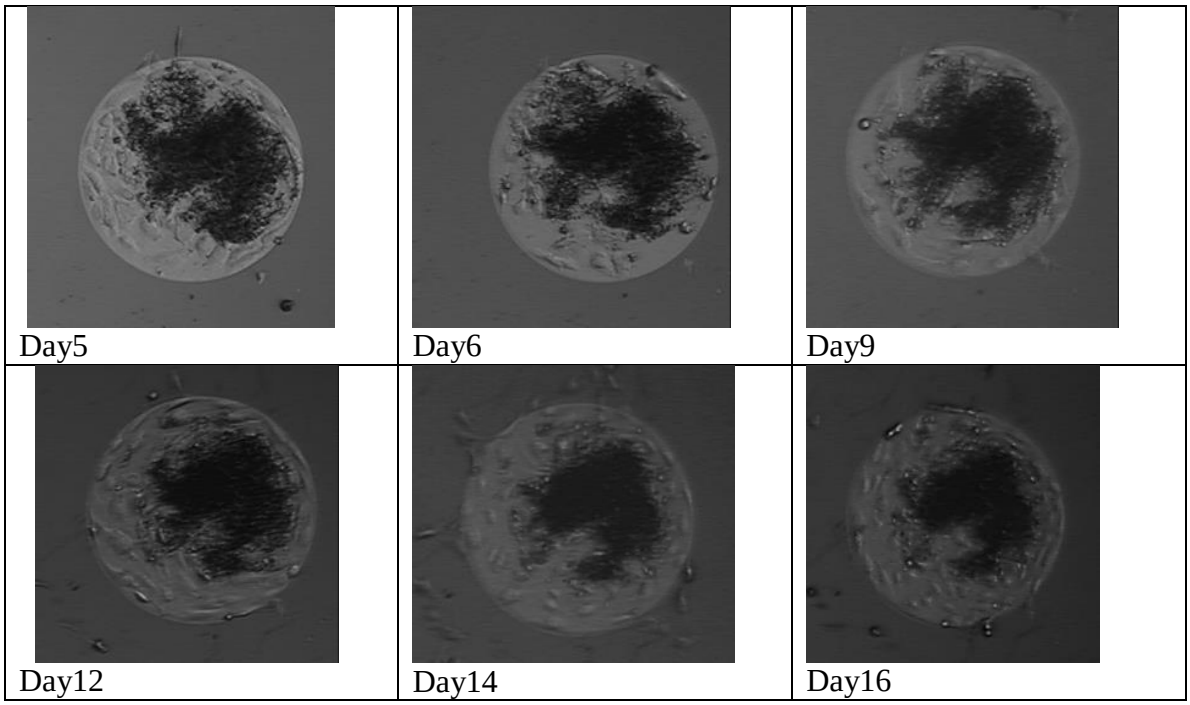

Figure 6.23 Optical images of HUVEC and islet cultured on TiB_2 circle patterned (450 µm diameter)substrates. HUVEC cultured for 4 days and then islets were seeded on these substrates and culutred for 12 more days. Scale bar 150 µm.

6.2.1.3. HUVECs, MSCs and Islets

The Figure 6.24 shows the islets cultured on TiB_2 substrates with a day co-cultured monolayer of HUVEC and MSC. The substrates were cultured for a period of 24 days. The presence of MSC possibly causes migration of HUVECs into the islets. The co-culture provides islet attachment similar to islet with only HUVEC culture. Islet movement towards the HUVEC and MSC cultured pattern was also observed (Figure 6.25).

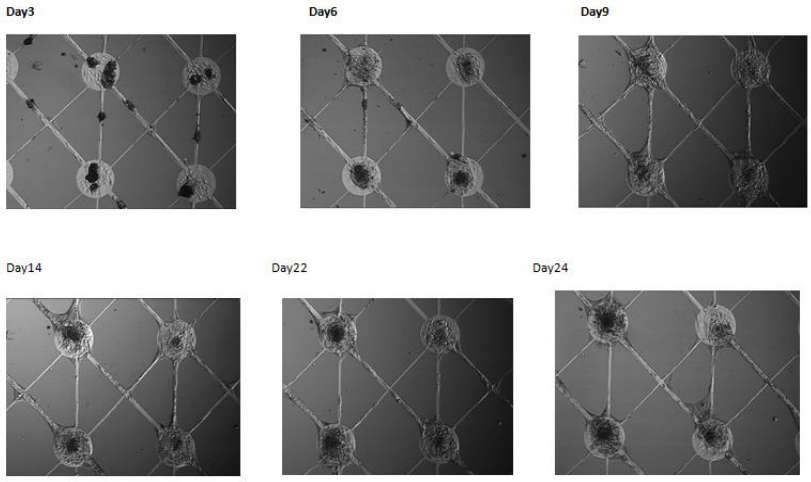

Figure 6.24 Optical images of EC, MSC and Islets on TiB_2 patterns. Islets seeded after 1 day confluent co-culturing of HUVEC and MSC (2:1, seeding density 2:1) on TiB_2 circle and line pattern substrates till day 24.

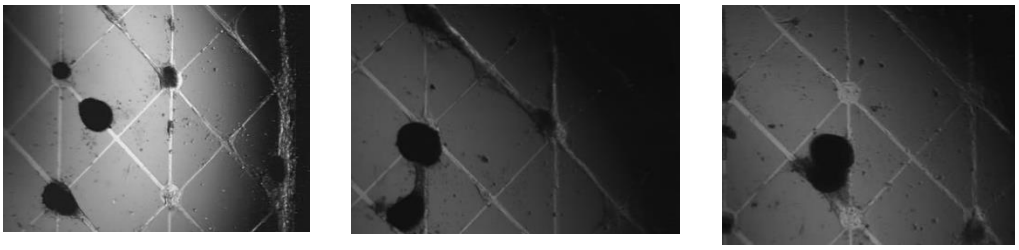

(a) (b) (c)

Figure 6.25 Islets on pre cultured HUVEC and MSC (Day 1) cultured on TiB2 patterned substrates. The HUVEC and MSC were co-cultured at seeding density of 30,000 cells per substrate at the ratio of 2:1. The optical images were captured on (a) Day 14, (b) Day 17 and (c) Day 21 respectively.

Previous studies have shown the growth factors released form endothelial cells enables migration of MSCs towards HUVECs [2, 7**Error! Reference source not found.**]. Previous studies have exhibited that HUVEC and MSC co culture possibly supports the viability of human islets [1, 21, 54, 41].

6.2.1.4. Scanning Electron Microscopy analysis of HUVECs, MSCs and Islets

Co-culture of HUVEC and MSC on titanium diboride line and circle pattern was done and on day2 islets were seeded on these co-cultured substrates. The substrates were cultured further for 22 more days and were fixed to be analyzed in SEM (Figure 6.26).

The SEM images exhibited islets in close attachment to the co-culture growing on the substrates. However, the mechanism of this attachment has not been clearly defined.

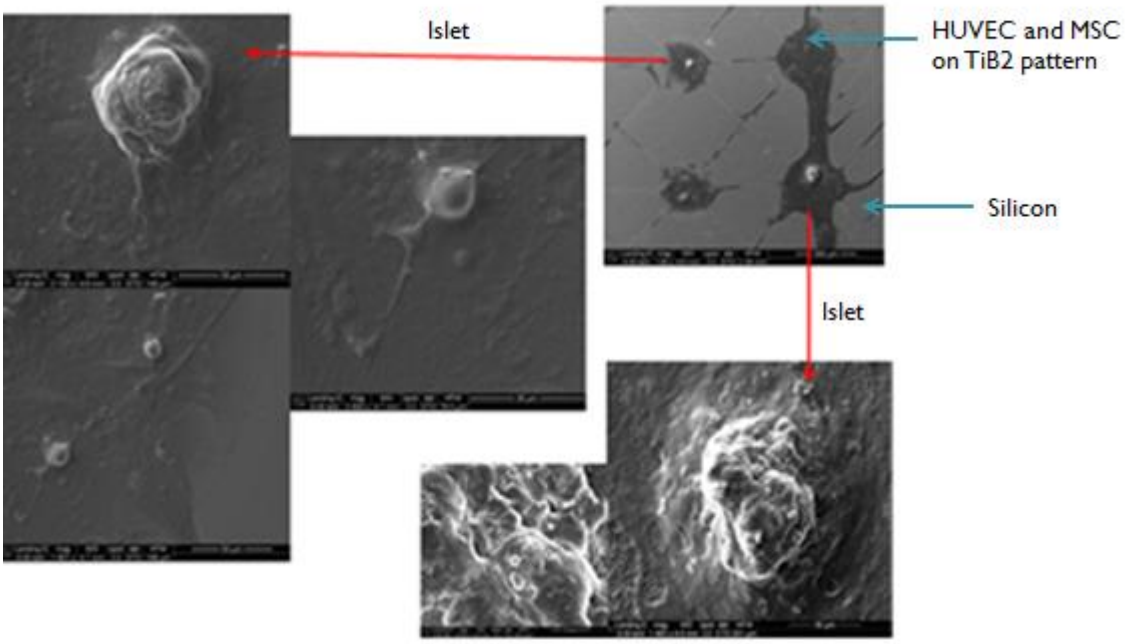

Figure 6.26 SEM images of Islets on pre cultured EC and MSC (Day1) cultured on TiB_2 patterned substrates for 24 days.

6.2.2. Immunocytochemical analysis

6.2.2.1. PECAM and islet antibodies

Human islets in-situ comprises of microvessels that support the functionality of islets and provide oxygen and nutrition. Luo et al. [236] co-cultured islets for 210 days and observed vascularization of the co-cultured islets. Presence of endothelial cells within the islet tissue possibly indicated the beginning of vascularization of islets in vitro. Their co-culture of HUVEC and MSC possibly released growth factors that facilitated islet viability. This in vitro technique could be critical for islets prior transplantation. Many modern tissue-engineering studies have used co-culture of HUVECs and MSCs to

improve the islet vascularization after transplantation [7]. Johansson et al. [6] have shown that significance of mesenchymal stem cells and endothelial co-culture that enhanced the viability and vascularization of islets as compared to islet culture with no co-culture.

Our results show that co-cultured islets have an overall strong expression of insulin, glucagon and endothelial cells vs the islets without co culture as seen in Figure 6.27. These immunohistochemistry results indicate islet function even after duration of three weeks to a month.

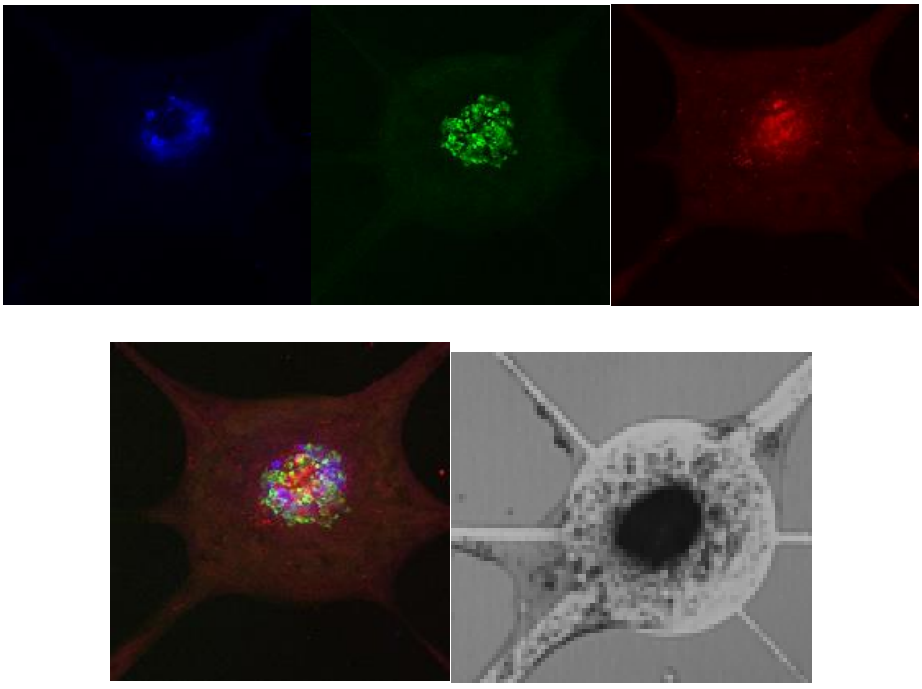

Figure 6.27 Immunohistochemistry of HUVEC, MSC and Islet of Langerhans post 26 days of culturing on TiB_2 patterned substrates in HUVEC media. HUVEC and MSC (2:1, seeding density of 30,000 total) per substrate) were cultured for 2 days and islets were seeded. These substrates were cultured for 26 days. Blue-Glucagon, Green-Insulin, Red-PECAM, overlay image and optical image.

Individual islets post-extraction are in the form of ball-like clusters of cells. Gradually these islets lose their cluster appearance and intra endothelial cells to reduce to a loose cluster of cells after three weeks. When the islets are co-cultured with HUVECs and MSCs on TiB_2 substrates for three weeks, the presence of endothelial cells within the

islets were observed in confocal imaging (Figure 6.27). Conventionally cultured islets were seen as a loose cluster of cells after three weeks as seen in Figure 6.28.

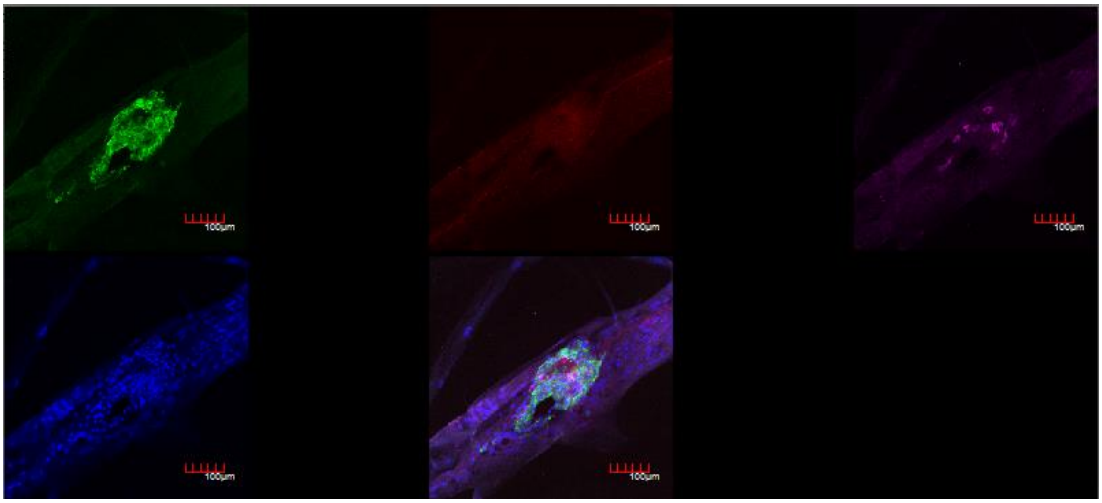

Figure 6.27 Immunohistochemistry of HUVEC, MSC and Islet of Langerhans post 26 days of culturing on TiB_2 patterned substrates in HUVEC media. Green-Insulin, Red-PECAM, Pink-Somatostatin, Blue-DAPI, and overlay image.

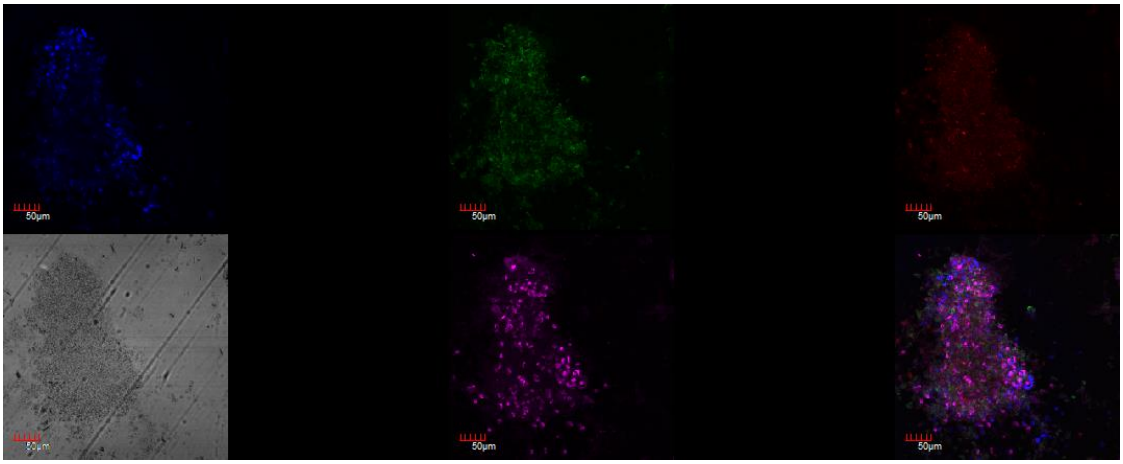

Figure 6.28 Immunohistochemistry of Islet of Langerhans post 26 days of culturing in normal islet media. Blue-Glucagon, Green-Insulin, Red-PECAM, brightfield image, Magenta-Somatostatin, and overlay image.

6.2.2.2. Actin filaments (Phalloidin) and vinculin

The cytoskeleton regulates the cell-substrate interface with the formation of focal adhesion and also controls cell function [235]. The focal adhesion points and cytoskeleton of the cells serve as a bidirectional communication path with the biomaterial

surface [81]. The blue, red and the green staining denote nuclei, actin filaments (cytoskeleton) and focal adhesion protein vinculin, respectively (Figure 6.30). The cytoskeleton is highly organized on thinner lines while the actin filaments are randomly oriented on the circles.

The HUVEC and MSC cultured substrates were stained with Rhodamine Phalloidin for Actin filaments, Vinculin for focal adhesions and DAPI for nuclei. The cells on the circle showed a disorganized orientation of the actin filaments while those on the lines indicated actin filaments oriented and stretching along the length of the lines. [54].

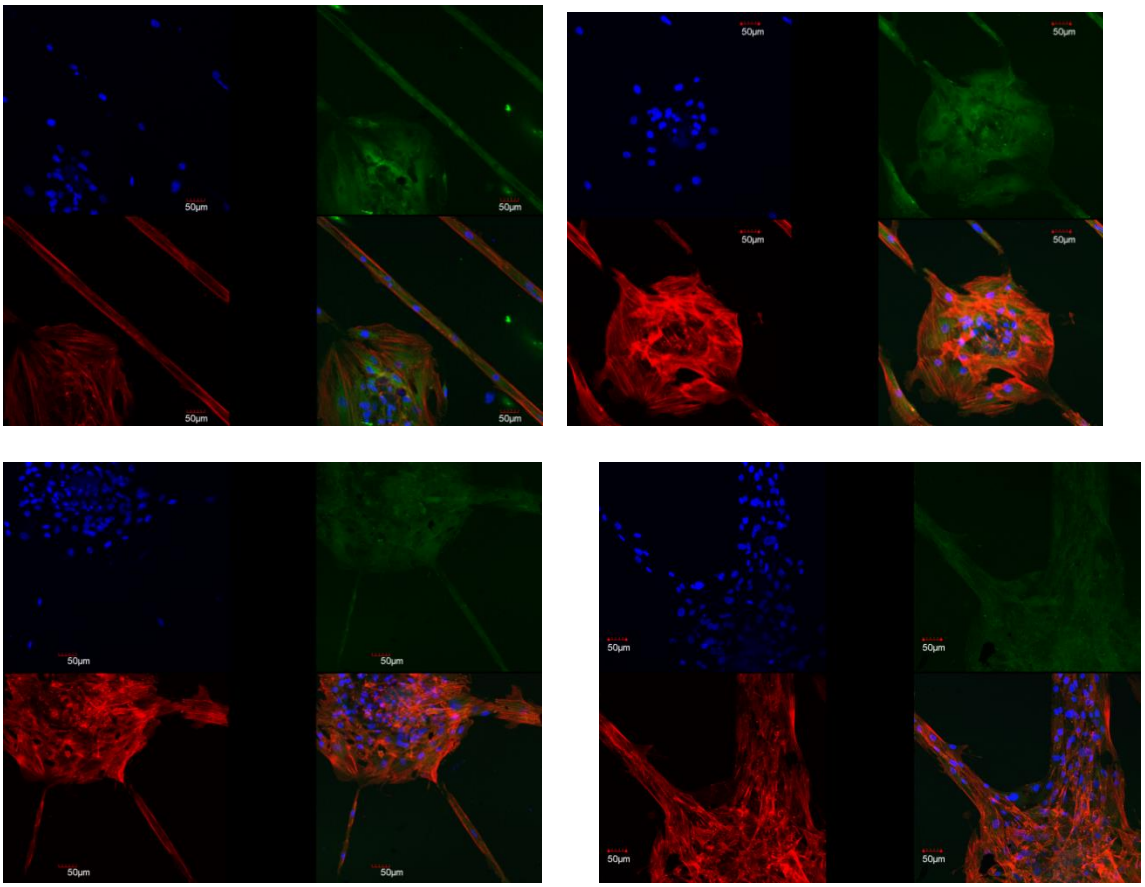

Figure 6.30 Confocal images of EC and MSC co-culture on TiB_2 substrates on Day 8. HUVEC and MSC were seeded on the substrates at a density of 30,000 cell per substrate (2:1). Blue-Nuclei (DAPI), Green-Focal adhesions (Vinculin) and Red-Actin filaments (Phalloidin).

6.3 SUMMARY:

Biomaterial titanium (Ti) that is extensively been used for implantable devices has a biocompatible oxide surface layer, which provides a high wear resistance to the biomaterial. For acceptable efficacy of a biomaterial, the HUVEC need to adhere to its surface in the presence of cellular microenvironment [237]. Direct physical adsorption of protein on substrate could be unspecific and unstable and could possibly give irreproducibility of results. The cleaning and sterilization method is one of issues that might affect cell-surface interactions [107]. Our substrate cleaning and sterilizing protocol was optimized to ensure selective cell growth and was explained in section 4.5.

Our results demonstrate that the endothelial cells can be geometrically confined on TiB_2 patterns on silicon substrates. In few past studies of cell patterning, there were limitations on the long term cell growth and the relation to selection of specific substrates. It is important that the cells retain their pattern specificity over the entire experimental/culturing period without causing cytoxicity to the adherent cells. Our method enabled cell adhesion in predefined regions of TiB_2 for a prolonged duration of 21 days.

Chapter 7: Conclusions and Future work

We investigated TiB_2 as a material with potential for biomedical applications where controlled growth of cells is required or high mechanical strength and corrosion resistance are important. Our immediate goal was to implement TiB_2 in the growth of various cell types (HUVEC, MSC and Islet of Langerhans) and to analyze in vitro conditions leading to vascularization of islets and possible constrains. Our project was designed to evaluate TiB_2 as a possible biomaterial by using complementary material characterization techniques (XPS, XRD, TEM, Nanoindentation, AFM and BioAFM, Contact Angle) to assess its various mechanical and physical properties.

We determined that TiB_2 was biocompatible in cell cultures for these three types of cells. The material properties showed certain similarities to Ti, which is known for its surface oxides such as TiO_2 and Ti-O suboxides. They form readily as a passivating layer, contribute to high biocompatibility of Ti and affect cell growth. However, boron oxides were also formed at the very surface as detected by XPS. TiB_2 exhibits very high hardness and Young's modulus, which due to mechanotransduction effects enhance and control cell growth. Surface roughness of our titanium diboride samples ranged from 2 nm to 6 nm depending on annealing conditions, hardness of 18 GPa and Young's modulus of 180 GPa. Cells typically displayed durotaxis behavior showing preference to grow and proliferate on stiff and hard TiB_2 as opposed to surrounding Si or SiO_2. Interesting cases of nonselective growth were also observed in special experimental conditions.

The BioAFM studies of substrates cultured and fixed with HUVEC indicated differences in the Young's modulus and adhesion of the material surface depending on

specific (i.e. selectively on TiB_2) and non-specific (i.e. indiscriminatory on TiB_2 and Si or SiO_2/Si cell growth. There was also a noted decrease in the Young's modulus measured on clean patterned substrates due to the presence of the glutaraldehyde fixative. For selective HUVEC growth (cells growing only on TiB_2 pattern), differences in the Young's modulus of titanium diboride and silicon/silicon dioxide was observed. For cell cultured fixed substrates we detected very large modifications of mechanical properties (hardness, stiffness, and adhesion forces) when cell grew nonselectively possibly due to ECM secreted by the HUVECs cultured on contaminated surfaces. The non selective HUVEC growth showed no difference in the Young's modulus of both the materials thus indicating presence a layer on the material surface formed due to the substrate cleaning and handling can change the cells capability to sense the micropattern on the material.

For substrates having cell growth, the surface chemistry, roughness, hydrophilicity, hardness, Young's modulus and the surface preparation plays an important role on protein adsorption and cell attachment. All these effects were observed in our experiments with TiB_2 patterned arrays and despite of complexity linking various cues and regulatory mechanisms, we can conclude that TiB_2 results in very reproducible and nontoxic behavior as a cell culture substrate for the controlled growth of HUVEC and MSC and as a passive substrate for Islets of Langerhans.

TiB_2 material patterned into circles and lines of various geometries provided prolonged viability of HUVECs for 24 days. The growth and orientation of HUVECs on various width dimension lines was also sustained with a clear demonstration of contact guidance, where the patterns control cell growth results in cell alignment, change in size, orientation and mobility. However, the formation of a network did not occur with only

the HUVEC since the substrate was 2D. The 2D circle and line patterns with in vitro co-culturing of HUVECs and MSCs were seeded with Islets of Langerhans to test the islet viability over the culture period time of 21 days.

Titanium diboride patterned substrates were also cultured with MSC only and these cells grew all over the whole substrate i.e. initially not adhering specifically to the TiB_2 patterns. After culturing for 7 to 9 days they became completely pattern specific. Then, the MSC gradually started agglomerating into the circles only to form spheroids. This spheroidal formation of MSC can be used for further differentiation processes such as into Islets of Langerhans. This was again a clear indication of mechanical forces controlling cell behavior. The implantation of the TiB_2 substrates with HUVEC, MSC and Islet of Langerhans in mice would be a good in vivo experiment in the future to complete biocompatibility studies of TiB_2 material.

There is still much to be learned for understanding the cell biology of vascularization in vitro using inorganic materials. Designing grafts and patterns of biomaterials to selectively bind cells for long duration with normal cell morphology enables a path in studying the biocompatibility of an artificial material.

Future work includes analysis of the same materials implanted in animal models will help to validate the in vitro models. This will allow an understanding of how unique molecules can result in an effect and are affected by cell–cell interactions at different time points and locations in the tissue-like models. These studies are slowly beginning to shed light on the intricacies of the complexity of the in vivo tissue regenerative niche and information from these studies should help to design and prepare novel biomaterials for increasingly better survival and functioning after implantation.

References

1. Brissova, M., & Powers, A. C. (2008). Revascularization of transplanted islets: can it be improved? *Diabetes*, *57*(9), 2269–71. doi:10.2337/db08-0814.

2. Brissova M, Shostak A, Shiota M, Wiebe PO, Poffenberger G, Kantz J, Chen Z, Carr C, Jerome WG, Chen J, Baldwin HS, Nicholson W, Bader DM, Jetton T, Gannon M, Powers AC: Pancreatic islet production of vascular endothelial growth factor–a is essential for islet vascularization, revascularization, and function. Diabetes 55:2974–2985, 2006.

3. Brissova M, Fowler MJ, Wiebe P, Shostak A, Shiota M, Radhika A, Lin PC, Gannon M, Powers AC: Intra-islet endothelial cells contribute to revascularization of transplanted pancreatic islets. Diabetes 53:1318–1325, 2004.

4. Rackham, C. L., Chagastelles, P. C., Nardi, N. B., Hauge-Evans, a C., Jones, P. M., & King, a J. F. (2011). Co-transplantation of mesenchymal stem cells maintains islet organisation and morphology in mice. *Diabetologia*, *54*(5), 1127–35. doi:10.1007/s00125-011-2053-4.

5. Song, H.-J., Xue, W.-J., Li, Y., Tian, X.-H., Song, Y., Ding, X.-M., … Li, Z.-L. (2009). Improved islet survival and funtion with rat endothelial cells in vitro co-culture. *Transplantation proceedings*, *41*(10), 4302–6. doi:10.1016/j.transproceed.2009.09.071.

6. Johansson, U., Rasmusson, I., Niclou, S. P., Forslund, N., Gustavsson, L., Nilsson, B., … Magnusson, P. U. (2008). Formation of Composite Endothelial Cell – Mesenchymal. *Diabetes*, (10), 2393–2401. doi:10.2337/db07-0981.

7. Johansson, A. Properties of endothelium and its importance in endogenous and transplanted islets of Langerhans. Acta Universitatis Upsaliensis. Digital comprehensive summaries of Uppsala dissertations from the Faculty of Medicine 492,48 pp Uppsala. ISBN 978-91-554-7643-4. 2009

8. P. Langerhans. Beitrage zur mikroskopischen Anatomie der Bauchspeicheldruse. Inaugural dissertation; Berlin; 1869.

9. L. Jansson. The regulation of pancreatic islet blood flow. Diabetes Metab Rev 10(4):407-416; 1994.

10. L. Orci. The microanatomy of the islets of Langerhans. Metabolism 25(11 Suppl 1):1303-1313; 1976.

11. Lammert E, Gu G, McLaughlin M, Brown D, Brekken R, Murtaugh LC, Gerber HP, Ferrara N, Melton DA. Role of VEGF-A in vascularization of pancreatic islets. Curr Biol 13:1070–1074, 2003

12. G. Kloppel, M. Lohr, K. Habich, M. Oberholzer and P. U. Heitz, Islet pathology and the pathogenesis of type 1 and type 2 diabetes mellitus revisited. Surv Synth Pathol Res 4(2):110-125; 1985.

13. D. E. Sutherland, R. W. Gruessner, D. L. Dunn, A. J. Matas, A. Humar, R. Kandaswamy, S. M. Mauer, W. R. Kennedy, F. C. Goetz, R. P. Robertson, et al. Lessons learned from more than 1,000 pancreas transplants at a single institution. Ann Surg 233(4):463-501; 2001.

14. A. M. Shapiro, J. R. Lakey, E. A. Ryan, G. S. Korbutt, E. Toth, G.L. Warnock, N. M. Kneteman and R. V. Rajotte. Islet transplantation in seven patients with type 1

diabetes mellitus using a glucocorticoid-free immunosuppressive regimen. N Engl J Med 343(4):230-238; 2000.

15. www.daviddarling.info/encyclopedia/I/islets_of_Langerhans

16. American Diabetes Association- Fast Facts, Professional diabetes org, March 2013.

17. www.wikipedia.org/wiki/Islet_cell_transplantation

18. Carlsson PO, Palm F, Andersson A, Liss P: Markedly decreased oxygen tension in transplanted rat pancreatic islets irrespective of the implantation site. Diabetes 50:489–495, 2001

19. Mattsson G, Jansson L, Carlsson PO: Decreased vascular density in mouse pancreatic islets after transplantation. Diabetes 51:1362–1366, 2002

20. Nyqvist D, Kohler M, Wahlstedt H, Berggren PO: Donor islet endothelial cells participate in formation of functional vessels within pancreatic islet grafts. Diabetes 54:2287–2293, 2005

21. Contreras JL, Smyth CA, Eckstein C, Bilbao G, Thompson JA, Young CJ, Eckhoff DE: Peripheral mobilization of recipient bone marrow-derived endothelial progenitor cells enhances pancreatic islet revascularization and en-graftment after intraportal transplantation. Surgery 134:390–398, 2003

22. Miller R, Cirulli V, Diaferia GR, Ninniri S, Hardiman G, Torbett BE, Benezra R, Crisa L: Switching-on survival and repair response programs in islet transplants by bone marrow-derived vasculogenic cells. Diabetes 57:2402– 2412, 2008

23. E. A. Ryan, B. W. Paty, P. A. Senior, D. Bigam, E. Alfadhli, N. M. Kneteman, J. R. Lakey and A. M. Shapiro. Five-year follow-up after clinical islet transplantation. Diabetes 54(7):2060-2069; 2005.

24. R. Olsson, A. Maxhuni and P. O. Carlsson. Revascularization of transplanted pancreatic islets following culture with stimulators of angiogenesis. Transplantation 82(3):340-347; 2006.

25. J. O. Sandberg, B. Margulis, L. Jansson, R. Karlsten and O. Korsgren. Transplantation of fetal porcine pancreas to diabetic or normoglycemic nude mice. Evidence of a rapid engraftment process demonstrated by blood flow and heat shock protein 70 measurements. Transplantation 59(12):1665-1669; 1995.

26. P. O. Carlsson, F. Palm and G. Mattsson. Low revascularization of experimentally transplanted human pancreatic islets. J Clin Endocrinol Metab 87(12):5418-5423; 2002.

27. J. Lau and P. O. Carlsson. Low revascularization of human islets when experimentally transplanted into the liver. Transplantation 87(3):322-325; 2009.

28. A. Pries and W. Kuebler. Handbook of experimental Pharmacology: Normal Endothelium. Berlin: Springer-Verlag; 2006.

29. Francis, M. E., Uriel, S., & Brey, E. M. (2008). Endothelial cell-matrix interactions in neovascularization. *Tissue engineering. Part B, Reviews*, *14*(1), 19–32. doi:10.1089/teb.2007.0115

30. Jain RK (2005) Normalization of tumor vasculature: an emerging concept in antiangiogenic therapy. Science (New York, NY) 307(5706): 58–62.

31. Johnson PC, Mikos AG, Fisher JP, Jansen JA, Strategic directions in tissue engineering. Tissue Eng. 2007;13:2827–2837.

32. Sarkar S, Dadhania M, Rourke P, Desai TA, Wong JY. Vascular tissue engineering: microtextured scaffold templates to control organization of vascular smooth muscle cells and extracellular matrix. Acta Biomater. 2005 Jan;1(1):93–100.

33. Sudo R, Chung S, Zervantonakis IK, Vickerman V, Toshimitsu Y, Griffith LG, Kamm RD. Transport-mediated angiogenesis in 3D epithelial co-culture. FASEB J. 2009

34. Davis GE, Bayless KJ, Mavila A. Molecular basis of endothelial cell morphogenesis in three-dimensional extracellular matrices. Anat Rec. 2002;268:252-275.

35. Conway EM, Collen D, Carmeliet P. Molecular mechanisms of blood vessel growth.Cardiovasc Res. 2001;49:507–521.

36. Sorrell MJ, Baber MA, Caplan AI. Influence of Adult Mesenchymal Stem Cells on In Vitro Vascular Formation. Tissue Eng Part A. 2009.

37. Au P, Tam J, Fukumura D, et al. Bone marrow-derived mesenchymal stem cells facilitate engineering of long-lasting functional vasculature. Blood. 2008;111:4551–4558.

38. Armulik A, Abramsson A, Betsholtz C. Endothelial/pericyte interactions. Circ Res.2005;97:512–523.

39. Koike N, Fukumura D, Gralla O, Au P, Schechner JS, Jain RK. Tissue engineering: creation of long-lasting blood vessels. Nature. 2004;428: 138–139.

40. Zhang JQ, Shan P, Ma Y, Jiang P, Chen J, Wen Y. Differentiation potential of bone marrow mesenchymal stem cells into retina in normal and laser-injured rat eye. Sci China C: Life Sci 2004;47(3):241–50.

41. Chen LB, Jiang XB, Yang L. Differentiation of rat marrow mesenchymal stem cells into pancreatic islet beta-cells. World J Gastroenterol 2004;10(20):3016–20.

42. Derubeis AR, Cancedda R. Bone marrow stromal cells (BMSCs) in bone engineering: limitations and recent advances. Ann Biomed Eng 2004;32(1):160–5.

43. Fruttiger M. Development of the retinal vasculature. Angiogenesis. 2007; 10:77–88.

44. Rüster, B., Göttig, S., Ludwig, R. J., Bistrian, R., Müller, S., Seifried, E., … Henschler, R. (2006). Mesenchymal stem cells display coordinated rolling and adhesion behavior on endothelial cells. *Blood*, *108*(12), 3938–3944. doi:10.1182/blood-2006-05-025098.

45. Curran, J. M., Chen, R., & Hunt, J. A. (2006). The guidance of human mesenchymal stem cell differentiation in vitro by controlled modifications to the cell substrate. *Biomaterials*, *27*(27), 4783–4793.

46. Cancedda R, Dozin B, Giannoni P, Quarto R. Tissue engineering and cell therapy of cartilage and bone. Matrix Biol 2003;22(1):81–91.

47. Ali khademhosseini, Jeffery Borenstein, Mehmet Toner, Shuichi Takayama,"Micro and nanoengineering of the cell microenvironment-Technologies and Applications," 2008, ISBN-13:978-1-59693-148-0.

48. Loffredo, F., & Lee, R. T. (2008). Therapeutic vasculogenesis: it takes two. *Circulation research*, *103*(2), 128–30. doi:10.1161/CIRCRESAHA.108.180604.

49. Laranjeira, M. S., Fernandes, M. H., & Monteiro, F. J. (2012). Reciprocal induction of human dermal microvascular endothelial cells and human mesenchymal stem cells: time-dependent profile in a co-culture system. Cell proliferation, 45(4), 320–34. doi:10.1111/j.1365-2184.2012.00822.

50. Aguirre, a, Planell, J. a, & Engel, E. (2010). Dynamics of bone marrow-derived endothelial progenitor cell/mesenchymal stem cell interaction in co-culture and its implications in angiogenesis. *Biochemical and biophysical research communications*, *400*(2), 284–91. doi:10.1016/j.bbrc.2010.08.073.

51. Wang Z Z, Au P, Chen T, Shao Y, Daheron L M, Bai H, Arzigian M, Fukumura D, Jain RK, Scadden DT. Endothelial cells derived from human embryonic stem cells form durable blood vessels in vivo. Nat Biotechnol. 2007;25:317–318.

52. Lin, R.-Z., & Melero-Martin, J. M. (2011). Bioengineering human microvascular networks in immunodeficient mice. *Journal of visualized experiments : JoVE*, (53), e3065. doi:10.3791/3065.

53. Phelps, E. A., & García, A. J. (2010). Engineering more than a cell: vascularization strategies in tissue engineering. *Current opinion in biotechnology*, *21*(5), 704–9. doi:10.1016/j.copbio.2010.06.005.

54. Kirkpatrick, C. J., Fuchs, S., & Unger, R. E. (2011). Co-culture systems for vascularization--learning from nature. *Advanced drug delivery reviews*, *63*(4-5), 291–9. doi:10.1016/j.addr.2011.01.009.

55. Rouwkema J, Rivron N.C, and Van Blitterswijk, (2008), "Vascularization in tissue engineering," Trends in biotechnology, 26(8), 434-441, doi:10.1002/jbm.a.32507.

56. Capila, I., and Linhardt,R J.,(2002), " Heparin-protein interactions," Angew Chem Int Ed.;59 (10):2558-68.

57. Stepehen L. Wolfe, "An introduction to cell and molecular biology,"; Wadsworth Pub. Co. 1995.

58. **www.mechanobio.info**

59. Harvey Lodish, Arnold Berk, Chris A. Kaiser, Monty Krieger, Anthony Bretscher, Hidde Ploegh, Angelika Amon, Matthew P. Scott; "Molecular Cell Biology;" W.H. Freeman & Company; Seventh edition: 2012.

60. www.mechanobio.info/topics/cytoskeleton-dynamics/go-0005856/go-0005884

61. University of reading,UK,Cell migration lab,matrix

62. Wendy F. Liu and Christopher S. Chen, Cellular and multicellular form and function. Adv Drug Deliv Rev. 2007 November 10; 59(13): 1319-1328.

63. Goldmann, W. H. (2012). Mechanotransduction and focal adhesions. *Cell biology international*, *36*(7), 649–52. doi:10.1042/CBI20120184.

64. John D. Catravas, Allan D. Callow, Una S. Ryan; "Vascular Endothelium: Mechanisms of Cell Signaling;" NATO science series, IOS press, Vol38, June 1998.

65. Avner Friedman, B. Aguda, "Tutorials in Mathematical Biosciences III: Cell Cycle, Proliferation, and Cancer," Springer,2000, doi-10.1007/11561606.

66. Massia, S. P. (1999). Cell-Extracellular Matrix Interactions Relevant to Vascular Tissue Engineering.

67. Balcells, M., & Edelman, E. R. (2002). Effect of pre-adsorbed proteins on attachment, proliferation, and function of endothelial cells. *Journal of cellular physiology*, *191*(2), 155–61. doi:10.1002/jcp.10087

68. Anderson, D. E. J., & Hinds, M. T. (2012). Extracellular matrix production and regulation in micropatterned endothelial cells. *Biochemical and Biophysical Research Communications*, *427*(1), 159–164. doi:10.1016/j.bbrc.2012.09.034.

69. Steed, E., Balda, M. S., & Matter, K. (2010). Dynamics and functions of tight junctions. *Trends in cell biology*, *20*(3), 142–9. doi:10.1016/j.tcb.2009.12.002.

70. Lai, M., Yang, X., Liu, Q., Li, J., Hou, Y., & Chen, X. (2014). The surface nanostructures of titanium alloy regulate the proliferation of endothelial cells, *1*(1), 45–58. doi:10.3934/matersci.2014.1.45.

71. HINDS, D. E. J. A. and M. T. (2011). Endothelial Cell Micropatterning : Methods, Effects , and Applications. *Annals of Biomedical Engineering*, *39*(9), 2329–2345. doi:10.1007/s10439-011-0352-z.

72. Roach, Paul, David Eglin, Kirsty Rohde, and Carole C Perry. 2007. "Modern Biomaterials: a Review - Bulk Properties and Implications of Surface Modifications." Journal of Materials Science. Materials in Medicine 18 (7) (July): 1263–77. doi:10.1007/s10856-006-0064-3.

73. Byfield, F. J., Reen, R. K., Shentu, T., Levitan, I., & Gooch, K. J. (2009). Endothelial actin and cell stiffness is modulated by substrate stiffness in 2D and

3D. *Journal of Biomechanics*, *42*, 1114–1119. doi:10.1016/j.jbiomech.2009.02.012.

74. Menzies, K. L., & Jones, L. (2010). The impact of contact angle on the biocompatibility of biomaterials. *Optometry and vision science : official publication of the American Academy of Optometry*, *87*(6), 387–99. doi:10.1097/OPX.0b013e3181da863e.

75. Wittmer, C. R., Phelps, J. a, Saltzman, W. M., & Van Tassel, P. R. (2007). Fibronectin terminated multilayer films: protein adsorption and cell attachment studies. *Biomaterials*, *28*(5), 851–60. doi:10.1016/j.biomaterials.2006.09.037.

76. Neyra, M. P. (2009). Interactions between titanium surfaces and biological components. *PhD thesis Dissertation*, (July).

77. Bruce Alberts, Alexander Johnson, Julain Lewis, Martin Raff, Keith Roberts, and Peter Walter; "Molecular Biology of the cell,"; New York:Garland Science; 2002;ISBN-10:0-8153-3218-1.

78. Gentile, F., Tirinato, L., Battista, E., Causa, F., Liberale, C., di Fabrizio, E. M., & Decuzzi, P. (2010). Cells preferentially grow on rough substrates. *Biomaterials*, *31*(28), 7205–12. doi:10.1016/j.biomaterials.2010.06.016.

79. Chen, J., Wan, G., Leng, Y., Yang, P., Sun, H., Wang, J., … Tang, R. (2006). Antithrombogenic investigation and biological behavior of cultured human umbilical vein endothelial cells on Ti-O film. *Science in China Series E*, *49*(1), 20–28. doi:10.1007/s11431-004-5108-7.

80. Chung, T.-W., Liu, D.-Z., Wang, S.-Y., & Wang, S.-S. (2003). Enhancement of the growth of human endothelial cells by surface roughness at nanometer scale. *Biomaterials*, *24*(25), 4655–4661. doi:10.1016/S0142-9612(03)00361-2.

81. Donald E. Ingber, The architecture of life, Scientific American, January 1998.

82. Vogel, V., & Sheetz, M. (2006). Local force and geometry sensing regulate cell functions. *Nature reviews. Molecular cell biology*, *7*(4), 265–75. doi:10.1038/nrm1890.

83. Ingber, Donald E. (2011). From cellular mechanotransduction to biologically inspired engineering. *NIH Public access Author manuscript*, *38*(3), 1148–1161. doi:10.1002/term.231.Micropatterned.

84. Ingber, D E. (1998). Cellular basis of mechanotransduction. *Marine Biological Laboratory*, *194*(3), 3232–327.

85. www.scienceforums.net/topic/37584-art-is-life-cell-tensegrity-artefact-of-fact

86. Ingber, D. E. (2002). Mechanical Signaling and the Cellular Response to Extracellular Matrix in Angiogenesis and Cardiovascular Physiology. *Circulation Research*, *91*(10), 877–887. doi:10.1161/01.RES.0000039537.73816.E5.

87. Nemir, S., & West, J. L. (2010). Synthetic materials in the study of cell response to substrate rigidity. *Annals of biomedical engineering*, *38*(1), 2–20. doi:10.1007/s10439-009-9811-1.

88. Krishnan, R., Klumpers, D. D., Park, C. Y., Rajendran, K., Trepat, X., van Bezu, J.,van Hinsberg, VW., Carman, CV., Brain, JD., Fredberg, JJ., Butler, JP., van Nieuw Amerongen, G. P. (2011). Substrate stiffening promotes endothelial

monolayer disruption through enhanced physical forces. *American journal of physiology. Cell physiology*, *300*(1), C146–54. doi:10.1152/ajpcell.00195.2010.

89. Yeung, T., Georges, P. C., Flanagan, L. A., Marg, B., Ortiz, M., Funaki, M., … Janmey, P. A. (2005). Effects of Substrate Stiffness on Cell Morphology , Cytoskeletal Structure , and Adhesion. *Cell motility and the cytoskeleton*, *34*(April 2004), 24–34. doi:10.1002/cm.20041.

90. www.usm.edu/pattonresearchgroup/PSC475/Lecture%20Notes/Lec13_Surfaces.pdf

91. www.iom3.org/feature/superhydrophobic-materials.

92. www.ndt-ed.org/EducationResources/CommunityCollege/PenetrantTest/PTMaterials/surfaceenergy.

93. Arima, Y., & Ã, H. I. (2007). Effect of wettability and surface functional groups on protein adsorption and cell adhesion using well-defined mixed self-assembled monolayers. *Elsevier*, *28*, 3074–3082. doi:10.1016/j.biomaterials.2007.03.013.

94. Berg, M. C., Yang, S. Y., Hammond, P. T., & Rubner, M. F. (2004). Controlling mammalian cell interactions on patterned polyelectrolyte multilayer surfaces. *Langmuir : the ACS journal of surfaces and colloids*, *20*(4), 1362–8.

95. Tzoneva, R., Faucheux, N., & Groth, T. (2007). Wettability of substrata controls cell – substrate and cell – cell adhesions. *Sciencedirect*, *1770*, 1538–1547. doi:10.1016/j.bbagen.2007.07.008.

96. Absolom, D. R., Zingg, W., & Neumann, A. W. (1987). Protein adsorption to polymer particles: role of surface properties. *Journal of biomedical materials research*, *21*(2), 161–71. doi:10.1002/jbm.820210202.

97. Wilson, C. J., Clegg, R. E., Leavesley, D. I., & Pearcy, M. J. (2005). Mediation of biomaterial-cell interactions by adsorbed proteins: a review. *Tissue engineering*, *11*(1-2), 1–18. doi:10.1089/ten.2005.11.1.

98. Zhu, Y., Gao, C., Liu, Y., & Shen, J. (2004). Endothelial cell functions in vitro cultured on poly(L-lactic acid) membranes modified with different methods. *Journal of biomedical materials research. Part A*, *69*(3), 436–43. doi:10.1002/jbm.a.30007.

99. Mathes, J. M. (2010). Protein Adsorption to Vial Surfaces – Quantification , Structural and Mechanistic Studies. *PhD dissertation*.

100. Marsh, R. J., Jones, R. A. L., & Sferrazza, M. (2002). Adsorption and displacement of a globular protein on hydrophilic and hydrophobic surfaces, Colloids and Surfaces B, *23*, 31–42.

101. Fields C, Cassano A, Makhoul RG, Allen C, Sims R, Bulgrin J, Meyer A, Bowlin GL, Rittgers SE., 2002, "Evaluation of electrostatically endothelial cell seeded expanded polytetrafluoroethylene grafts in a canine femoral artery model,", Journal of Biomaterial Applications, 17 (2),135-52.

102. Macdonald, D. E., Deo, N., Markovic, B., Stranick, M., & Somasundaran, P. (2002). Adsorption and dissolution behavior of human plasma fibronectin on thermally and chemically modified titanium dioxide particles. *Biomaterial*, *23*, 1269–1279.

103. Liu, Y., Yang Tan, T. T., Yuan, S., & Choong, C. (2013). Multifunctional P(PEGMA)–REDV conjugated titanium surfaces for improved endothelial cell

selectivity and hemocompatibility. *Journal of Materials Chemistry B*, *1*(2), 157. doi:10.1039/c2tb00014h.

104. Moon, J. J., Saik, J. E., Poché, R. A, Leslie-Barbick, J. E., Lee, S.H., Smith, A. A, Dickinson, M.E., West, J. L. (2010). Biomimetic hydrogels with pro-angiogenic properties. *Biomaterials*, *31*(14), 3840–7. doi:10.1016/j.biomaterials.2010.01.104.

105. Lele, T. P., Sero, J. E., Matthews, B. D., Kumar, S., Xia, S., Montoya-Zavala, M., Polte, T., Overby, D., Wang, N., Ingber, D. E. (2007). Tools to study cell mechanics and mechanotransduction. *Methods in cell biology*, *83*, 443–472. doi:10.1016/S0091-679X(07)83019-6.

106. Kotzar, G., Freas, M., Abel, P., Fleischman, A., Roy, S., Zorman, C., Moran, J. M., Melzak, J. (2002). Evaluation of MEMS materials of construction for implantable medical devices, *23*, 2737–2750.

107. Kasemo, B. (1988). Biomaterial and implant surfaces : On the role of cleanliness, contamination , and preparation. *Journal of biomedical materials research*, *22*, 145–158.

108. Park, H. J., Olivares-navarrete, R., Baier, R. E., Meyer, A. E., Tannenbaum, R., Boyan, B. D., & Schwartz, Z. (2012). Effect of cleaning and sterilization on titanium implant surface properties and cellular response. *Acta Biomaterialia*, *8*(5), 1966–1975. doi:10.1016/j.actbio.2011.11.026.

109. Wenzel, R. N. (2010). Influence of surface roughness on contact angle and wettability. *attension theory note 7*, 1–3.

110. Rupp, F., Scheideler, L., Rehbein, D., & Axmann, D. (2004). Roughness induced dynamic changes of wettability of acid etched titanium implant modifications. *Biomaterials*, *25*, 1429–1438. doi:10.1016/j.biomaterials.2003.08.015.

111. An, N., Schedle, A., Wieland, M., Andrukhov, O., Matejka, M., & Rausch-fan, X. (2009). Proliferation , behavior , and cytokine gene expression of human umbilical vascular endothelial cells in response to different titanium surfaces. *Wiley InterScience*. doi:10.1002/jbm.a.32539.

112. Rausch-fan, X., Qu, Z., Wieland, M., Matejka, M., & Schedle, A. (2007). Differentiation and cytokine synthesis of human alveolar osteoblasts compared to osteoblast-like cells (MG63) in. *Elsivier*, *4*, 102–110. doi:10.1016/j.dental.2007.03.001.

113. Cai, K., Bossert, J., & Jandt, K. D. (2006). Does the nanometre scale topography of titanium influence protein adsorption and cell proliferation? *Colloids and surfaces. B, Biointerfaces*, *49*(2), 136–44. doi:10.1016/j.colsurfb.2006.02.016.

114. Klinger, a, Steinberg, D., Kohavi, D., & Sela, M. N. (1997). Mechanism of adsorption of human albumin to titanium in vitro. *Journal of biomedical materials research*, *36*(3), 387–92.

115. Sommerfeld, J., Richter, J., Niepelt, R., Kosan, S., Keller, T. F., Jandt, K. D., & Ronning, C. (2012). Protein adsorption on nano-scaled, rippled TiO2 and Si surfaces. *Biointerphases*, (55), 7. doi:10.1007/s13758-012-0055-5.

116. Tzoneva-Velonova, R. (2003). The wettability of biomaterials determines the protein adsorption and the cellular responses. *PhD dissertation*.

117. De Mel, A., Jell, G., Stevens, M. M., & Seifalian, A. M. (2008). Biofunctionalization of biomaterials for accelerated in situ endothelialization: a review. Biomacromolecules, 9(11), 2969–79. doi:10.1021/bm800681k.

118. Treves, C., Martinesi, M., Stio, M., Gutiérrez, A., Jiménez, J. A., & López, M. F. (2010). In vitro biocompatibility evaluation of surface-modified titanium alloys. *Journal of biomedical materials research. Part A*, *92*(4), 1623–34. doi:10.1002/jbm.a.32507.

119. Bruni, S., Martinesi, M., Stio, M., Treves, C., Bacci, T., & Borgioli, F. (2005). Effects of surface treatment of Ti-6Al-4V titanium alloy on biocompatibility in cultured human umbilical vein endothelial cells. *Acta biomaterialia*, *1*(2), 223–34. doi:10.1016/j.actbio.2004.11.001.

120. Neumann, A., Reske, T., Held, M., Jahnke, K., Ragoss, C., & Maier, H. R. (2004). Comparative investigation of the biocompatibility of various silicon nitride ceramic qualities in vitro. Journal of materials science. Materials in medicine, 15(10), 1135–40. doi:10.1023/B:JMSM.0000046396.14073.92.

121. Bacáková, L, E Filová, F Rypácek, V Svorcík, and V Starý. 2004. "Cell Adhesion on Artificial Materials for Tissue Engineering." Physiological Research/ Academia Scientiarum Bohemoslovaca 53 Suppl 1 (January): S35–45.

122. Guo, C. Y., Matinlinna, J. P., Tin, A., & Tang, H. (2012). Effects of Surface Charges on Dental Implants : Past , Present , and Future. *International Journal of Biomaterials*, 5 pages. doi:10.1155/2012/381535.

123. Taddei, E. B., Henriques, V. a. R., Silva, C. R. M., & Cairo, C. a. a. (2004). Production of new titanium alloy for orthopedic implants. *Materials Science and Engineering: C*, *24*(5), 683–687. doi:10.1016/j.msec.2004.08.011.

124. Edited by Andreas Adam, Robert Dondelinger, Peter Mueller, "Textbook of Metallic Stents,", 1997, Isis Medical Media Ltd, ISBN 1 899066 32 2.

125. Lam, M. T., & Wu, J. C. (2013). Biomaterial applications in cardiovascular tissue repair and regeneration. *NIH Public access Author manuscript*, *10*(8), 1039–1049. doi:10.1586/erc.12.99.Biomaterial.

126. Ratner, B. D, A HISTORY OF BIOMATERIALS. doi:10.1016/B978-0-08-087780-8.00154-6.

127. Zaveri, N. A. (2007). Biocorrosion stuides of surface modified bioimplant in simulated body fluids. *Utah State University, Master's Thesis*, 144.

128. Oshida, Y. (2013). Bioscience and bioengineering of Titanium materials. *Elsivier*. doi:10.1016/B978-0-444-62625-7.00002-9.

129. Liu, X., Chu, P., & Ding, C. (2004). Surface modification of titanium, titanium alloys, and related materials for biomedical applications. *Materials Science and Engineering: R: Reports*, *47*(3-4), 49–121. doi:10.1016/j.mser.2004.11.001.

130. Lomholt, T. C., Pantleon, K., & Somers, M. a. J. (2011). In-vivo degradation mechanism of Ti-6Al-4V hip joints. *Materials Science and Engineering: C*, *31*(2), 120–127. doi:10.1016/j.msec.2010.08.007.

131. Ravi, V. A., Rogers, S., Malek, M., Surmenian, D., Priddy, I., Harrison, B., Schissler, A., Divi, S. C., Tamirisakandala, S., Miracle, D. (2011), "The

environmental stability of Boron-containing titanium alloys for Biomedical applications". *Corrosion in Biological environments*, *63*(6), 7 pages.

132. Miracle, D. B., State, W., Gunasekera, J. S., & Tamirisakandala, S. (2006). Titanium alloyed with boron. *Wright State University CORE Scholar*, *164*, 41–43.

133. Mayrhofer, P. H., Mitterer, C., Hultman, L., & Clemens, H. (2006). Microstructural design of hard coatings. *Progress in Materials Science*, *51*(8), 1032–1114. doi:10.1016/j.pmatsci.2006.02.002.

134. K alfagiannis, N, G Volonakis, L Tsetseris, and S Logothetidis. 2011. "Excess of Boron in TiB 2 Superhard Thin Films: a Combined Experimental and Ab Initio Study." Journal of Physics D: Applied Physics 44 (38) (September 28): 385402. doi:10.1088/0022-3727/44/38/385402.

135. M. Textor, C. Sittig, V. Frauchiger, S. Tosatti, D.M. Brunette;" Properties and biological significance of natural oxide films on titanium and its alloys" in: D.M. Brunette, P. Tengvall, M. Textor, P. Thomsen (Eds.), Titanium in Medicine, Springer, Berlin, 2001, pp. 171–230.

136. Bakir, M. (2012). Haemocompatibility of titanium and its alloys. *Journal of Biomaterails Applicationspplications*, *27*(1), 3–15. doi:10.1177/0885328212439615.

137. Edited by D. M. Brunette, P.Tengvall, M.Textor, P.Thomsen, "Titanium in medicine," Springer, Berlin, 2001.

138. J.Cl. Puippe. (2003). Surface treatment of titanium implants, *European Cells and Materails, Vol.5.Supp,* 32–33.

139. Takeuchi, M., Abe, Y., Yoshida, Y., Nakayama, Y., Okazaki, M., & Akagawa, Y. (2003). Acid pretreatment of titanium implants. *Biomaterial*, *24*, 1821–1827. doi:10.1016/S0142-9612(02)00576-8.

140. Chen, J.Y, Wan, G., Leng, Y., Yang, P., Sun, H., Wang, J., & Huang, N. (2004). Behavior of cultured human umbilical vein endothelial cells on titanium oxide films fabricated by plasma immersion ion implantation and deposition. *Surface and Coatings Technology*, *186*(1-2), 270–276. doi:10.1016/j.surfcoat.2004.02.050.

141. Oh, W. S., Xu, C., Kim, D. Y., & Goodman, D. . (1997). Preparation and characterization of epitaxial titanium oxide films on Mo (100), *15*(100), 1710–1716.

142. Aronsson, B. O., Lausmaa, J., & Kasemo, B. (1997). Glow discharge plasma treatment for surface cleaning and modification of metallic biomaterials. *Journal of biomedical materials research*, *35*(1), 49–73.

143. Hanawa, T. (1999). In vivo metallic biomaterials and surface modification. *Materials Science and Engineering: A*, *267*(2), 260–266. doi:10.1016/S0921-5093(99)00101-X.

144. Jiang, X., Chen, J., & Huang, N. (2008). Effect of micro-characterization on thrombus formation ability of TiO 2 film. *Material Science*, *2*(4), 386–391. doi:10.1007/s11706-008-0058-9.

145. www3.physik.uni-greifswald.de/method/afm/AFM_laser.gif

146. Abdulraheem, Y. M., Ghoraishi, S., Arockia-thai, L., Zachariah, S. K., & Ghannam, M. (2013). The Effect of Annealing on the Structural and Electron Beam Assisted PVD, *2013*.

147. Karagkiozaki, V., Karagiannidis, P. G., Kalfagiannis, N., Kavatzikidou, P., Patsalas, P., Georgiou, D., & Logothetidis, S. (2012). Novel nanostructured biomaterials: implications for coronary stent thrombosis. *International journal of nanomedicine*, *7*, 6063–76. doi:10.2147/IJN.S34320

148. Zagozdzon-Wosik, W., Darne, C., Radhakrishnan, D., Rusakova, I., Heide, P. Van Der, Zhang, Z-H., Bennett, J., Trombetta, L., Majhi, P.,Matron, D. (2004). Applications of metallic borides for gate electrodes I CMOS integarted circuits, *8*.

149. Ranjit, R., Zagozdzon-Wosik, W., Rusakova, I., Heide, P. Van Der, Bennett, J., & Marton, D. (2004). FORMATION OF CONTACTS AND INTEGRATION WITH SHALLOW JUNCTIONS USING DIBORIDES OF Ti , Zr AND Hf. *Advanced Material Science*, *8*, 176–184, PhD Dissertation.

150. Munro, R. G. (2000). Material properties of titanium diboride. *Journal of Research of the National Institute of Standards and Technology*, *105*(5), 709. doi:10.6028/jres.105.057.

151. Chu, K., Lu, Y. H., & Shen, Y. G. (2008). Structural and mechanical properties of titanium and titanium diboride monolayers and Ti/TiB2 multilayers. *Thin Solid Films*, *516*, 5313–5317. doi:10.1016/j.tsf.2007.07.042.

152. Bruker NanoScope Analysis1.50 User Manual.

153. Bruker, Measuring Absolute Values of Modulus of Elasticity for Soft Materials with AFM Part I : Recent developments in PeakForce QNM and Force Volume: A brief review of AFM imaging technology. (2012).

154. Hoffman, D. (2011). Measuring the elastic modulus of polymers using the atomic force microscope, Master's Thesis, Michigan Technological University.

155. Hao, Liang and Lawrence, Jonathan, Surface Modification of Biomaterials, Laser Surface Treatment of Bio-Implant Materials, ISBN 0470016876, pp. 11 – 22.

156. Zagozdzon-Wosik W, Ranjit R, Rusakova I, van der Heide P, Zhang Z, Bennett J. RTP of titanium boride for applications in front end processing. Advanced Thermal Processing of Semiconductors, 2003 RTP 2003 11th IEEE International Conference on2003. p. 209-13.

157. Feng Huang WJL, J. F. Sullivan, J. A. Barnard and M. L. Weaver Room-temperature oxidation of ultrathin TiB2 films. Journal of Materials Research 2002;17:805-13.

158. Koh, kim h-w, Kim H-E. Improvement in oxidation resistance of TiB2 by formation of protective SiO2 layer on surface. 2000.

159. Kulpa A, Troczynski T. Oxidation of TiB2 Powders below 900°C. Journal of the American Ceramic Society 1996;79:518-20.

160. Ong CW, Huang H, Zheng B, Kwok RWM, Hui YY, Lau WM. X-ray photoemission spectroscopy of nonmetallic materials: Electronic structures of boron and BxOy. Journal of Applied Physics 2004;95:3527-34.

161. Oshida Y. 4 - Oxidation and Oxides. Bioscience and Bioengineering of Titanium Materials (Second Edition). Oxford: Elsevier; 2013. p. 87-115.

162. Voitovich VB, Lavrenko VA, Adejev VM. High-temperature oxidation of titanium diboride of different purity. Oxidation of Metals 1994;42:145-61.

163. Zaleska A, Grabowska E, Sobczak JW, Gazda M, Hupka J. Photocatalytic activity of boron-modified TiO2 under visible light: The effect of boron content, calcination temperature and TiO2 matrix. Applied Catalysis B-Environmental 2009;89:469-75.

164. Dadgour HF, Endo K, De VK, Banerjee K. Grain-Orientation Induced Work Function Variation in Nanoscale Metal-Gate Transistors - Part II: Implications for Process, Device, and Circuit Design. IEEE Transactions on Electron Devices 2010;57:2515-25.

165. Dadgour HF, Endo K, De VK, Banerjee K. Grain-Orientation Induced Work Function Variation in Nanoscale Metal-Gate Transistors - Part I: Modeling, Analysis, and Experimental Validation. IEEE Transactions on Electron Devices 2010;57:2504-14.

166. Zagozdzon-Wosik W, Rusakova I, Darne C, Zhang ZH, Van Der Heide P, Majhi P. Microstructure and electrical properties of diborides modified by rapid thermal annealing. Journal of Microscopy 2006;223:227-30.

167. Zagozdzon-Wosik W and Marton D. unpublished.

168. Yoo, D., Kim, I., Kim, S., Hahn, C. H., Lee, C., & Cho, S. (2007). Effects of annealing temperature and method on structural and optical properties of TiO2 films prepared by RF magnetron sputtering at room temperature. *Applied Surface Science, 253*(8), 3888–3892. doi:10.1016/j.apsusc.2006.08.019.

169. Awan, G. H., & Aziz, S. (2005). SYNTHESIS AND APPLICATIONS OF TiO 2 NANOPARTICLES. *Pakistan Engineeering Congress, 70th Annual Session Proceedings*, *676*, 404–412.

170. Petersson, I. U., Lo, J. E. L., Fredriksson, A. S., & Ahlberg, E. K. (2009). Semi-conducting properties of titanium dioxide surfaces on titanium implants. *Biomaterials*, *30*, 4471–4479. doi:10.1016/j.biomaterials.2009.05.042.

171. Zagonel, L. F., Bäurer, M., Bailly, A., Renault, O., & Hoffmann, M. (2009). Orientation dependent work function of in situ annealed strontium titanate. *Journal of Physics: Condensed Matter*, *21*. doi:10.1088/0953-8984/21/31/314013

172. Rechendorff, K., Hovgaard, M. B., Foss, M., Zhdanov, V. P., & Besenbacher, F. (2006). Enhancement of protein adsorption induced by surface roughness. *Langmuir : the ACS journal of surfaces and colloids*, *22*(26), 10885–8. doi:10.1021/la0621923.

173. Dolatshahi-Pirouz, a, Rechendorff, K., Hovgaard, M. B., Foss, M., Chevallier, J., & Besenbacher, F. (2008). Bovine serum albumin adsorption on nano-rough platinum surfaces studied by QCM-D. *Colloids and surfaces. B, Biointerfaces*, *66*(1), 53–9. doi:10.1016/j.colsurfb.2008.05.010.

174. Jiang, X., Chen, J., & Huang, N. (2008). Effect of micro-characterization on thrombus formation ability of TiO 2 film. *Material Science*, *2*(4), 386–391. doi:10.1007/s11706-008-0058-9.

175. Cai, K., Bossert, J., & Jandt, K. D. (2006). Does the nanometre scale topography of titanium influence protein adsorption and cell proliferation? *Colloids and surfaces. B, Biointerfaces*, *49*(2), 136–44. doi:10.1016/j.colsurfb.2006.02.016

176. Chen, J.Y, Wan, G. ., Leng, Y. ., Yang, P., Sun, H., Wang, J., & Huang, N. (2004). Behavior of cultured human umbilical vein endothelial cells on titanium oxide films fabricated by plasma immersion ion implantation and deposition. *Surface and Coatings Technology*, *186*(1-2), 270–276. doi:10.1016/j.surfcoat.2004.02.050

177. Chen, J.Y., Tian, R. L., Leng, Y. X., Yang, P., Wang, J., Wan, G. J., … Huang, N. (2007). Effect of Ar plasma etching of Ti–O film surfaces on biological behavior of endothelial cell. *Surface and Coatings Technology*, *201*(15), 6901–6905. doi:10.1016/j.surfcoat.2006.09.110.

178. Zyganitidis, I., Kalfagiannis, N., & Logothetidis, S. (2009). Ultra sharp Berkovich indenter used for nanoindentation studies of TiB 2 thin films. *Materials Science and Engineering B*, *165*, 198–201. doi:10.1016/j.mseb.2009.07.016.

179. Bhushan, B., & Li, X. (2003). Nanomechanical characterisation of solid surfaces and thin films. *International Materials Reviews*, *48*(3), 125–164. doi:10.1179/095066003225010227

180. Saha, R., & Nix, W. D. (2002). Effects of the substrate on the determination of thin film mechanical properties by nanoindentation. *Acta Materialia*, *50*, 23–38. doi:10.1016/S1359-6454(01)00328-7.

181. Yu HY, Sanday SC, Rath BB. J Mech Phys Solids 1990;38:745.

182. Beegan, D., Chowdhury, S., & Laugier, M. T. (2004). The nanoindentation behaviour of hard and soft films on silicon substrates. *Thin Solid Films*, *466*, 167–174. doi:10.1016/j.tsf.2004.03.006

183. Chadwick, R. S. (2012). Determination of the elastic moduli of thin samples and adherent cells using conical atomic force microscope tips, *7*(September). doi:10.1038/NNANO.2012.163.

184. Berger, M., Larsson, M., & Hogmark, S. (2000). Evaluation of magnetron-sputtered TiB intended for tribological applications. *Surface and Coatings Technology*, *124*, 253–261.

185. Ternary phase equilibria in transition metal-boron-carbon-silicon systems. Part i. related binary systems. Volume vii.tib system; E. Rudy, Aerojet-General Corp Sacramento CA materials research lab; . Ft. Belvoir Defense Technical Information Center JAN 1966.

186. Oliver, W. C., & Pharr, G. M. (2011). Measurement of hardness and elastic modulus by instrumented indentation: Advances in understanding and refinements to methodology. *Journal of Materials Research*, *19*(01), 3–20. doi:10.1557/jmr.2004.19.1.3.

187. Han, S. M., Saha, R., & Nix, W. D. (2006). Determining hardness of thin films in elastically mismatched film-on-substrate systems using nanoindentation. *Acta Materialia*, *54*(6), 1571–1581. doi:10.1016/j.actamat.2005.11.026.

188. "Indentation Rules of Thumb — Applications and Limits; Agilent Technologies," 2010.

189. Weng, Shinuo, and Jianping Fu. 2011. "Synergistic Regulation of Cell Function by Matrix Rigidity and Adhesive Pattern." Biomaterials 32 (36) (December): 9584–93. doi:10.1016/j.biomaterials.2011.09.006.

190. Cretel, E., Pierres, A., Benoliel, A.-M., & Bongrand, P. (2008). How Cells feel their environment: a focus on early dynamic events. *Cellular and molecular bioengineering*, *1*(1), 5–14. doi:10.1007/s12195-008-0009-7.

191. Grevesse, T., Versaevel, M., Circelli, G., Desprezb, S., & Gabriele, S. (2013). A simple route to functionalize polyacrylamide hydrogels for the independent tuning of mechanotransduction cues. *The Royal Society of Chemsitry*, *13*, 777–780. doi:10.1039/c2lc41168g.

192. Introduction to Bruker ' s ScanAsyst and PeakForce Tapping AFM Technology; Application Note # 133., 1–12.

193. Pittenger, B. B., Erina, N., & Su, C. (1993). Quantitative Mechanical Property Mapping at the Nanoscale with PeakForce QNM.

194. Cappella, B., & Dietler, G. (1999). Force-distance curves by atomic force microscopy. *Surface Science Reports*, *34*(1-3), 1–104. doi:10.1016/S0167-5729(99)00003-5.

195. Scanning probe microscopy for industrial applications: Nanomechanical characterization; Dalai G. Yablon; Wily; 2013.

196. Chtcheglova, L. a, Wildling, L., Waschke, J., Drenckhahn, D., & Hinterdorfer, P. (2010). AFM functional imaging on vascular endothelial cells. *Journal of molecular recognition : JMR*, *23*(6), 589–96. doi:10.1002/jmr.1052.

197. Kloxin, A. M., Benton, J. A., & Anseth, K. S. (2010). In situ modulation with dynamic substraes to direct cell phenotype. *NIH Public access Author manuscript*, *31*(1), 1–8. doi:10.1016/j.biomaterials.2009.09.025.In.

198. Kuznetsova, T. G., Starodubtseva, M. N., Yegorenkov, N. I., Chizhik, S. a, & Zhdanov, R. I. (2007). Atomic force microscopy probing of cell elasticity. *Micron*, *38*(8), 824–33. doi:10.1016/j.micron.2007.06.011.

199. Guo, Q., Xia, Y., Sandig, M., & Yang, J. (2012). Characterization of cell elasticity correlated with cell morphology by atomic force microscope. *Journal of Biomechanics*, *45*(2), 304–309. doi:10.1016/j.jbiomech.2011.10.031.

200. Maiorano, G., Sabella, S., Sorce, B., Brunetti, V., Malvindi, M. A., Cingolani, R., & Pompa, P. P. (2010). Effects of cell culture media on the dynamic formation of protein-nanoparticle complexes and influence on the cellular response. *ACS nano*, *4*(12), 7481–91. doi:10.1021/nn101557e.

201. Tedja, R., Lim, M., Amal, R., & Marquis, C. (2012). Eff ects of Serum Adsorption on Cellular Uptake Profile and Consequent Impact of Titanium Dioxide Nanoparticles. *American Chemical Society Nano*, (5), 4083–4093.

202. Horie, M., Nishio, K., Fujita, K., Endoh, S., Miyauchi, A., Saito, Y.,Iwahashi, H., Yamamoto, K., Murayama, A., Nakano, H., Nanashima, N., Niki, E.,Yoshida,Y., Protein adsorption of ultrafine metal oxide and its influence on cytotoxicity toward cultured cells. *Chemical research in toxicology*, *22*(3), 543–53. doi:10.1021/tx800289z.

203. Birch, W., Carre, A., & Mittal, K. L. (2008). Wettability Techniques to Monitor the Cleanliness of Surfaces, 1–32.

204. Mason, B. N., Califano, J. P., & Reinhart-king, C. A. (2012). Engineering Biomaterials for Regenerative Medicine. (S. K. Bhatia, Ed.)*Engineering Biomaterials for Regenerative Medicine*, 19–38. doi:10.1007/978-1-4614-1080-5.

205. Chen, C. S., Mrksich, M., Huang, S., Whitesides, G. M., & Ingber, D. E. (1997). Geometric Control of Cell Life and Death. *Science*, *276*(5317), 1425–1428. doi:10.1126/science.276.5317.1425.

206. Chiou, Y.-W., Lin, H.-K., Tang, M.-J., Lin, H.-H., & Yeh, M.-L. (2013). The influence of physical and physiological cues on atomic force microscopy-based cell stiffness assessment. *PloS one*, *8*(10), e77384. doi:10.1371/journal.pone.0077384.

207. Sato, H., Katano, M., Takigawa, T., & Masuda, T. (2001). Estimation for the elasticity of vascular endothelial cells on the basis of atomic force microscopy and Young's modulus of gelatin gels. *Polymer Bulletin*, *47*(3-4), 375–381. doi:10.1007/s289-001-8195-z.

208. Mathur, A. B. (2001). Engineering endothelial cell adhesion on artificial surfaces to improve vascular graft biocompatibility: An application of the AFM-TIRFM system. *PhD dissertation, Duke University*.

209. Xue, X., Wang, J., Zhu, Y., Tu, Q., & Huang, N. (2010). Biocompatibility of pure titanium modified by human endothelial cell-derived extracellular matrix. *Applied Surface Science*, *256*, 3866–3873. doi:10.1016/j.apsusc.2010.01.042.

210. Tu, Q., Zhao, Y., Xue, X., Wang, J., & Huang, N. (2010). Improved endothelialization of titanium vascular implants by extracellular matrix secreted from endothelial cells.

211. Lavigne, D., Guerrier, L., Gueguen, V., Michel, J., & Boschetti, E. (2010). Culture of human cells and synthesis of extracellular matrix on materials

compatible with direct analysis by mass spectrometry. *The Royal Society of Chemsitry*, *135*, 503–511. doi:10.1039/b914539g

212. Alexander Fridman, Gary Friedman, Plasma Medicine; February 2013, ISBN 978-0-470-68970-7.

213. Khang, D., Lu, J., Yao, C., Haberstroh, K. M., & Webster, T. J. (2008). The role of nanometer and sub-micron surface features on vascular and bone cell adhesion on titanium. *Biomaterials*, *29*(8), 970–83. doi:10.1016/j.biomaterials.2007.11.009.

214. Lu, J., Khang, D., & Webster, T. J. (2010). Greater endothelial cell responses on submicron and nanometer rough titanium surfaces. *Journal of biomedical materials research. Part A*, *94*(4), 1042–9. doi:10.1002/jbm.a.32778.

215. Li, B., Li, Y., Li, J., & Fu, X. (2014). Influence of nanostructures on the biological properties of Ti implants after anodic oxidation. *Journal of materials science. Materials in medicine*, *25*, 199–205. doi:10.1007/s10856-013-5064-5.

216. Tengvall, P., & Ingemar, L. (1992). Physio-chemical considerations of titanium as a biomaterial. *Clinical Materials*, *9*, 115–134.

217. Van Wachem, P. B., Beugeling, T., Feijen, J., Bantjes, a, Detmers, J. P., & van Aken, W. G. (1985). Interaction of cultured human endothelial cells with polymeric surfaces of different wettabilities. *Biomaterials*, *6*(6), 403–8. Retrieved from http://www.ncbi.nlm.nih.gov/pubmed/4084642.

218. Choi, S. S., Anh, V. V, Joo, M. S., & Kim, D. W. (2006). HF Treatment of a Si Surface and its Effect on Biomolecule AFM Imaging. *Journal of Korean Physical Society*, *48*(4), 589–593.

219. Xi, X., Shi, J., Maghsoudy-Louyeh, S., Tittmann, B. R., Thompson, D. O., & Chimenti, D. E. (2010). Characterization of Silicon Wafer Surfaces After Hydrophilic and Hydrophobic Treatments By Atomic Force Microscopy. *AIP conference proceedings*, *1493*(1211), 1493–1498. doi:10.1063/1.3362245.

220. Maghsoudy-Louyeh, S., Ju, H. S., & Tittmann, B. R. (2010). Surface Roughness Study in Relation With Hydrophilicity/Hydrophobicity of Materials Using Atomic Force Microscopy. *AIP proceedings*, *1487*(1211), 1487–1492. doi:10.1063/1.3362244.

221. Oldani, C., Dominguez, A., & Eli, T. (2012). Titanium as a Biomaterial for Implants. *Recent Advances in Arthroplasty*.

222. Melchiorri, A. J., Hibino, N., & Fisher, J. P. (2013). Strategies and Techniques to Enhance the In Situ Endothelialization of Small-Diameter Biodegradable Polymeric Vascular Grafts. *Tissue engineering. Part B,*, *19*(4). doi:10.1089/ten.teb.2012.0577.

223. Ni, M., Tong, W. H., Choudhury, D., Rahim, N. A. A., Iliescu, C., & Yu, H. (2009). Cell culture on MEMS platforms: A review. *International journal of molecular sciences*, *10*(12), 5411–41. doi:10.3390/ijms10125411.

224. Parfitt, G. D. (1976). SURFACE CHEMISTRY OF OXIDES. *Pure & Appl. Chem.*, *48*(4), 415–418.

225. Roessler, S., Zimmermann, R., Scharnweber, D., Werner, C., & Worch, H. (2002). Characterization of oxide layers on Ti6Al4V and titanium by streaming potential and streaming current measurements. *Colloids and surfaces B*, *26*, 387–395.

226. Fenoglio, I., Fubini, B., Ghibaudi, E. M., & Turci, F. (2011). Multiple aspects of the interaction of biomacromolecules with inorganic surfaces. *Advanced drug delivery reviews*, *63*(13), 1186–209. doi:10.1016/j.addr.2011.08.001.

227. Edited by Tofail Syed, Syed A. M. Tofail, Paul O'Brien, Harold Craighead, "Biological interactions with surface charge in biomaterials,"2011, RSC Nanoscience & nanotechnology.

228. Kasemo, B. (1988). Biomaterial and implant surfaces : On the role of cleanliness , contamination , and preparation. *Journal of biomedical materials research*, *22*, 145–158.

229. Park, H. J., Olivares-navarrete, R., Baier, R. E., Meyer, A. E., Tannenbaum, R., Boyan, B. D., & Schwartz, Z. (2012). Effect of cleaning and sterilization on titanium implant surface properties and cellular response. *Acta Biomaterialia*, *8*(5), 1966–1975. doi:10.1016/j.actbio.2011.11.026.

230. Myllymaa, S., Kaivosoja, E., Myllymaa, K., Sillat, T., Korhonen, H., Lappalainen, R., & Konttinen, Y. T. (2010). Adhesion, spreading and osteogenic differentiation of mesenchymal stem cells cultured on micropatterned amorphous diamond, titanium, tantalum and chromium coatings on silicon. *Journal of materials science. Materials in medicine*, *21*(1), 329–41. doi:10.1007/s10856-009-3836-8.

231. Iskandar, M. E., Cipriano, A. F., Lock, J., Gott, S. C., Rao, M. P., & Liu, H. (2012). Improved bone marrow stromal cell adhesion on micropatterned titanium surfaces. *Conference proceedings : ... Annual International Conference of the IEEE Engineering in Medicine and Biology Society. IEEE Engineering in*

Medicine and Biology Society. Conference, *2012*, 5666–9. doi:10.1109/EMBC.2012.6347280.

232. Joie, J., Lei, Y., Colin, T., Durrieu, M. C., Poignard, C., & Saut, O. (2013). Modelling of migration and orientation of endothelial cells on micropatterned polymers. *Research Report n 8252*, 17 pages.

233. Matsuda, T., & Sugawara, T. (1996). Control of cell adhesion, migration, and orientation on photochemically microprocessed surfaces. *Journal of Biomedical Materials Research*, *32*, 165–173.

234. Cenni, E., Granchi, D., Ciapetti, G., Verri, E., Cavedagna, D., Gamberini, S., Cervellati, M., Leo, A.Di., Pizzoferrato, A. (1997). Expression of adhesion molecules on endothelial cells after contact with knitted Dacron. *Biomaterials*, *18*(6), 489–94. Retrieved from http://www.ncbi.nlm.nih.gov/pubmed/9111953.

235. Sanborn, Sharon L, Gurunathan Murugesan, Roger E Marchant, and Kandice Kottke-Marchant. 2002. "Endothelial Cell Formation of Focal Adhesions on Hydrophilic Plasma Polymers." Biomaterials 23 (1) (January): 1–8.

236. Luo, J Z Q, F Xiong, a S Al-Homsi, T Roy, and L G Luo. 2011. "Human BM Stem Cells Initiate Angiogenesis in Human Islets in Vitro." Bone Marrow Transplantation 46 (8) (August): 1128–37. doi:10.1038/bmt.2010.278.

237. Kang, Tae-Yun, Jung Min Hong, Bum Jin Kim, Hyung Joon Cha, and Dong-Woo Cho. 2013. "Enhanced Endothelialization for Developing Artificial Vascular Networks with a Natural Vessel Mimicking the Luminal Surface in Scaffolds." Acta Biomaterialia 9 (1) (January): 4716–25. doi:10.1016/j.actbio.2012.08.042.

238. In-Sung, Y., Seung-Ki, M., & Youngbai, A. (2010). Influence of Bioactive Material Coating of Ti Dental Implant Surfaces on Early Healing and Osseointegration of Bone. *Journal of the Korean Physical Society*, *57*(61), 1717. doi:10.3938/jkps.57.1717.

239. Makau, F. M., Morsi, K., Gude, N., Alvarez, R., Sussman, M., & May-Newman, K. (2013). Viability of Titanium-Titanium Boride Composite as a Biomaterial. *ISRN Biomaterials*, 1–8. doi:10.5402/2013/970535

APPENDIX A: Staining Protocol

Fixed staining of HUVECs and Islets for confocal imaging:

- Rinse the substrates twice with 1X Phosphate Buffered Saline.
- Put 4% formaldehyde (100 µl) on the substrate for 25 minutes.
- After the cells are fixed, wash the wafers thrice in 1X PBS (1ml) each 30minutes at room temperature.
- Permealize the islets in 0.3% Triton for 3 to 4 hours.
- 5% Donkey serum made with 5 parts of BSA and 95 parts of 0.15%Triton. Remove the 0.3% Triton and put 100 µl of Donkey serum on each wafer overnight at 4 °C

Day 1 staining

- Prepare primary antibody with 1:100 of CD31(ab28364-Rabbit) + 1:200 of Insulin (ab7842-Guine Pig) + 1:100 off Glucagon (ab10988-Mouse) + 1:500 of Somatostatin (ARP13-2366-Sheep) and remaining of antibody dilution buffer. Antibody Dilution buffer is prepared with 0.2% Triton-X 100, 1%BSA and 1X PBS.
- Place paraffin film on the base of the box.
- Equilibrate the islets twice in antibody dilution buffer for 20 minutes each at room temperature.
- Put 100 µl of primary antibody on the substrate placed in the box. Make sure no bubbles are present in the drop and have enough antibody to cover the wafer. Refrigerate overnight (4 °C). Place a small piece of wet tissue in the box.

Day 2 staining

- Wash the wafer thrice with 0.2% Triton-X/ 1X PBS for 30 minutes each at room temperature . Place the wafer on a box with a new paraffin film at the base of the box.
- Prepare secondary antibody with 1:500 of Dylight 405 (anti Mouse) + 1:500 of Alexa Flour 488 (anti Guine Pig) + + 1:500 of Alexa Flour 647 (anti Sheep) + 1:500 of Alexa Flour 594 (anti Rabbit) and antibody dilution buffer.
- Put 50 µl to 150 µl on each wafer and keep for an hour at room temperature or overnight at 4 °C.
- Wash the wafer thrice with 0.2% Triton-X/ 1X PBS for 30 minutes each at room temperature. Mount the wafers on a cover slide with 50 µl of Aqua Poly or Vectasheild and refrigerate overnight (4 °C).
- Image the substrates with the fixed cells on the confocal microscope.

4.8.3. Fixed staining of HUVECs on substrates:

- Rinse the substrates twice with 1X Phosphate Buffered Saline.
- Put 2 ml of 4% formaldehyde on the substrate in the 35mm*10mm petri dish for 2 minutes. Aspirate the formaldehyde and put 1 ml of 2% formaldehyde for 20 minutes.
- After the cells are fixed, wash the wafers thrice in 1X PBS (1ml) each 5 minutes at room temperature.
- Permealize the islets in 0.3% Triton for 10 minutes.

- 5% Donkey serum (1ml) made with 5 parts of BSA and 95 parts of 0.15%Triton. Remove the 0.3% Triton and put 1ml of Donkey serum on the wafer for 2 hours 45 minutes at room temperature.
- Wash twice with 1X PBS for 10 minutes.
- Prepare primary antibody with 1:100 of CD31 (ab28364-Rabbit) + remaining of antibody dilution buffer. Antibody Dilution buffer is prepared with 0.2% Triton-X 100, 1%BSA and 1X PBS.
- Place paraffin film on the base of the box.
- Put 100 µl of primary antibody on the substrate placed in the box. Make sure no bubbles are present in the drop and have enough antibody to cover the wafer. Refrigerate overnight (4 °C). Place a small piece of wet tissue in the box.

Day 1 staining

- Wash the wafer thrice with 0.2% Triton-X/ 1X PBS for 30 minutes each at room temperature. Place the wafer on a box with a new paraffin film at the base of the box.
- Prepare secondary antibody with 1:500 of Cy3 + antibody dilution buffer.
- Put 50 µl to 150 µl on each wafer and keep for an hour at room temperature.
- Wash the wafer thrice with 0.2% Triton-X/ 1X PBS for 30 minutes each at room temperature .Mount the wafers on a cover slide with 50 µl of Aqua Poly or Vecatshield with DAPI and refrigerate overnight (4 °C).

Day2 staining

- DAPI staining for nuclei of endothelial cells
    - Put a drop of Vectashield with DAPI on the wafer for 5 minutes. Cover the wafer with coverslip and image it in the confocal microscope.

Fixed staining for Actin filaments (cytoskeleton) and focal adhesions:

4.8.4. SEM fixing and imaging:

- Preparation of stock components
    - 0.2M sodium cacodylate: Dissolve 42.9g sodium cacodylate distilled water and make up to a final volume of 1 liter.
    - 0.2M HCl: Add 1.7ml concentrated HCl to 98.3ml.
    - Store stock components in refrigerator until required for use.
- Preparation of 0.1M Buffer
    - Add 27ml 0.2M HCl stock to 250ml 0.2M sodium cacodylate stock (add approximately half the volume of HCl then add the rest while monitoring the pH using either the pH meter or pH paper)
    - Make upto 500ml with distilled water.
    - Check pH of the mixed buffer is between 7.0 to 7.2 using pH meter or pH paper.
- Preparation of 3% glutaraldehydefixative
    - Dispense approximately 11ml of buffer into a container.
    - Pipette 1.5ml of glutaraldehyde (25% Glutaraldehyde, EM grade-Agar Scientific).
- Preparation of cells
    - Grow cells (HUVEC, MSC and Islets) on the substrate.

- Remove the cell culture media and wash with pre warmed 37 °C HBSS twice.
- Incubate the substrate with cells in an abundance of 3% glutarledyde for 30 minutes at room temperature on a rocking platform.
- Remove excess fixative and rinse the cells with dH_2O twice.
- For cell drying, take the cells through an additional ethanol series (75, 85, 90 and 100% ethanol and incubate with HMDS for 5 minutes) to speed the evaporation of surface liquid and limit the cell stress.
- Seal the petri dish in order to avoid any re-hydration and store in the dark at room temperature for upto 3 weeks.

- SEM imaging
  - Nano SEM equipment at the Methodist Hospital Research Institute was used for the SEM imaging.

APPENDIX B: AFM data-Surface roughness

Distance (μm)	Surface roughness (nm)	Distance (μm)	Surface roughness (nm)
0	7.241	4.786	2.651
0.137	7.241	4.922	3.704
0.273	-3.289	5.059	4.431
0.41	-4.167	5.196	3.872
0.547	-2.874	5.333	4.447
0.684	-0.056	5.469	5.573
0.82	-3.265	5.606	5.581
0.957	-0.128	5.743	5.341
1.094	-0.519	5.879	7.521
1.231	-1.325	6.016	4.383
1.367	-2.283	6.153	4.79
1.504	0.287	6.29	7.289
1.641	-0.423	6.426	5.126
1.778	-0.663	6.563	5.213
1.914	0.064	6.7	7.952
2.051	0.551	6.837	5.86
2.188	1.277	6.973	7.561
2.324	0.639	7.11	6.275
2.461	2.738	7.247	7.888
2.598	7.002	7.384	7.409
2.735	0.735	7.52	6.044
2.871	1.062	7.657	6.371
3.008	5.732	7.794	5.413
3.145	0.671	7.93	6.06
3.282	0.99	8.067	7.034
3.418	1.724	8.204	4.463
3.555	0.599	8.341	5.189
3.692	2.778	8.477	5.118
3.829	3.744	8.614	6.73
3.965	2.786	8.751	5.932
4.102	5.126	8.888	4.647
4.239	3.201	9.024	3.768
4.375	3.928	9.161	4.974
4.512	5.7	9.298	3.537
4.649	3.776	9.435	3.617

Distance (μm)	Surface roughness (nm)
9.571	4.67
9.708	3.944
9.845	11.992
9.981	3.872
10.118	4.439
10.255	3.082
10.392	8.072
10.528	6.786
10.665	4.215
10.802	3.178
10.939	4.231
11.075	4.391
11.212	4.878
11.349	9.796
11.486	7.385
11.622	7.952
11.759	1.517
11.896	2.491
12.032	3.297
12.169	4.032
12.306	1.78
12.443	4.359
12.579	6.219
12.716	4.527
12.853	3.808
12.99	2.371
13.126	0.846
13.263	4.87
13.4	1.014
13.536	2.786
13.673	2.794
13.81	3.122
13.947	1.517
14.083	6.666
14.22	0.639
14.357	2.012
14.494	2.579

Distance (μm)	Surface roughness (nm)
14.63	0.415
14.767	1.301
14.904	0.982
15.041	6.06
15.177	1.317
15.314	-0.846
15.451	7.6
15.587	4.144
15.724	-0.184
15.861	-0.343
15.998	-0.415
16.134	-0.247
16.271	-2.259
16.408	1.198
16.545	0.639
16.681	-0.072
16.818	2.579
16.955	-1.269
17.092	0.176
17.228	0.902
17.365	-1.413
17.502	-0.12
17.638	-3.657
17.775	-2.363
17.912	0.766
18.049	-1.309
18.185	-0.822
18.322	-0.575
18.459	-0.088
18.596	0.311
18.732	-2.251
18.869	-1.924
19.006	-2.483
19.143	-3.609
19.279	-0.144
19.416	-1.429
Average	2.790636

APPENDIX C: Nanoindenter-Hardness and modulus data of TiB_2

Sr. no	E Average Over Defined Range	H Average Over Defined Range	Modulus From Unload	Hardness From Unload
	GPa	GPa	GPa	GPa
1	191.98	14.38	187.27	13.66
2	194.37	14.61	197.24	13.52
3	186.74	13.61	187.10	12.75
4	189.06	13.89	189.37	13.24
5	191.28	13.92	177.20	13.62
6	187.13	13.55	186.05	12.75
7	177.97	12.57	179.23	11.99
Mean	188.36	13.79	186.21	13.07
Std. Dev.	5.33	0.66	6.63	0.61

Displacement Into Surface
Nm
3.658817
7.411321
12.75402
18.4589
24.49008
30.66508
37.30054
44.04205

Hardness	STANDARD DEVIATION (Hardness)	Modulus	STANDARD DEVIATION (Modulus)
GPa	GPa	GPa	GPa
0.835501	0.333296	63.74777	15.18887
3.163102	0.742764	119.7906	14.91643
6.710155	1.170846	153.917	12.89625
9.088381	1.095508	169.1775	10.38895
10.78225	0.968532	178.1377	8.482605
12.01849	0.888199	182.6592	7.058317
13.03885	0.838145	185.6224	5.999966
13.7725	0.724904	187.848	5.725137

Displacement Into Surface
Nm
3.7716
7.490657
12.73695
18.44362
24.47167
30.65624
37.20578
43.97801

Hardness	STANDARD DEVIATION (Hardness)	Modulus	STANDARD DEVIATION (Modulus)
GPa	GPa	GPa	GPa
0.66289	0.167345	60.63659	7.133862
2.778197	0.335171	110.6277	7.974688
6.183425	0.598951	139.2533	5.349817
8.558839	0.518271	152.4205	4.209207
10.23878	0.45417	162.0114	4.0018
11.42702	0.494481	168.1348	3.937911
12.37599	0.494084	172.3311	3.880556
13.22187	0.447335	175.4047	3.182259